

Syracuse University

SURFACE

Physics - Dissertations

College of Arts and Sciences

2011

Topics in Cosmic Acceleration and Braneworlds

Eric J. West

Syracuse University

Follow this and additional works at: https://surface.syr.edu/phy_etd



Part of the [Physics Commons](#)

Recommended Citation

West, Eric J., "Topics in Cosmic Acceleration and Braneworlds" (2011). *Physics - Dissertations*. 110.
https://surface.syr.edu/phy_etd/110

This Dissertation is brought to you for free and open access by the College of Arts and Sciences at SURFACE. It has been accepted for inclusion in Physics - Dissertations by an authorized administrator of SURFACE. For more information, please contact surface@syr.edu.

Abstract

Cosmic acceleration has come to be a standard, and perhaps required, ingredient in our current understanding of the universe. In the early universe, under the name of inflation, a phase of accelerated expansion is used to solve many problems with the standard Hot Big Bang cosmology. In the late universe, cosmic acceleration seems to best explain a wide variety of observations. In both cases, we lack a complete theory of what drives cosmic acceleration. In this thesis I discuss some open issues in our understanding of cosmic acceleration, both in the early and late universe.

Topics in Cosmic Acceleration and Braneworlds

by

Eric J. West

B.S. University of Minnesota Duluth, 1999

B.A. University of Minnesota Duluth, 1999

DISSERTATION

Submitted in partial fulfillment of the requirements for the
degree of Doctor of Philosophy in Physics
in the Graduate School of Syracuse University

May, 2011

Copyright 2010 Eric J. West

All rights Reserved

Contents

List of Figures	viii
Preface	ix
1 Introduction	1
1.1 Basics of General Relativity	1
1.1.1 The Curvature of Space-Time	1
1.1.2 The Dynamics of Space-Time	3
1.1.3 The Action Principle	4
1.2 The FRW Universe	5
1.2.1 The FRW Metric	5
1.2.2 Kinematics in an FRW Universe	6
1.2.3 Dynamics of an FRW Universe	12
1.3 The Hot Big Bang Cosmology	16
1.3.1 Hubble's Law	16
1.3.2 Big Bang Nucleosynthesis	17
1.3.3 The Cosmic Microwave Background	19
1.4 Concordance and Λ CDM Cosmology	19
2 Reheating the Post-Inflationary Universe	22
2.1 Three Shortcomings	23
2.1.1 The Horizon Problem	23

2.1.2	The Flatness Problem	24
2.1.3	The Origin of Structure Problem	26
2.2	Solving the Horizon and Flatness Problems	26
2.3	Slow-Roll Inflation	28
2.4	The Origin of Structure	33
2.5	Perturbative Reheating	35
2.6	Preheating and Parametric Resonance	37
2.7	Preheating in Models with Derivative Coupling	41
2.7.1	Preheating into Derivatively-Coupled Scalars	44
2.7.2	Preheating into Gauge Fields	48
2.8	Conclusions	53
3	Brief Interlude: Is the Universe Really Accelerating?	55
3.1	LTB Cosmology	55
3.2	Cosmic Parallax in an LTB Void	58
3.3	Axisymmetric Bianchi Type I Models	63
3.4	Cosmic Parallax in Axisymmetric Bianchi-I Models	71
4	Building Braneworlds	81
4.1	Why Extra Dimensions?	81
4.2	Factorizable Extra Dimensions	82
4.3	The Randall-Sundrum Braneworlds	83
4.4	Inclusion of Bulk Fields	85
4.5	Kinked Scalar in a Flat Extra Dimension	87
4.6	Kinked Scalar in a Warped Background	92
4.7	Bulk Scalars in Gravitating Warped Extra Dimensions	97
4.8	Stability of Kink Solutions	106
4.9	Discussion and Outlook	114
	Conclusion	117

List of Figures

1.1	Comoving vs. physical coordinates	7
1.2	Conformal vs. cosmic time	8
1.3	Illustration of luminosity distance.	11
1.4	Illustration of angular diameter distance.	12
1.5	Hubble diagram	17
1.6	Primordial abundances of the light elements	18
1.7	CMB angular power spectrum	20
1.8	Concordance cosmology	20
2.1	Conformal horizons, past and present	24
2.2	Energy density vs. scale-factor	25
2.3	Decay channels of the inflaton	36
2.4	Instability diagram of the Mathieu equation	39
2.5	One-loop correction to the inflaton mass	42
2.6	Instability diagram for a derivatively-coupled scalar field	47
2.7	Zero mode of a derivatively-coupled scalar field during preheating	49
2.8	Instability diagram for a derivatively-coupled gauge field	52
3.1	Illustration of an LTB void	57
3.2	A geodesic in an LTB void	59
3.3	Illustration of cosmic parallax in an LTB void	62
3.4	Cosmic parallax in realistic LTB models	63

3.5	Observation angle γ_0 in Bianchi I models	74
3.6	Location of sources used to measure cosmic parallax	75
3.7	Cosmic parallax in Bianchi-I models: varying Δt , fixed ϵ	76
3.8	Cosmic parallax in Bianchi-I models as a function of Δt	77
3.9	Cosmic parallax in Bianchi-I models: varying ϵ , fixed Δt	78
3.10	Cosmic parallax in Bianchi-I models as a function of ϵ	79
3.11	Estimated cosmic parallax in Bianchi-I models	80
4.1	Illustration of the RS1 model	84
4.2	The RS1 solution to the hierarchy problem	86
4.3	Bulk scalar field profiles	88
4.4	Nodeless scalar field profiles	90
4.5	Possible stable scalar field configurations	92
4.6	Solutions with a quartic potential	104
4.7	Parameter space of solutions with a quartic potential	105
4.8	Solutions with a higher-order potential	107
4.9	Parameter space of solutions with a higher-order potential	108

Preface

It is an exciting time for cosmology. For most of human history, ideas about the origin, evolution, and fate of the universe have occupied the realm of philosophical speculation. In stark contrast, in a little over 100 years cosmology has grown into a legitimate science. Advances in technology have allowed us to develop instruments with extraordinary precision, making it possible to test our ideas about the cosmos and to pit one idea against another. In the process, we have learned an unprecedented amount about the universe we live in. We have learned that our solar system is but one amongst billions in a galaxy we call the Milky Way, which in turn is just one amongst billions of other galaxies that we know of. We have learned that the universe is not static, but that it is in fact expanding. We have learned that the universe (or at least its latest incarnation) is very close to 13.7 billion years old, and we have a good idea what it was like when it was only 1 second old. We have learned that we are immersed in the radiation after-glow of the universe as it was when it was only about 300,000 years old, and we have learned that the universe at that time was much more uniform than it is today. So we have learned a lot.

On the other hand, we have discovered many things about the cosmos that we do not understand. We know, for instance, that ordinary matter only makes up about 5% of the total energy density budget of the universe, while 20% is made up of so-called dark matter, and 75% is made up of so-called dark energy, both of which we have yet to understand the nature of. We know that virtually all of the material in the observable universe is made up of matter rather than anti-matter, but we do not

know why. We know that the effects of the vacuum energy is 120 orders of magnitude smaller than it should be, according to our “best” theory of matter, but again, we do not know why. And finally, we know that the universe is very close to being spatially flat, that the CMB is very close to uniform, and that the seeds of structure are distributed very evenly on all length scales that we have observed, yet we do not really know why. So we still have a lot to learn.

Unfortunately it would require too much space to discuss all of these outstanding puzzles in cosmology. Instead, I will only have space and time to discuss a few of them, namely those which my own research has involved me with. The outline of the dissertation is as follows. In Chapter 1 I review the Hot Big Bang (HBB) cosmology, the observational evidence supporting it, and some of its shortcomings which motivate the later chapters. In Chapter 2 I will discuss the idea of inflation as a way of solving many of the outstanding problems in HBB cosmology. I will also discuss the theory of reheating at the end of inflation, which is the crucial bridge between inflation and HBB cosmology. In Chapter 3 I present evidence for, and possible explanations of, the recent acceleration of the universe. One of these explanations actually attempts to explain away cosmic acceleration all together. I will discuss this scenario in detail and present one possible method to test it with observations. Finally, I change gears slightly in Chapter 4 to discuss spacetime models with extra spatial dimensions. Inflation and dark energy both require a foothold in some fundamental theory beyond the standard model of particle physics or the gravitational theory of Einstein. Models of spacetime with extra dimensions, and braneworld models in particular, are able to provide such a foothold. And so, rather than directly solving some outstanding problem in HBB cosmology, braneworld models can be seen as providing a theoretical foundation for various solutions of those problems.

Chapter 1

Introduction

The standard model of cosmology is based on Einstein's theory of General Relativity (GR) and the Friedmann-Robertson-Walker (FRW) model of the universe. This model of space-time eventually led to the hugely successful Hot Big Bang (HBB) cosmology. In this chapter I will briefly review the elements of GR that will be needed in this and the remaining chapters, I will discuss basic properties of an FRW universe, and I will summarize the observational successes of the HBB cosmology. Finally I will briefly explain some of the shortcomings of the HBB cosmology, which provide the motivation for the remaining chapters as well as much research in theoretical cosmology today.

1.1 Basics of General Relativity

1.1.1 The Curvature of Space-Time

In Einstein's theory of General Relativity (GR), gravity is identified with the curvature of space-time. To see what this means, we need to introduce some notation. Let us define coordinates (x^0, x^1, x^2, x^3) around an observer in space-time, where x^0 is the time coordinate and the x^i (for $i = 1, 2, 3$) are space coordinates. The line element, or space-time interval, which defines how clocks measure time and how rods measure

distance in this coordinate system, is given by

$$ds^2 = g_{\mu\nu} dx^\mu dx^\nu. \quad (1.1)$$

Here greek indices range from 0 to 3 and repeated indices are summed over. The quantity $g_{\mu\nu}$ is called the metric of space-time in these coordinates. In general, the components of the metric are themselves functions of the coordinates. In other words, the rate of identical clocks and the lengths of identical rods may vary from one space-time point to another. We also introduce a dual metric with raised indices, $g^{\mu\nu}$, obeying the condition

$$g^{\mu\lambda} g_{\lambda\nu} = \delta^\mu{}_\nu, \quad (1.2)$$

where $\delta^\mu{}_\nu = \text{diag}(1, 1, 1, 1)$ is the Kroenecker delta symbol. The metric tensors $g_{\mu\nu}$ and $g^{\mu\nu}$ are used to lower and raise indices on other tensors, respectively.

Next we define a geodesic as a path that extremizes the interval between two points. In Euclidean space, these are straight lines; on a globe, they are great circles. Formally, these paths obey the geodesic equation

$$\frac{d^2 x^\rho}{d\lambda^2} = -\Gamma^\rho{}_{\mu\nu} \frac{dx^\mu}{d\lambda} \frac{dx^\nu}{d\lambda}, \quad (1.3)$$

where λ is an arbitrary affine (i.e., monotonically increasing) parameter and we have introduced a useful quantity called the Christoffel symbol

$$\Gamma^\rho{}_{\mu\nu} = \frac{1}{2} g^{\rho\sigma} \left(\frac{\partial g_{\sigma\nu}}{\partial x^\mu} + \frac{\partial g_{\mu\sigma}}{\partial x^\nu} - \frac{\partial g_{\mu\nu}}{\partial x^\sigma} \right). \quad (1.4)$$

The Christoffel symbol is also used to define a covariant derivative

$$\nabla_\mu A^\nu = \partial_\mu A^\nu + \Gamma^\nu{}_{\mu\lambda} A^\lambda \quad (1.5)$$

$$\nabla_\mu \omega_\nu = \partial_\mu \omega_\nu - \Gamma^\lambda{}_{\mu\nu} \omega_\lambda. \quad (1.6)$$

The covariant derivative ∇_μ is assumed to be a linear operator that obeys the Leibniz rule (so that $\nabla_\mu(T^\rho S_\nu) = (\nabla_\mu T^\rho)S_\nu + T^\rho(\nabla_\mu S_\nu)$, etc), commutes with contraction (so that $\nabla_\mu(T^\nu{}_\nu) = \nabla_\mu T^\nu{}_\nu$, etc), is metric compatible ($\nabla_\mu g_{\rho\sigma} = 0$), is torsion-free ($[\nabla_\mu, \nabla_\nu]f = 0$), and reduces to the ordinary derivative ∂_μ in flat space-time.

The intrinsic curvature of a space is completely characterized by the Riemann curvature tensor, defined as

$$[\nabla_\mu, \nabla_\nu] A^\rho = R^\rho{}_{\sigma\mu\nu} A^\sigma \quad (1.7)$$

$$[\nabla_\mu, \nabla_\nu] \omega_\sigma = -R^\rho{}_{\sigma\mu\nu} \omega_\rho, \quad (1.8)$$

or equivalently in terms of the Christoffel symbols

$$R^\rho{}_{\mu\sigma\nu} = \frac{\partial}{\partial x^\sigma} \Gamma^\rho{}_{\nu\mu} - \frac{\partial}{\partial x^\nu} \Gamma^\rho{}_{\sigma\mu} + \Gamma^\lambda{}_{\nu\mu} \Gamma^\rho{}_{\sigma\lambda} - \Gamma^\lambda{}_{\sigma\mu} \Gamma^\rho{}_{\nu\lambda}. \quad (1.9)$$

The Ricci tensor is the only independent and non-trivial trace of the Riemann tensor

$$R_{\mu\nu} = R^\rho{}_{\mu\rho\nu} \quad (1.10)$$

(all other traces either vanish or are identical up to a sign). Taking another trace gives the Ricci scalar

$$R = R^\mu{}_\mu. \quad (1.11)$$

These can be combined to form a covariantly conserved quantity called the Einstein tensor

$$G_{\mu\nu} = R_{\mu\nu} - \frac{1}{2} R g_{\mu\nu}, \quad (1.12)$$

where by covariantly conserved we mean that $\nabla_\mu G^\mu{}_\nu = 0$. These traces of the Riemann tensor contain only part of the information about the curvature of space-time in greater than three dimensions. The remaining content is contained in the trace-free part of the Riemann tensor called the Weyl tensor.

1.1.2 The Dynamics of Space-Time

We can now describe how space-time is dynamically influenced by matter, according to GR. The master equations are the Einstein equations, covariantly written as

$$G_{\mu\nu} + \Lambda g_{\mu\nu} = 8\pi G T_{\mu\nu}, \quad (1.13)$$

where Λ is an arbitrary cosmological constant, G is Newton's gravitational constant and $T_{\mu\nu}$ is the energy-momentum tensor describing a given matter source. The left-hand side of equation (1.13) contains second-derivatives of the metric, and in particular second time-derivatives, while the right-hand side describes some matter distribution. So (1.13) contains equations of motion for the metric, $g_{\mu\nu}$, under the influence of matter, $T_{\mu\nu}$, as advertised. However, equation (1.13) also contains constraint equations that need to be enforced. In addition, there is a gauge redundancy that needs to be accounted for in order to eliminate gauge artifacts. One way to deal with this is to impose further gauge-fixing conditions, as is often done in electromagnetism. Finally, from the fact that the Einstein tensor is covariantly conserved, equation (1.13) implies that the energy-momentum tensor is also covariantly conserved, yielding four additional constraints on the system's dynamics

$$\nabla_{\mu} T^{\mu}_{\nu} = 0. \quad (1.14)$$

Together the dynamical equations contained in (1.13), the constraints contained in (1.13) and (1.14), and any gauge-fixing conditions along with initial conditions determine the dynamical behavior of the metric components. In general this leads to a non-linear system of coupled partial differential equations, which can be difficult to solve. But, as we will see, in many situations there are simplifying assumptions that make life a bit easier.

1.1.3 The Action Principle

It should be mentioned in passing that the Einstein equations (1.13) and conservation equations (1.14) can be derived from an action principle. The gravitational action is given by

$$S_{\text{grav}}[g_{\mu\nu}] = \frac{1}{16\pi G} \int d^4x \sqrt{-g} [R - 2\Lambda], \quad (1.15)$$

where g is the determinant of $g_{\mu\nu}$, R is the Ricci scalar (1.11), Λ is the cosmological constant appearing in (1.13), and the metric signature is $(-, +, +, +)$. Varying this

action with respect to the metric $g^{\mu\nu}$ yields a term proportional to the left-hand side of (1.13) plus a total derivative. The action for matter in curved space-time can be written generically as

$$S_{\text{matter}} [g_{\mu\nu}, (\text{matter fields})] = \int d^4x \sqrt{-g} \mathcal{L}_{\text{matter}}. \quad (1.16)$$

Note that the matter action is a functional of both matter fields and the metric $g_{\mu\nu}$, and so must be varied with respect to both. Requiring the variation with respect to matter fields to vanish yields their equations of motion. Variation with respect to the metric $g^{\mu\nu}$ yields a definition of the energy-momentum tensor

$$T_{\mu\nu} = -\frac{2}{\sqrt{-g}} \frac{\delta \sqrt{-g} \mathcal{L}_{\text{matter}}}{\delta g^{\mu\nu}}. \quad (1.17)$$

The total action, of course, is just

$$S_{\text{tot}} [g_{\mu\nu}, (\text{matter fields})] = S_{\text{grav}} [g_{\mu\nu}] + S_{\text{matter}} [g_{\mu\nu}, (\text{matter fields})]. \quad (1.18)$$

By requiring the variation of the total action to vanish (and neglecting boundary terms) one obtains the Einstein equations.

1.2 The FRW Universe

1.2.1 The FRW Metric

Now we begin discussing cosmology as a special case of GR. Cosmology is concerned with the evolution of the universe, or space-time, as a whole. As such, it is concerned with physics on length scales much larger than galaxies or even galaxy clusters. On these scales ($\gtrsim 100$ Mpc), observations indicate that the universe is very approximately homogeneous and isotropic. That is, on large scales the universe looks approximately the same in every direction (isotropy), and would look approximately the same from any vantage point (homogeneity). Such a space-time can be modeled by the Friedmann-Robertson-Walker (FRW) metric

$$ds^2 = -dt^2 + a^2(t) \left(\frac{dr^2}{1 - Kr^2} + r^2 d\theta^2 + r^2 \sin^2 \theta d\phi^2 \right), \quad (1.19)$$

where t is the cosmic time coordinate, (r, ϕ, θ) are the comoving spherical-polar spatial coordinates, and K is a constant which may be positive, negative, or zero. Also note that we are working in natural units where the speed of light is set to $c = 1$. The spatial sections in this space-time have constant Gaussian curvature proportional to K . These spatial sections are conformally re-scaled from one moment to the next by the scale-factor $a(t)$ (i.e., they retain their characteristic Gaussian curvature).

It is sometimes convenient to work in so-called conformal time coordinates instead of cosmic time coordinates. The conformal time coordinate η is defined by the relation

$$d\eta = \frac{dt}{a(t)}. \quad (1.20)$$

In these coordinates the FRW metric (1.19) becomes

$$ds^2 = a^2(\eta) \left[-d\eta^2 + \left(\frac{dr^2}{1 - Kr^2} + r^2 d\theta^2 + r^2 \sin^2 \theta d\phi^2 \right) \right]. \quad (1.21)$$

which is related to the flat Minkowski metric by a conformal transformation (this is obvious in the case when $K = 0$, but it also holds in the case when $K \neq 0$).

1.2.2 Kinematics in an FRW Universe

As mentioned in passing above, the spatial coordinates in (1.19) and (1.21) are comoving coordinates. This means that the coordinates scale with the conformal rescaling of the universe. To illustrate this, imagine a coordinate-mesh on a spatial section with two or more observers (represented as test particles) located at various intersections of the mesh, as shown in Fig. 1.1. If the scale-factor is increasing in time, then at a later time this spatial section will have expanded by an amount given by the scale-factor. As space expands, the observers move further away from each other (shown in the lower part of Fig. 1.1). In comoving coordinates, the coordinate-position of the observers remains the same for all time, and therefore the coordinate-distance between them also remains constant. Alternatively one may choose to work in physical coordinates, which do not expand or contract with space, but remain fixed. As

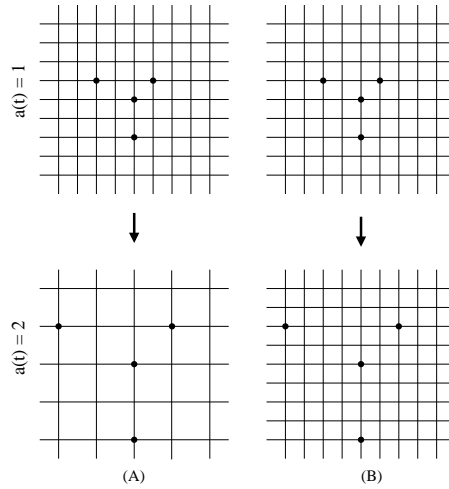


Figure 1.1: Illustration of comoving vs. physical spatial coordinates. Shown are four comoving test particles, at two different times. In (A) comoving coordinates are used, while in (B) the same situation is shown in physical coordinates.

a result, in these coordinates comoving observers change their coordinate-position as time evolves, as shown in Fig. 1.1B. The two coordinate choices are equally valid descriptions of the same physical situation, and in fact are complementary to one another in comoving coordinates, the coordinate system expands with space, and so comoving observers remain at rest with respect to it; in physical coordinates the coordinate system remains at rest, and so comoving observers move with respect to it. Comoving coordinates are often the more convenient choice, but as we will see there will be times when results are more easily interpreted in physical coordinates.

From the above illustration it is clear that we should be able to relate a comoving distance, x_{co} , to a physical distance, d_{phys} , with a simple rescaling by the scale-factor

$$d_{\text{phys}}(t) = a(t) x_{\text{co}}. \quad (1.22)$$

However, we have not yet said how to measure these distances. In special relativity we could have defined proper distances as measured by rods in the rest frame of some inertial observer. But this relies on the observer's notion of simultaneity. In GR, this

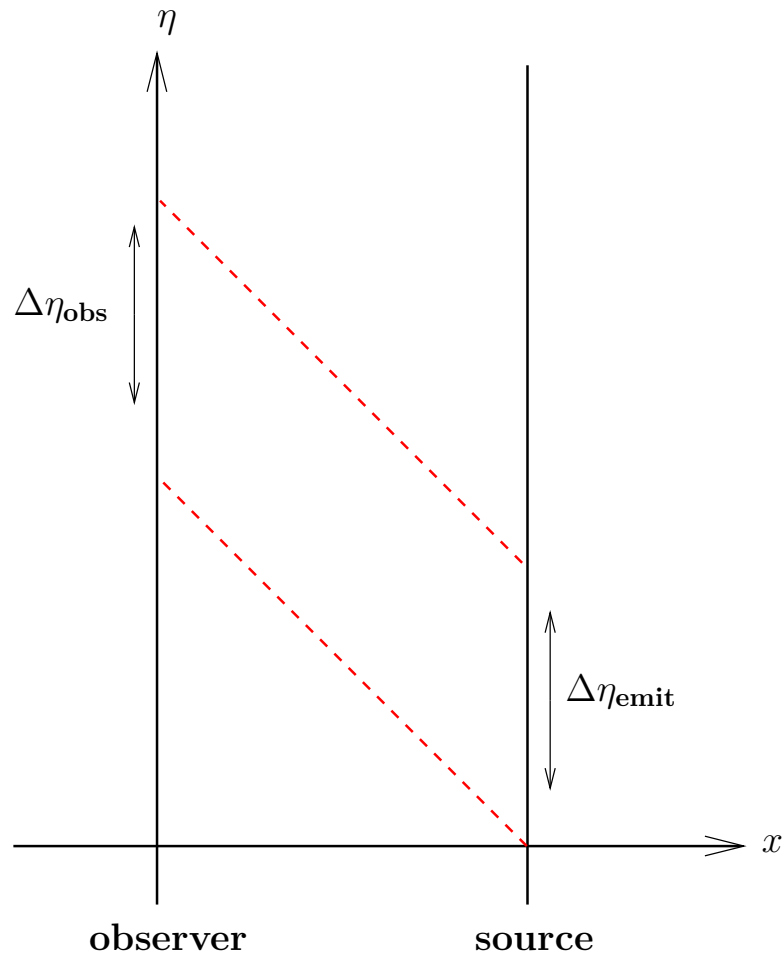


Figure 1.2: Conformal space-time diagram of two light signals emitted from a comoving source and received by a comoving observer. The conformal time between the emitted and received wavefronts is the same (shown here), but the physical (cosmic) time between the fronts is not.

becomes problematic, since two observers in the “same” frame can disagree about how to define time globally. Instead, we define *proper* distance between an observer at $r = 0$ and a source at $r = r_0$, at some time t , as the distance that freely propagating light would have had to travel from the source in order to reach the observer at time

t . In comoving coordinates this is easily shown to be

$$\begin{aligned}\chi(r, t) &= \int_r^0 \frac{dr'}{\sqrt{1 - Kr'^2}} \\ &= \int_{t_0}^t \frac{dt'}{a(t')}.\end{aligned}\tag{1.23}$$

where t_0 is the time of emission at the source and we have made use of the fact that $ds^2 = 0$ for light. In physical coordinates the proper distance is expressed as

$$d_p(r, t) = a(t)\chi(r, t).\tag{1.24}$$

Note that for $K = 1, 0, -1$, we can integrate (1.23) to give

$$\chi(r) = \begin{cases} \sin^{-1} r, & K = +1 \\ r, & K = 0 \\ \sinh^{-1} r, & K = -1 \end{cases}\tag{1.25}$$

This can also be inverted

$$r(\chi) = \begin{cases} \sin \chi, & K = +1 \\ \chi, & K = 0 \\ \sinh \chi, & K = -1 \end{cases}\tag{1.26}$$

The above relations seem to indicate that to measure distances, we need two things: the relevant portion of the expansion history of the universe, and the time of emission at the source. The trouble is that we never have an independent handle on the time that a particular light signal was emitted from its source. So we need some other handle.

Luckily, as the universe expands, the wavelength of light is stretched and becomes red shifted. One way to see this is to consider two pulses of light emitted sequentially from a source. Here we will assume a flat FRW universe ($K = 0$) for the sake of illustration, but the result is general. In conformal time coordinates the space-time diagram of this situation can be drawn as in Fig. 1.2. In these conformal-time coordinates light propagates at 45 deg as they would in Minkowski space-time. The

time delay between the light signals emitted at the source is therefore the same as the time delay between the signals received at the observer's end, in conformal time (i.e., $\Delta\eta_{\text{emit}} = \Delta\eta_{\text{obs}} = \Delta\eta$). This implies (through (1.20)) that in cosmic time coordinates, $\Delta t_{\text{emit}} = a(t_{\text{emit}})\Delta\eta$ and $\Delta t_{\text{obs}} = a(t_{\text{obs}})\Delta\eta$. Therefore we find that

$$\frac{\lambda_{\text{obs}}}{\lambda_{\text{emit}}} = \frac{\Delta t_{\text{obs}}}{\Delta t_{\text{emit}}} = \frac{a(t_{\text{obs}})}{a(t_{\text{emit}})}. \quad (1.27)$$

Astronomers define redshift as

$$z = \frac{\lambda_{\text{obs}} - \lambda_{\text{emit}}}{\lambda_{\text{emit}}}. \quad (1.28)$$

Equations (1.27) and (1.28) then yield an important relation between redshift and scale-factor

$$\frac{a(t_{\text{obs}})}{a(t_{\text{emit}})} = 1 + z. \quad (1.29)$$

We can use this to express comoving distance (1.23) in terms of redshift

$$\begin{aligned} \chi(z) &= \int_{t_0}^t \frac{dt'}{a(t')} \\ &= \int_0^z \frac{dz'}{H(z')}, \end{aligned} \quad (1.30)$$

where we have introduced the Hubble parameter, $H(t) = \frac{\dot{a}(t)}{a(t)}$. From (1.26) we then have

$$r(z) = \begin{cases} \sin \chi(z), & K = +1 \\ \chi(z), & K = 0 \\ \sinh \chi(z), & K = -1 \end{cases} \quad (1.31)$$

We have just seen that redshift is roughly linearly proportional to how much the universe has expanded since the light signal was emitted. So if we know the expansion history of the universe, and if we can measure redshift accurately, we can use this to determine distances of interest.

When observing objects in the sky, we can basically only measure three things: spectra (from which we obtain redshift), brightness, and angular diameter. We have already mentioned how redshift can be related to proper distance. Now let us consider

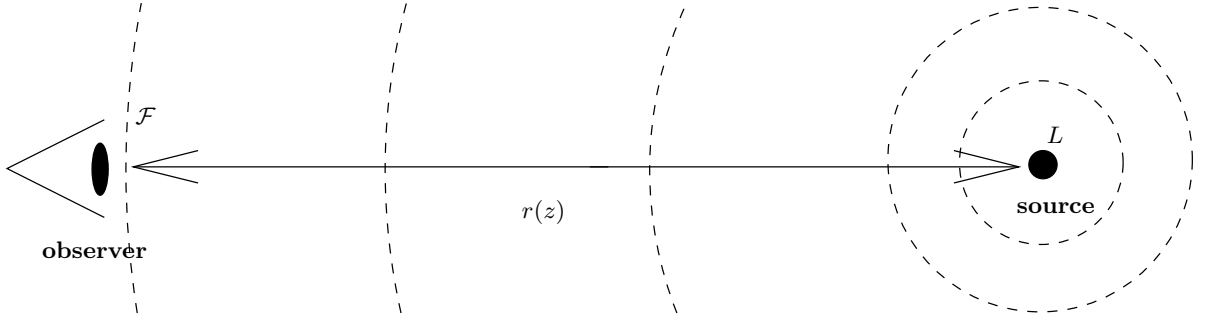


Figure 1.3: Illustration of luminosity distance.

how we might use an object's brightness and angular size to measure distances. The flux, \mathcal{F} , of an object in the sky is can be shown to be

$$\mathcal{F} = \frac{L}{4\pi r^2(z)(1+z)^2}, \quad (1.32)$$

where L is the luminosity of the source. The factor of $(1+z)$ enters twice in the denominator because in addition to the red shifting occurring due to the expansion, the energy of each individual photon also decreases as $E \propto a^{-1} \propto (1+z)^{-1}$. Matching this to the usual $1/r^2$ law defines an effective distance called the luminosity distance

$$\begin{aligned} d_L(z) &\equiv \sqrt{\frac{L}{4\pi\mathcal{F}}} \\ &= r(z)(1+z) \end{aligned} \quad (1.33)$$

The apparent size of an object, in physical coordinates, is given by

$$\begin{aligned} l_{\text{phys}} &= a(t_{\text{emit}})l_{\text{co}} \\ &= \frac{\theta r(z)}{1+z}, \end{aligned} \quad (1.34)$$

where θ is the subtended angle of the object along the line of sight. Matching this to the Euclidean formula for a small subtended angle defines an effective distance called the angular diameter distance

$$\begin{aligned} d_A(z) &\equiv \frac{l_{\text{co}}}{\theta} \\ &= \frac{r(z)}{1+z}. \end{aligned} \quad (1.35)$$

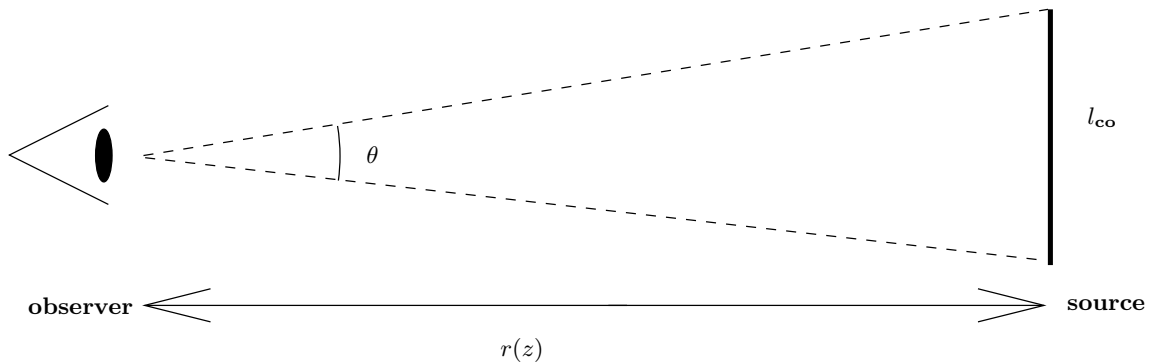


Figure 1.4: Illustration of angular diameter distance.

Note that if we know the comoving size of an object and we know our comoving distance to it, then the observed subtended angle gives us a way to test how close space is to being Euclidean (i.e., $K = 0$). Whether luminosity or angular diameter distance is more useful depends on the context. Galaxies and supernovae, for example, have poorly defined edges, making luminosity distance a more useful notion. The peaks of the CMB, on the other hand, can be related to angular diameter sizes, making the angular diameter distance a more useful notion. Both measures of distance, however, depend on the function $r(z)$, which we saw from equations (1.31) and (1.30) depends on $H(z)$. Therefore measures of distance in the universe are degenerate with the expansion history $H(z)$.

1.2.3 Dynamics of an FRW Universe

So far all of the results we have seen have been purely kinematical, relying only on the FRW metric, but not on the dynamical solutions for the scale-factor. In that sense, nothing in the previous section made any assumptions about how the metric of space-time is dynamically coupled to matter. We now turn to the task of examining the dynamical solutions of the scale-factor, according to GR.

Using the metric (1.19) and the results from Section 1.1 we can derive the left-

hand side of the Einstein equations (1.13) in an FRW universe. For consistency, matter in an FRW universe must also be homogeneously and isotropically distributed. Otherwise, inhomogeneity and anisotropy in the metric would be sourced from matter through the Einstein equations. An homogeneous and isotropic matter source, in the above comoving coordinates, has an energy-momentum tensor that resembles a perfect fluid

$$T^\mu{}_\nu = \text{diag}(-\rho, p, p, p) \quad (1.36)$$

where ρ is the energy density and p is the pressure of the fluid. With this ansatz for the matter content the Einstein equations give

$$\left(\frac{\dot{a}}{a}\right)^2 = \frac{8\pi G}{3}\rho - \frac{K}{a^2} + \frac{\Lambda}{3} \quad (1.37)$$

$$\frac{\ddot{a}}{a} = -\frac{4\pi G}{3}(\rho + 3p) + \frac{\Lambda}{3} \quad (1.38)$$

$$\dot{\rho} = -3\frac{\dot{a}}{a}(\rho + p). \quad (1.39)$$

Only two of these three equations are independent. But the system describes three time-dependent variables $a(t)$, $\rho(t)$, and $p(t)$. So to close the system, we need a third independent equation, which is usually taken to be a relationship between the energy density and pressure called an equation of state. In cosmology often sufficient to assume that the equation of state takes the simple form

$$p(t) = w\rho(t), \quad (1.40)$$

where w is a constant. This is a reasonable assumption, since ordinary matter obeys this equation of state, at least on the scales that are of interest in cosmology. From statistical mechanics we know that a distribution of non-relativistic particles (i.e., whose mean velocity is much smaller than the speed of light) has negligible pressure, whereas a distribution of relativistic particles (i.e., whose mean velocity is comparable to the speed of light) has a pressure which is 1/3 the energy density. This gives

$$w = \begin{cases} 0, & \mathbf{matter} \\ 1/3 & \mathbf{radiation} \end{cases} \quad (1.41)$$

Cosmologists generically call any distribution of non-relativistic particles, “dust” or sometimes simply “matter”; any distribution of relativistic particles is called “radiation”, regardless of the actual particle content.

Integrating equation (1.39) we find how energy density scales for a fluid with constant equation of state (i.e., w constant)

$$\rho(a) = \left(\frac{a}{a_0}\right)^{-3(1+w)}, \quad (1.42)$$

where a_0 is the scale-factor at some initial time. It is sometimes convenient to rewrite (1.37) as

$$H^2 = \frac{8\pi G}{3}(\rho_M + \rho_R + \rho_K + \rho_\Lambda) \quad (1.43)$$

where we have simply defined

$$\rho_K = -\frac{3}{8\pi G} \frac{K}{a^2}, \quad (1.44)$$

$$\rho_\Lambda = \frac{\Lambda}{8\pi G}, \quad (1.45)$$

Comparison with (1.42) shows that spatial curvature behaves as a fluid with equation of state $w = -1/3$, and the cosmological constant term behaves as a fluid with equation of state $w = -1$. From the scaling behavior of the energy density of these various components (matter, radiation, curvature, and a cosmological constant) we expect radiation to be the dominant contribution to the total energy density at very early times, followed by a periods of matter domination, curvature domination, and finally cosmological constant domination.

Using the above solution for the energy density in equation (1.37), we can solve for the scale-factor as a function of time. In the case of a spatially flat universe ($K = 0$) with no cosmological constant ($\Lambda = 0$) this becomes

$$a(t) = a_0 (t - t_0)^{2/3(1+w)} \quad (1.46)$$

where t_0 is the initial time corresponding to when a_0 is fixed. When spatial curvature or a cosmological constant is included, solutions may be found numerically.

We can recast the Friedmann equation (1.37) in terms of dimensionless quantities as follows. Define a critical energy density at a given time by

$$\rho_{\text{crit}}(t) = \frac{3H^2(t)}{8\pi G}. \quad (1.47)$$

This is the energy density required, for a given value of the Hubble parameter, in order for the universe to be spatially flat (in the absence of a cosmological constant).

Next define the density parameter for a species X by

$$\Omega_X(t) = \frac{\rho_X(t)}{\rho_{\text{crit}}}. \quad (1.48)$$

Treating the spatial curvature and cosmological constant as fluid components, as in (1.43), the Friedmann equation can then be written in terms of Ω_X 's as the simple rule

$$\Omega_{\text{tot}} = \Omega_M + \Omega_R + \Omega_K + \Omega_\Lambda = 1. \quad (1.49)$$

It is also useful to write the Hubble parameter in terms of redshift and the density parameters today

$$H(z) = H_0 \sqrt{\Omega_{M,0}(1+z)^3 + \Omega_{R,0}(1+z)^4 + \Omega_{K,0}(1+z)^2 + \Omega_{\Lambda,0}}. \quad (1.50)$$

So if we know the expansion rate and energy density budget of the universe today, we simply integrate this expression to reconstruct the expansion history of the universe, as a function of redshift. Once we have the expansion history as a function of redshift, we can determine distances to, and age of, various objects of interest.

Once we determine $H(z)$, we can calculate the age of the universe by

$$\begin{aligned} t_0 &= \int_0^{a_0} \frac{da}{aH} \\ &= \int_0^z \frac{dz}{H_0(1+z) \sqrt{\Omega_{M,0}(1+z)^3 + \Omega_{R,0}(1+z)^4 + \Omega_{K,0}(1+z)^2 + \Omega_{\Lambda,0}}} \end{aligned} \quad (1.51)$$

Using the best fit cosmological parameters yields an age of the universe of 13.75 ± 15 billion years. Now that we have laid out some basic features of an FRW universe, let us see what observations tell us about the kind of universe that we seem to inhabit.

1.3 The Hot Big Bang Cosmology

Making use of the FRW metric, the model of the universe that has emerged in the last century as the most successful, and which still forms the core of our understanding of the cosmos today, is the Hot Big Bang (HBB) Cosmology. There are three main observations in support of the HBB: the expansion of the universe according to Hubble's law, the primordial abundance of light elements, and the cosmic microwave background radiation.

1.3.1 Hubble's Law

We saw above that as light travels across the universe, its wavelength stretches when universe is expanding and is squeezed when the universe is contracting. In the 1920's, Edwin Hubble began noticing that almost all of the galaxies he observed were red shifted. Moreover, he noticed that distance and redshift were roughly linearly correlated, indicating that the further away a source was, the faster its recessional velocity. This relationship is known as Hubble's law. The fact that nearly all galaxies are moving away from us provides powerful evidence that the universe is expanding. To first order in redshift, Hubble's law is expressed as

$$H_0 d_L = z \tag{1.52}$$

where H_0 is the expansion rate of the universe today, d_L is the luminosity distance as defined above, and z is redshift. This says that luminosity distance is linearly proportional to redshift, where the proportionality constant is just the expansion rate of the universe.

The discovery that the universe is expanding rather than static fueled the search for models of an expanding universe and eventually gave credibility to the FRW universe, described above. Today the Hubble law is measured out to about a redshift of 1, providing conclusive evidence that the universe is expanding. Figure 1.5 shows the Hubble diagram for various sources out to a redshift of about 1, compiled by

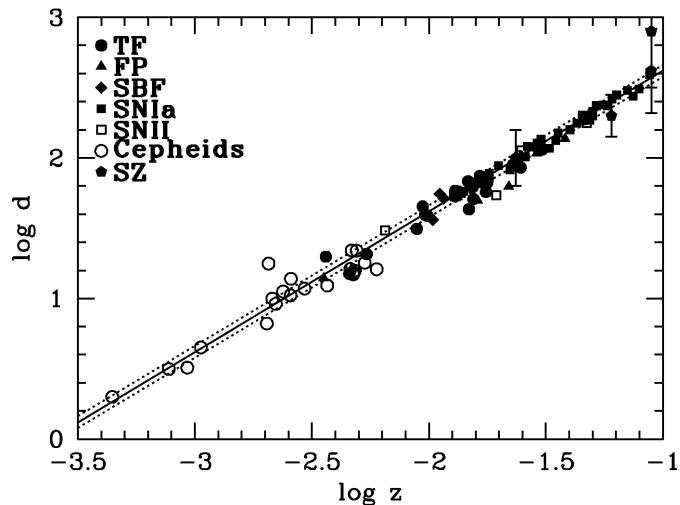


Figure 1.5: Plot of log distance in Mpc vs. log redshift from the final results of the HST Key Project [1]. The solid line is for $H_0 = 72 \text{ km s}^{-1} \text{ Mpc}^{-1}$, with the dashed lines representing $\pm 10\%$.

the Hubble Space Telescope Key Project whose determined value for H_0 was $72 \pm 8 \text{ km s}^{-1} \text{ Mpc}^{-1}$ [1]. Since this is such an important parameter in cosmology, efforts to reduce the uncertainties are always on-going. Recently H_0 has been pinned down to $74.2 \pm 3.6 \text{ km s}^{-1} \text{ Mpc}^{-1}$ [2].

1.3.2 Big Bang Nucleosynthesis

The fact that the universe is expanding today implies that it was much smaller in the distant past. Furthermore, when the universe was smaller than it is today, its temperature was also higher. By extrapolating this backwards, eventually we get to a time when the universe was so hot that nuclei would have undergone fusion. Going still further backwards in time, the universe would have been too hot even for fusion to occur (any nuclei produced would immediately be dissociated by energetic collisions). This leaves a window of time in which fusion would have occurred after the Hot Big Bang. Since the rate at which the universe cools is connected to the rate at which it expands, careful predictions can be made for abundances of the light

elements that would have been produced for a given expansion history. This gives a prediction from the Hot Big Bang Cosmology, according to which fusion would only be able to occur during a radiation-dominated epoch of the universe, about 3 minutes after the initial Big Bang.

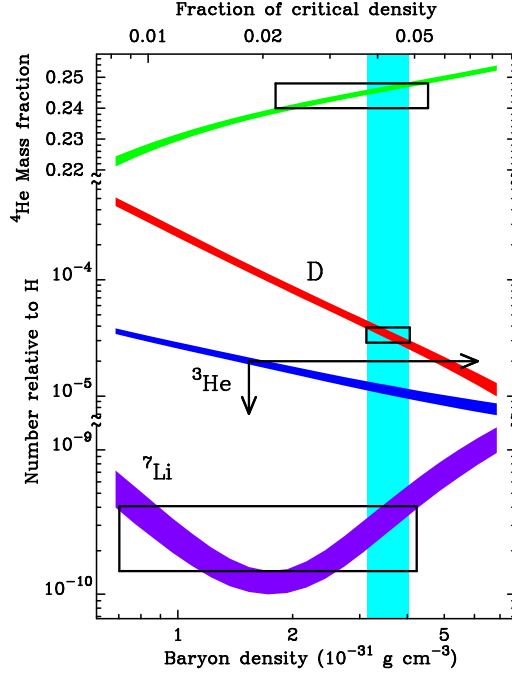


Figure 1.6: Comparison of theoretical predictions (solid curves) of the primordial abundances of light elements with allowed abundances from observations (boxed regions), from [3]. The vertical bar shows the region in which agreement of all abundances is possible.

On the other hand, astronomers are able to estimate the abundance of light elements in the universe by observing the spectra of stars. Since the nuclear physics involved in the fusion of light elements in the interior of stars is well understood, and we know roughly how long stars have been around for, one can estimate how much of the total abundance of light elements could have been produced in stars. The rest would have to have been produced primordially, that is, prior to star formation. When we compare the estimated primordial abundances of light elements inferred from observations with the predicted abundances from the Hot Big Bang, shown in

Fig. 1.6, we find remarkable agreement [3]. Due to both the theoretical and experimental uncertainties, it is generally accepted that an agreement within an order of magnitude would be the best that one could hope for. Instead all of the abundances of ^4He , D, ^3He , and ^7Li overlap in a region by a factor of about 2.

1.3.3 The Cosmic Microwave Background

As the universe expanded and cooled, at some point atoms would form. As atoms formed the universe would have become relatively neutral. Eventually photons would decouple from the plasma and freely propagate for most of the rest of the history of the universe. This light would propagate to us until today. In 1964 this radiation background was discovered by Penzias and Wilson. Since then numerous experiments and observations have been made of the CMB with growing precision. The analysis of the CMB is a lengthy and technical topic, but the most important features that we have discovered about the CMB is that it has a thermal distribution corresponding to a temperature of 2.7 K, it is uniform over the entire sky to one part in 10^5 , and its angular power spectra have distinct peaks corresponding to the acoustic oscillations of the baryon fluid at the time of decoupling. Figure 1.7 shows the (temperature-temperature) angular power spectrum as measured by different experiments, taken from the the WMAP 7-year results [4].

1.4 Concordance and Λ CDM Cosmology

Combining the above cosmological observations as well as observations of galaxy distributions and high redshift Type Ia supernovae has led to remarkable consistency. This consistency, or concordance, is despite the fact that the observations probe very different physics. In addition, what emerges from this concordance is a new and surprising picture of the universe that is nearly flat ($\Omega \simeq 1$ or equivalently $\Omega_K \simeq 0$) and vacuum-dominated, that is, accelerating. In particular, it appears that matter

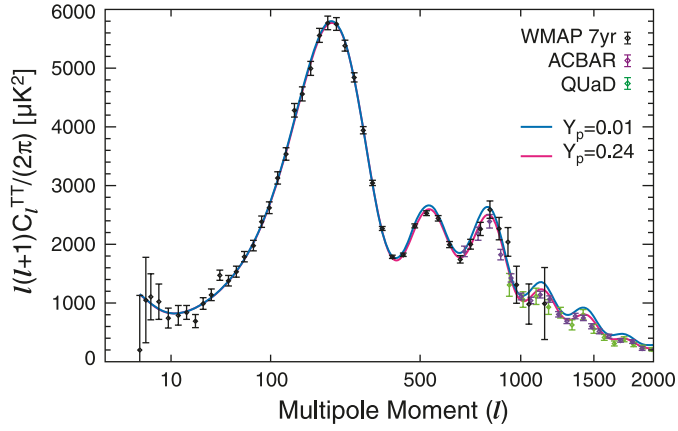


Figure 1.7: Combined angular power spectrum from WMAP 7-year results [4].

and radiation only makes up about 30% of the energy density budget of the universe. The rest is made up of something behaving like a cosmological constant with equation of state $w \simeq -1$, often called dark energy. Figure 1.8 shows the preferred regions of

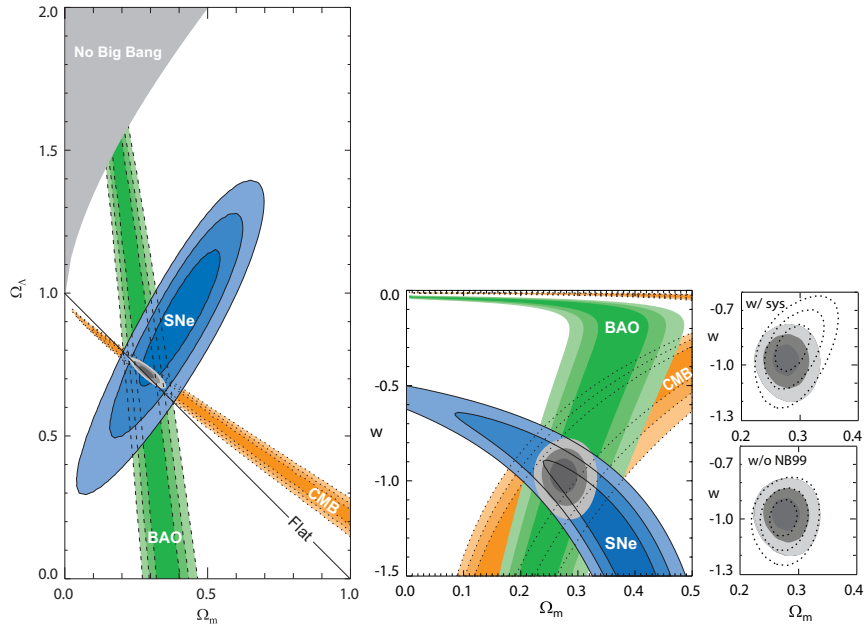


Figure 1.8: Confidence levels for combined data sets, from [5].

$\Omega_M - \Omega_\Lambda$ parameter space from CMB observations, Type Ia Supernovae, and baryon

acoustic oscillations (BAO) observed in the distribution of galaxies. Clearly $\Omega_\Lambda = 0$ is disfavored by these data. The resulting model of the universe is called the Λ CDM model, comprised of roughly 5% ordinary matter and radiation, 23% cold dark matter, and 72% dark energy.

Chapter 2

Reheating the Post-Inflationary Universe

As successful as the HBB cosmology is, it does not provide answers to some very important questions about the early universe. In particular the HBB cosmology seems to require fine-tuning of initial conditions across causally separated regions of space-time. Remarkably, many of these fine-tunings can be explained at once with a simple mechanism called inflation. In order for inflation to be a successful addition to the HBB, as a minimal requirement it has to smoothly transition to a hot early universe in time for BBN to occur. This transitional period is known as reheating. In this chapter I will first discuss how the idea of inflation solves various problems in the HBB cosmology, using slow-roll inflation as the canonical example. Then I will turn to the theory of reheating.

2.1 Three Shortcomings

2.1.1 The Horizon Problem

The early universe was extremely uniform, as indicated by the fact that the temperature fluctuations in the CMB are on the order $\sim 10^{-5}$. Since the CMB is essentially a snapshot of the radiation distribution in the early universe, this suggests that the entire observable universe had enough time to thermalize between the time of the big bang ($t = 0$) and the release of the CMB ($t \simeq 400,000$ years). This would only be possible if every portion of the sky that we observe today could have been in causal contact with every other portion of the sky we observe. So we can ask, how many causally disconnected patches of sky do we observe today? If the answer is none, that every patch is causally connected to every other patch, then the uniformity of the CMB would come as no surprise.

One way of estimating the number of causally disconnected patches is in terms of entropy density of the universe. The entropy density of the universe today is $s_0 \approx 6 \times 10^4 \text{cm}^{-3}$, while the Hubble radius of the observable universe today is $H_0^{-1} \approx 9 \times 10^{27} h^{-1} \text{cm}$, yielding the entropy within the current observable universe $S_0 \simeq 10^{88}$. Using similar values at decoupling yields the entropy within a Hubble volume at that time to be $S_{dec} \simeq 10^{83}$.

This corresponds to $\sim 10^5$ causally disconnected patches of sky that we observe today! None of these patches had time for light to travel to its nearest neighbor before today, much less to thermalize the entire sky. And yet when we compare the temperature in all of those different regions, they all agree to one part in 10 million. The universe therefore shows remarkable isotropy over regions that were never in causal contact with one another, but the HBB cosmology offers no explanation why.

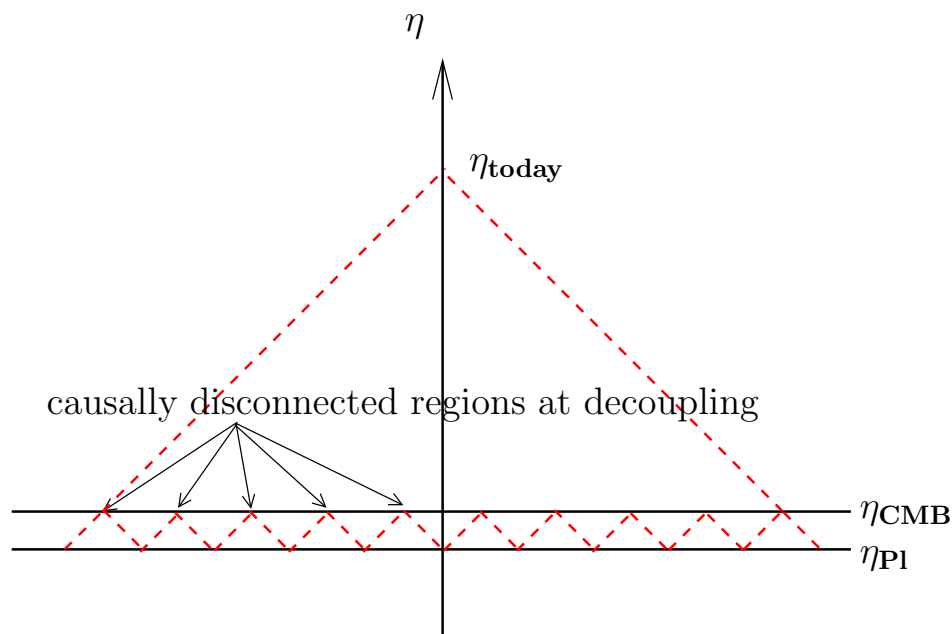


Figure 2.1: Conformal diagram of our horizon today compared with the horizon size at decoupling, when the CMB formed. The diagram is not to scale, but it illustrates that our current horizon contains many patches that had not been in causal contact before the time of decoupling.

2.1.2 The Flatness Problem

The universe today is extremely flat, but the HBB cosmology cannot explain why. This is called the *flatness problem*. Recall that the Friedmann equation can be written as

$$|\Omega - 1| = \frac{|K|}{a^2 H^2}. \quad (2.1)$$

Differentiating this with respect to the scale factor, and using the equation of motion for a fluid with constant equation of state gives the differential equation

$$\frac{d\Omega}{d \ln a} = \Omega(\Omega - 1)(1 + 3w). \quad (2.2)$$

Typical solutions for $w > -1/3$ are shown in Fig. 2.2, indicating that the flat FRW universe ($\Omega = 1$) is a repeller solution. Since the universe today is close to flat $\Omega(a_0) \sim 1$, it must have been even closer to flat in the past. In quantitative terms

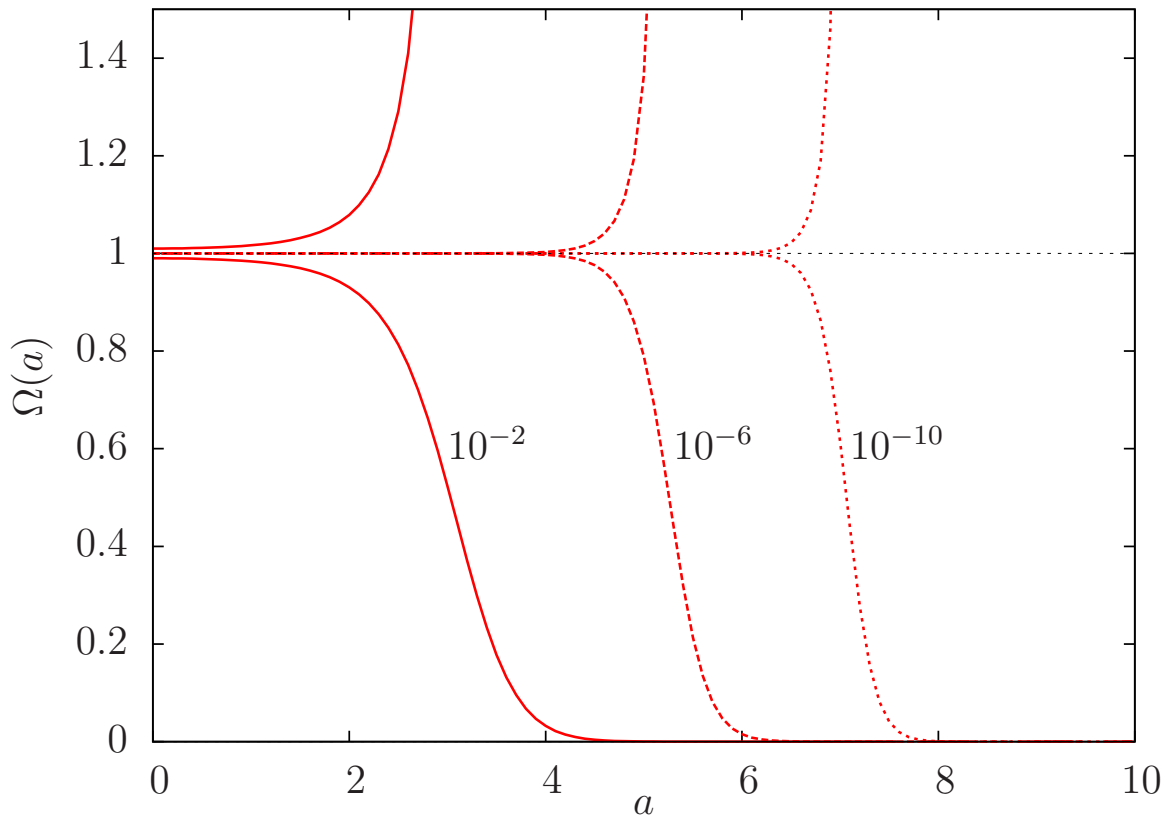


Figure 2.2: Plot of typical solutions of (2.2) for $w = 0$. So long as $w > -1/3$ the $\Omega = 1$ solution is a repellor. Shown are solutions whose initial values for $|\Omega - 1|$ are 10^{-2} , 10^{-6} , and 10^{-10} .

this requires

$$|\Omega(a_{\text{BBN}}) - 1| \leq \mathcal{O}(10^{-16})$$

$$|\Omega(a_{\text{GUT}}) - 1| \leq \mathcal{O}(10^{-55})$$

$$|\Omega(a_{\text{Pl}}) - 1| \leq \mathcal{O}(10^{-61}).$$

The energy density at the Planck epoch must be tuned to a value 60 orders of magnitude smaller than its naturally expected value in order to explain why it is so small today.

Another way to say this is that the natural time scale for curvature to dominate the energy density of the universe is on the order of the Planck time $t_{\text{Pl}} \sim 10^{-43}$ sec.

But the age of the universe is on the order of $10^{60} t_{P1}$ and it has not yet recollapsed or become curvature-dominated. The HBB cosmology does not tell us why that should be.

2.1.3 The Origin of Structure Problem

By now it is widely accepted that the formation of large-scale structure resulted from gravitational collapse of matter density fluctuations present in the very early universe. The evolution and growth of these density fluctuations is well understood in the regime where they are taken to source small metric perturbations on an FRW background. What is less understood is how such perturbations were produced in the first place. It has been shown [6] that they could not have formed spontaneously in an expanding universe through gravitational collapse alone. That means they were either produced by some physical mechanism very early on or were part of the initial conditions of the universe.

Unfortunately, the HBB cosmology does not provide any mechanism for generating super-horizon fluctuations. In fact, in the HBB cosmology, the horizon is always growing. As it grows radially away from us, comoving Fourier modes (with a characteristic comoving wavelength) are always entering our visible universe. Since the horizon (by definition) is moving at the speed of light, it would appear that there is no causal way to generate Fourier modes inside the horizon and then push them out to super-horizon scales. So in the HBB cosmology, these super-horizon density fluctuations must be taken as initial conditions of the universe.

2.2 Solving the Horizon and Flatness Problems

In the last section we saw that two of the problems of the HBB are that it has no way to explain why the universe today is so unnaturally flat (the flatness problem) and why the early universe as indicated by the CMB was so unnaturally uniform (the horizon

problem). In addition to these problems, many extensions to the standard model of particle physics would require the universe to pass through various phase transitions as it cooled. If so, then those phase transitions should have left defects behind, such as magnetic monopoles. Calculations have shown that the typical abundances of these relics would quickly cause the universe to recollapse [7–10]. This is often called the problem of unwanted relics [11].

In the early 1980's the inflationary universe scenario was proposed [10, 12, 13] and subsequently developed [14–18] as a way to simultaneously solve all three of these problems in one fell swoop. The basic idea was that in the universe expanded at an exponentially fast rate for a sufficiently long time, the universe would become flat, uniform, and diluted of any heavy relics.

To see this, suppose that the universe is being driven by a matter source that temporarily mimics a cosmological constant. In this case the Friedmann equations in cosmic-time coordinates are

$$H^2 = \frac{\rho_\Lambda}{3M_{\text{Pl}}^2} \quad (2.3)$$

$$\frac{\ddot{a}}{a} = \frac{\rho_\Lambda}{3M_{\text{Pl}}^2} \quad (2.4)$$

$$\dot{\rho}_\Lambda = 0. \quad (2.5)$$

The first and last equations together tell us that $H = \text{const}$, which implies

$$a(t) = a_0 e^{Ht} \quad (2.6)$$

for some initial condition $a_0 = a(t_0)$ set at time t_0 . Recalling that

$$\Omega_K(t) = \frac{K}{a^2(t)H^2(t)} \quad (2.7)$$

shows that Ω_K decays exponentially when $H = \text{const}$, $a \propto e^{Ht}$. In particular, comparing the curvature density at the beginning and end of such a period of expansion, we see that

$$\Omega_K(t_{\text{end}}) = \Omega_K(t_{\text{init}})e^{-H\Delta t}, \quad (2.8)$$

where $\Delta t = t_{\text{end}} - t_{\text{init}}$. In order to solve the flatness problem, we need $\Omega_K(t_{\text{end}}) \sim 10^{-62}$, requiring also that t_{end} is prior to BBN. So for $\Omega_K(t_{\text{init}}) \sim 1$, we require

$$N \equiv H\Delta t \sim 60. \quad (2.9)$$

With this amount of expansion, the universe can be driven close enough to flat to survive until today.

The other problem that inflation is supposed to solve is the horizon problem. During accelerated expansion, the horizon shrinks rather than grows. It turns out that with $N \sim 60$ this stretches a single, uniform, causally connected patch to the size of our current horizon. This solves the horizon problem. Furthermore it can also be shown that this number of e-folds also solves the monopole problem for GUT's.

It should be said that there are other features about our universe that the HBB cosmology does not explain. Most notably these are the nature of dark matter, the nature dark energy, and the baryon asymmetry of the universe. Inflation by itself does not solve any of these.

2.3 Slow-Roll Inflation

Here we will review what is now taken to be the canonical example of inflation models, namely slow-roll inflation (for a comprehensive survey of inflationary models see [19]).

We have seen that a matter source that temporarily mimics a cosmological constant would cause the universe to expand exponentially and could solve the flatness and horizon problems. The simplest type of matter that could behave in this way is a real scalar field. The action for a canonical real scalar field can be written

$$S_\phi = - \int d^4x \sqrt{-g} \left[\frac{1}{2} g^{\mu\nu} \partial_\mu \phi \partial_\nu \phi + V(\phi) \right], \quad (2.10)$$

where $V(\phi)$ is some undetermined potential. Taking the variation of this action and requiring it to vanish yields its equation of motion. But without even examining the

equation of motion, we can already learn a lot from the energy-momentum tensor (1.17). For the real scalar field this is

$$T_{\mu\nu} = \partial_\mu\phi\partial_\nu\phi - g_{\mu\nu} \left[\frac{1}{2}g^{\rho\sigma}\partial_\rho\phi\partial_\sigma\phi + V(\phi) \right]. \quad (2.11)$$

If we want to consider the scalar field in an FRW universe, then for consistency it must be spatially homogeneous and isotropic. As a result the field can have only time-dependence, and in particular its spatial gradients vanish. The resulting energy-momentum tensor is diagonal in a comoving frame, and we can define its components in direct analogy with a perfect fluid. In cosmic-time coordinates (1.19), using (1.36) these are

$$\rho_\phi = \frac{1}{2}\dot{\phi}^2 + V(\phi) \quad (2.12)$$

$$p_\phi = \frac{1}{2}\dot{\phi}^2 - V(\phi). \quad (2.13)$$

Recalling that we assumed the equation of state to take the form $p = w\rho$, the equation of state for the scalar field is

$$w_\phi = \frac{\frac{1}{2}\dot{\phi}^2 - V(\phi)}{\frac{1}{2}\dot{\phi}^2 + V(\phi)}. \quad (2.14)$$

In Chapter 1 we assumed the equation of state parameter w to be constant. Here w_ϕ is not constant, but we can still use the results of Chapter 1 in regimes when w_ϕ is approximately constant. Notice that w_ϕ depends on the potential, which we have not yet specified. This already suggests that we can construct a wide variety of models with a wide variety of behavior just by selecting different potentials. More importantly, notice that when the scalar field is dominated by kinetic energy ($\dot{\phi}^2 \gg V(\phi)$) the equation of state is $w_\phi \approx 1$, while when it is potential-dominated ($V(\phi) \gg \dot{\phi}^2$) the equation of state is $w_\phi \approx -1$. Recall that for a constant equation of state, the energy density scales as $a^{-3(1+w)}$. This tells us that in a kinetic-dominated phase, the energy density of a scalar field decreases as a^{-6} , faster than radiation (a^{-4}) or dust (a^{-3}). In a potential-dominated phase the energy density remains constant, mimicking a cosmological constant.

The simplest way for a scalar field to become potential-dominated is if it has no kinetic energy at all. For example if the field becomes trapped in a local minimum of its potential, and if that potential is lifted above the zero point, then the scalar field will act as a cosmological constant during this trapped phase. Eventually, due to quantum mechanical fluctuations the field will tunnel to its stable vacuum. Another way in which a scalar field can become potential-dominated is by slowly rolling down its potential. This mechanism is the basis of a class of models called “slow-roll” inflation. These models are perhaps the simplest models of inflation, and more importantly for our purposes, they illustrate all of the key elements that one would care about in the context of cosmology. Let us now look at these models.

We consider a real scalar field, whose action is given by (2.10), in an FRW universe. In anticipation of the fact that this scalar field will drive inflation and solve the flatness problem, we neglect spatial curvature from the beginning ($K = 0$). Similarly in anticipation of the fact that inflation will exponentially dilute radiation and matter, $\rho_M \sim \exp(-3Ht)$ and $\rho_R \sim \exp(-4Ht)$ respectively, we will neglect them from the beginning as well. Finally for simplicity we assume a vanishing cosmological constant ($\Lambda = 0$). With these assumptions, in cosmic-time coordinates the Friedmann and acceleration equations (1.37) and (1.38) become

$$H^2 = \frac{1}{3M_{\text{Pl}}^2} \left(\frac{1}{2} \dot{\phi}^2 + V(\phi) \right) \quad (2.15)$$

$$\frac{\ddot{a}}{a} = -\frac{1}{3M_{\text{Pl}}^2} \left(\dot{\phi}^2 - 2V(\phi) \right), \quad (2.16)$$

while the equation of motion for the spatially uniform scalar field in these coordinates is

$$\ddot{\phi} + 3H\dot{\phi} = \frac{\partial V}{\partial \phi}. \quad (2.17)$$

We notice from the acceleration equation (2.16) that $\ddot{a}/a > 0$ when $V(\phi) \gg \dot{\phi}^2$. For self consistency we should also ensure that $\dot{\phi}$ remains small. From (2.15), this requires $\ddot{\phi} \ll 3H\dot{\phi}$. These so-called slow-roll conditions are sufficient to drive inflation (but

they are not necessary). When these conditions hold, we may approximate equations (2.15)-(2.17) by

$$H^2 \simeq \frac{V(\phi)}{3M_{\text{Pl}}^2} \quad (2.18)$$

$$\frac{\ddot{a}}{a} \simeq \frac{V(\phi)}{3M_{\text{Pl}}^2} \quad (2.19)$$

$$3H\dot{\phi} \simeq \frac{\partial V}{\partial \phi}. \quad (2.20)$$

In this regime $V(\phi)$ can be treated as roughly constant, as can be seen by a quick consistency check. From (2.18) and (2.19) we find that $\dot{H} \simeq 0$, which implies that $H \simeq \text{const}$, which from (2.18) again implies that $V(\phi) \simeq \text{const}$, as stated. Therefore we can use an adiabatic approximation to give

$$a(t) \propto \exp \left[\int^t H(t') dt' \right]. \quad (2.21)$$

Instead of $N = H\Delta t$ as above in the case when H was a true constant, we now define the number of e -foldings as

$$N \equiv \int^t H(t') dt'. \quad (2.22)$$

Using the Friedmann equations in the slow-roll approximation, this can be rewritten as

$$N \simeq \frac{1}{M_{\text{Pl}}^2} \int \frac{V(\phi)}{V'(\phi)} d\phi \quad (2.23)$$

so that for a given potential, one can immediately determine how many e -folds inflation will last for. In order to ensure that the flatness and horizon problems are solved, any potential with $N > 60$ will do.

It is often useful to re-write the above expressions in terms of different variables. For monotonic field values $\phi(t)$, we can use ϕ to parameterize time

$$t \longrightarrow \phi \quad (2.24)$$

$$H(t) \longrightarrow H(\phi) \quad (2.25)$$

Then the Friedmann equations can be rewritten as

$$H'(\phi) = -\frac{2}{M_{\text{Pl}}^2} \dot{\phi} \quad (2.26)$$

$$H^2(\phi) \left[1 - \frac{1}{3} \epsilon(\phi) \right] = \frac{1}{3M_{\text{Pl}}^2} V(\phi) \quad (2.27)$$

$$\frac{\ddot{a}}{a} = H^2(\phi) [1 - \epsilon(\phi)] \quad (2.28)$$

where we have defined the slow-roll parameter

$$\epsilon(\phi) \equiv 2M_{\text{Pl}}^2 \left(\frac{H'(\phi)}{H(\phi)} \right)^2. \quad (2.29)$$

The equation of state in these variables is

$$p = \rho \left(\frac{2}{3} \epsilon(\phi) - 1 \right). \quad (2.30)$$

Acceleration occurs when $w < -1/3$, which corresponds to $\epsilon < 1$. As $\epsilon \rightarrow 0$, $w \rightarrow -1$, mimicking a cosmological constant. It should be emphasized that these equations are exact, that is, we have not yet made use of the slow-roll approximation. The slow-roll limit is characterized by

$$H(\phi) \simeq \sqrt{\frac{V(\phi)}{3M_{\text{Pl}}^2}} \simeq \text{constant} \quad (2.31)$$

$$\epsilon \simeq \frac{M_{\text{Pl}}^2}{2} \left(\frac{V'(\phi)}{V(\phi)} \right)^2 \ll 1. \quad (2.32)$$

Note that we can use this expression for ϵ (valid in the slow-roll approximation) to re-express the number of e -foldings as

$$N \simeq \frac{1}{M_{\text{Pl}} \sqrt{2}} \int \frac{d\phi}{\sqrt{\epsilon(\phi)}}. \quad (2.33)$$

From this we see that when the slow-roll conditions are satisfied over sufficiently large field values (i.e., $\epsilon \ll 1$) inflation lasts for a large number of e -folds ($N \gg 1$). Again, any potential that gives rise to $N > 60$ e -folds of inflation is sufficient to solve the horizon and flatness problems.

2.4 The Origin of Structure

If inflation only solved the flatness and horizon problems, it would be interesting, but it is possible that it never would have become as widely embraced as it has. Infinitely many potentials can be cooked up to give sufficient inflation to solve the flatness and horizon problems. But very soon after the first models of inflation were proposed it was realized [20–22] that inflation could also provide a mechanism for generating the seeds of structure, thereby solving the origin of structure problem, for free.

According to quantum mechanics, all fields including the inflaton field experience quantum fluctuations. Decomposing these fluctuations of the scalar field ϕ into Fourier modes, $\delta\phi_k$, with comoving wavenumber k , we can solve their equations of motion and follow their behavior. The behavior of the modes depends on the characteristic length in the problem, which is the horizon scale $\sim H^{-1}$. The characteristic length scale of a given comoving mode is its corresponding *physical* wavelength $\sim a/k$ (k/a being its corresponding physical wavenumber). Comparing these two scales, modes far inside the horizon ($k \gg aH$) do not feel the curvature of space-time, and so behave as they would for a scalar field in Minkowski space-time. Due to the exponential expansion, however, modes are rapidly stretched to super-horizon scales, since $l_{\text{phys}} \sim a/k \sim e^{Ht}$. Once modes become super-horizon sized, they freeze in as classical perturbations. This is to be expected since the horizon sets a limit to the events that can be in causal contact. So as each mode exits the horizon, we should expect it to decouple from microphysical effects. Quantum mechanically what has happened is that the super-horizon modes have acquired stable non-zero occupation numbers. This corresponds to the modes forming a kind of condensate, which is just to say, a classical state. This effect is the result having a quantum field ϕ in a de Sitter-like space-time. What started inside the horizon as quantum fluctuations have ended up outside the horizon as classical fields. This important result is what enables inflation to seed structure formation.

Subsequent analysis showed [23–27] that primordial fluctuations produced during

inflation would result in a scale-invariant power spectrum, predicted by Harrison [6] and Zeldovich [28]. In particular, the power spectrum is found to be

$$\mathcal{P}_\phi(k) = \left(\frac{H}{2\pi} \right)^2 \Big|_{k=aH}, \quad (2.34)$$

where, for a given k , H is to be evaluated at the horizon crossing $k = aH$. The power spectrum tells us how distributed the cross-correlation of modes is in k -space. The important feature here is that the right-hand side has no k -dependence, indicating a scale-invariant power spectrum. This is often said to be the most important prediction of inflation.

These fluctuations of the scalar field then become imprinted as metric perturbations. It is this metric, or curvature perturbation which then influences how matter density or temperature fluctuations evolve. In terms of the slow-roll parameters the curvature perturbation power spectrum is found to be

$$\mathcal{P}_\mathcal{R}(k) = \frac{1}{24\pi^2} \frac{V}{\epsilon} \Big|_{k=aH}. \quad (2.35)$$

Therefore, for a given model of inflation it is straight forward to compute ϵ , which immediately yields the primordial curvature power spectrum for that model.

There are other useful quantities to define and calculate such as the the spectral index, the power spectrum of tensor perturbations, the tensor spectral index, and the scalar-to-tensor ratio. These are all important in order to relate the predictions of a model of inflation to observable quantities. And just as for the curvature power spectrum, these quantities can be related to the slow-roll parameters for slow-roll inflation models so that once a potential is given, all of the observationally relevant quantities can be easily calculated.

So far we have only discussed slow-roll inflation, with a single scalar field. There is a wide variety of inflation model in the literature, but what they all have in common is that they solve the horizon and flatness problems, that they give rise to a nearly scale-invariant power spectrum of fluctuations, and finally that they gracefully merge with the HBB cosmology. It is this merging that we will now turn our attention to.

2.5 Perturbative Reheating

At first sight, the requirement of merging inflation with the HBB cosmology might worry us. After all, because inflation dilutes away all sources of energy density, and because $T \propto \rho_R^{1/4}$, we can expect that the universe gets exponentially cooled during inflation. That means that after 60 e -folds of inflation, the temperature of the universe would be e^{60} (or about 10^{26}) times cooler than it was when inflation began. Using the naive estimate that inflation begins in the Planck era, where $T \sim 10^{19}\text{GeV}$, and assuming that inflation lasts for exactly 60 e -folds (which is just long enough to solve the horizon and flatness problems, but no longer), the temperature when inflation ends would be $T \sim 100\text{eV}$ or about 10^5K . That may seem hot, but BBN requires temperatures at least four orders of magnitude larger, at 1MeV . So even under the most conservative assumptions, inflation over cools the universe by several orders of magnitude. To merge with the HBB cosmology, and therefore reproduce the successes of BBN, some mechanism needs to “reheat” the universe to at least 1MeV at the end of inflation.

This re-population is typically achieved by the decay of the inflaton into ordinary matter particles. The perturbative theory of this process is called *reheating* [14, 29, 30], which we now review. Here we will only consider coupling between the inflaton field and another scalar field, but couplings to more general fields have also been considered.

The equations of motion can then be written as

$$\ddot{\phi} + 3H\dot{\phi} + \Gamma\dot{\phi} + \frac{\partial V}{\partial\phi} = 0 \quad (2.36)$$

$$\dot{\rho}_\chi + 3H\rho_\chi = \Gamma\rho_\phi \quad (2.37)$$

$$H^2 = \frac{8\pi G}{3}(\rho_\phi + \rho_\chi) \quad (2.38)$$

where we have added the Γ term by hand in order to model the decay of the inflaton ϕ into the matter field χ . We can then use this equation to estimate the reheating temperature, depending on the strength of the coupling. We calculate cross-sections

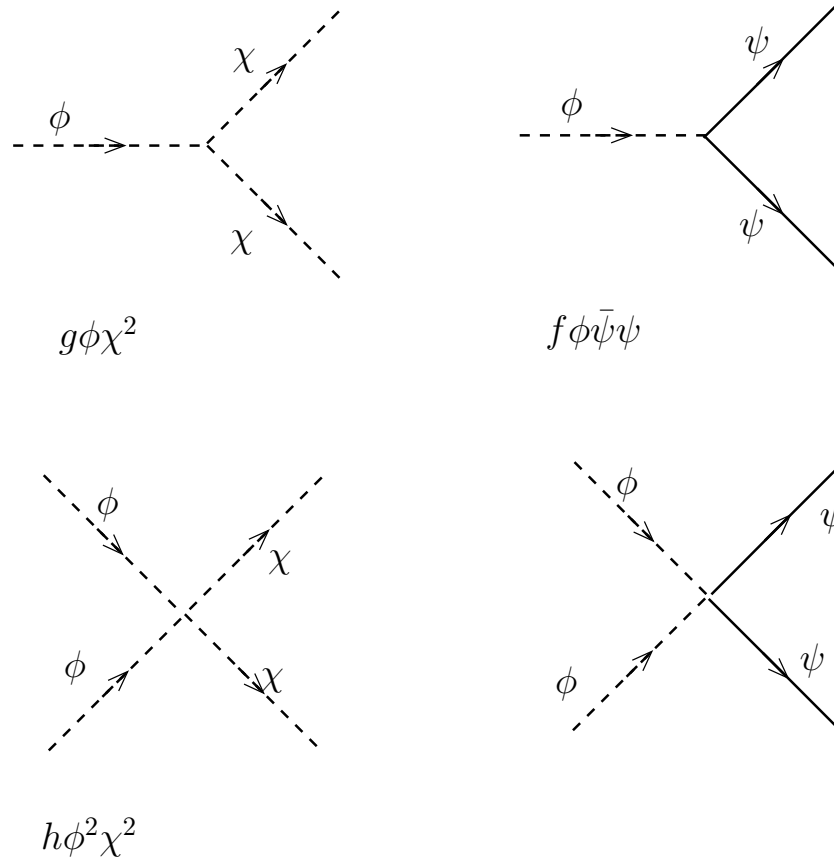


Figure 2.3: Some possible decay channels of the inflaton into a scalar field χ or fermion field ψ .

for the various possible interactions in the usual way using perturbative techniques from quantum field theory. Figure 2.3 shows some possible interactions that one may consider as decay channels of the inflaton. The estimated temperature needs to be high enough that BBN can still occur, but not so high that heavy relics are re-introduced. It was noticed, however, that these equations admit a regime where the decay of the inflaton into matter is not a perturbative one, but rather an explosive process that is far from equilibrium. This process is called *preheating*, which we discuss next.

2.6 Preheating and Parametric Resonance

The theory of reheating was refined by the discovery [31–33] that in many models the dynamics would proceed through a stage of parametric resonance, leading to the extremely efficient decay of the inflaton into a far from equilibrium distribution of matter. The understanding of this preliminary stage of reheating—*preheating*—has since been developed by many authors [34–43]. We begin by reviewing the basic results about preheating in a simple model with a direct coupling between the inflaton and matter fields. For detailed methods and results regarding the physics of reheating and preheating, we refer the reader to [42, 44].

For simplicity we assume inflation is driven by a single real scalar field ϕ , slow-rolling down a quadratic effective potential, and coupled to a massive real scalar field χ (representing matter fields) through a quartic interaction,

$$\mathcal{L} = -\frac{1}{2}(\partial^\mu \phi)\partial_\mu \phi - \frac{1}{2}(\partial^\mu \chi)\partial_\mu \chi - \frac{m_\phi^2}{2}\phi^2 - \frac{m_\chi^2}{2}\chi^2 - \frac{g^2}{2}\phi^2\chi^2. \quad (2.39)$$

We expand the field χ in terms of annihilation and creation operators

$$\chi(\mathbf{x}, t) = \int \frac{d^3k}{(2\pi)^{3/2}} (a_k \chi_k(t) e^{i\mathbf{k}\cdot\mathbf{x}} + \text{h.c.}). \quad (2.40)$$

Then the mode functions χ_k and the homogeneous inflaton ϕ satisfy the field equations

$$\ddot{\chi}_k + 3H\dot{\chi}_k + \left[\left(\frac{k}{a}\right)^2 + m_\chi^2 + g^2\phi^2 \right] \chi_k = 0, \quad (2.41)$$

$$\ddot{\phi} + 3H\dot{\phi} + (m_\phi^2 + g^2\chi_k^2)\phi = 0, \quad (2.42)$$

where the Hubble parameter $H(t) \equiv \dot{a}/a$ is determined by the Friedmann equation

$$H^2 = \frac{1}{6M_{\text{Pl}}^2} (\dot{\phi}^2 + m_\phi^2\phi^2), \quad (2.43)$$

and where we have denoted a time derivative by an overdot. Note that we have assumed $\rho_\chi \ll \rho_\phi$. Similarly, we will henceforth also neglect the back-reaction term $g^2\chi^2\phi$ in (2.42).

Slow-roll inflation occurs when $\dot{\phi} \ll m_\phi \phi$ and $\ddot{\phi} \ll 3H\dot{\phi}$. During slow-roll, the interaction between ϕ and χ in (2.41) simply increases the effective mass of the field χ ,

$$m_{\text{eff}}^2 = m_\chi^2 + g^2 \phi^2. \quad (2.44)$$

There are several arguments (see, for example, [45]) that suggest that this mass should not be much lower than the Hubble scale. If m_χ is negligible, the requirement $m_{\text{eff}} > H$, in combination with (2.43), then leads to the bound

$$g \gtrsim \frac{m_\phi}{M_{\text{Pl}}} \approx 10^{-6}. \quad (2.45)$$

Hence, the coupling between the inflaton and any other light scalar cannot be too weak. The same bound also guarantees that the effective mass of χ , equation (2.44), is adiabatically constant during inflation, even if m_χ is negligible.

Once inflation ends, the inflaton field begins oscillating around the minimum of its effective potential and the field evolution rather quickly follows the equation

$$\phi(t) \approx \phi_e \frac{\sin(m_\phi t)}{m_\phi t}, \quad (2.46)$$

where $\phi_e \approx 0.3M_{\text{Pl}}$ denotes the value of the inflaton at the beginning of the oscillating stage. Because of the rapid oscillations, the effective mass of χ ceases being adiabatically constant for sufficiently light fields and this non-adiabatic evolution leads to particle production for appropriate couplings between matter and the inflaton. More importantly, parametric resonance can excite χ very efficiently.

If we neglect the expansion of the universe and the back-reaction from χ , (2.42) and (2.41) can be combined into the Mathieu equation,

$$\ddot{\chi}_k + [\delta - 2\epsilon \cos(2t)] \chi_k = 0, \quad (2.47)$$

where we have defined a dimensionless time $t \rightarrow m_\phi^{-1}t$, and used

$$\delta \equiv \left(\frac{k}{m_\phi}\right)^2 + \left(\frac{m_\chi}{m_\phi}\right)^2 + 2\epsilon \quad \text{and} \quad \epsilon \equiv \left(\frac{g\phi_e}{2m_\phi}\right)^2. \quad (2.48)$$

Solutions of the Mathieu equation are known to exhibit parametric resonance—resonance for certain values of the dimensionless parameters δ and ϵ . In the δ - ϵ plane, these resonant solutions form instability bands. Along these unstable solutions, the mode functions grow exponentially,

$$\chi_k \propto \exp(\mu m_\phi t), \quad (2.49)$$

where the characteristic exponent μ depends on δ and ϵ . A numerical plot of the bands is shown in figure 2.4.

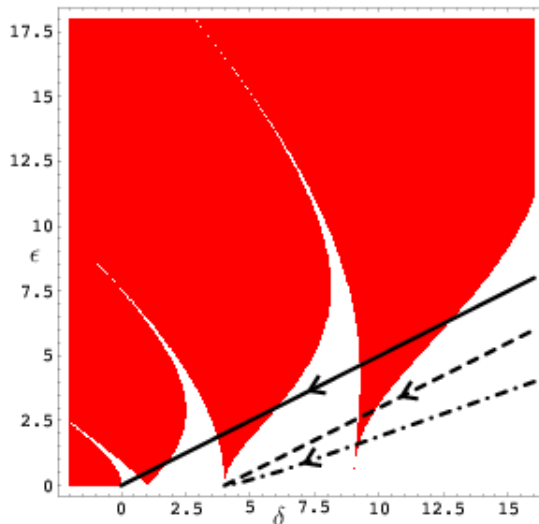


Figure 2.4: Instability diagram for solutions of the Mathieu equation in the δ - ϵ plane. In this diagram, shaded regions indicate resonant, or unstable, solutions of the Mathieu equation. Unshaded regions indicate stable solutions. We also show the evolution of the parameters in (2.50) for different comoving modes and fields: $k = 0, m_\chi = 0$ (continuous), $k = 0, m_\chi \neq 0$ (dashed) and $k \neq 0, m_\chi \neq 0$ (dot-dashed).

Since we have neglected the expansion of the universe, the parameters of the Mathieu equation are time-independent and a mode that lies within one of the instability bands therefore continues to grow indefinitely. Of course this unending particle production is simply a consequence of the approximation scheme.

When the expansion of the universe is included, the inflaton undergoes damped oscillations and the expansion of the universe redshifts all momenta. Both effects tend to decrease the efficiency of parametric resonance. Making the approximation $a \propto t^{2/3}$ and substituting into (2.42) and (2.41), the rescaled field $\tilde{\chi}_k \equiv \chi_k a^{3/2}$ then satisfies the Mathieu equation (2.47), but now with time-dependent parameters δ and ϵ

$$\delta = \left(\frac{k}{m_\phi a}\right)^2 + \left(\frac{m_\chi}{m_\phi}\right)^2 + 2\epsilon \quad \text{and} \quad \epsilon = \left(\frac{g\phi_e}{2m_\phi t}\right)^2. \quad (2.50)$$

Even though δ and ϵ are time-dependent, their values are nearly constant during the oscillating phase. For instance, the relative change in ϵ during an oscillation of ϕ is

$$\frac{1}{m_\phi} \frac{\dot{\epsilon}}{\epsilon} = -\frac{3H}{m_\phi}. \quad (2.51)$$

Hence, at late times, $t \approx H^{-1} \gg m_\phi^{-1}$, we can think of the parameters δ and ϵ as being (locally) constant. The same assumption of late times has been actually made in the derivation of (2.50).

The time-dependence in δ and ϵ will cause comoving modes to migrate in the δ - ϵ plane. Thus, when the expansion of the universe is taken into account, particle production in a given k -mode may take place for a brief time interval as this mode passes in and then out of an instability band. We also plot the trajectories of different modes in the δ - ϵ plane in figure 2.4. The longer a particular mode remains inside an instability band, the more efficient is the production of the corresponding particles. It is clear from the figure that parametric resonance is always more effective for longer wavelengths and lighter fields [46].

Other models with canonical couplings between the inflaton and matter can be similarly examined, but although the quantitative results differ, similar qualitative results emerge. What is less explored is whether models with non-canonical couplings between the inflaton and matter yield similar results. In the next section we examine such couplings.

2.7 Preheating in Models with Derivative Coupling

Most work on preheating has focused on models with direct, non-derivative, couplings to matter. Little is known about the strength of these couplings, but theoretical arguments suggest that they have to be rather weak. Indeed, in order for the inflaton to drive a phenomenologically acceptable stage of inflation, its potential has to be extremely “flat”. A variety of different ways to stabilize these flat potentials have been studied in single-field [47] and multiple-field inflationary models like hybrid inflation [48], but perhaps the most compelling idea that has emerged to date is that inflation is driven by a pseudo-Nambu-Goldstone boson [49]. In the simplest realization of this idea, the inflaton sector is invariant under an approximate global $U(1)$ symmetry that shifts the inflaton field by a constant. Because only a constant potential is invariant under shifts of the inflaton, this approximate symmetry guarantees that deviations from flatness are small. But at the same time, because direct couplings between the inflaton and matter violate the shift symmetry, they are also expected to be extremely weak, and perhaps even negligible. For this reason preheating via direct couplings in models with such approximate shift symmetries, as studied in [50], is not expected to be very efficient.

On the other hand, derivative couplings of the inflaton to matter do satisfy the shift symmetry, and so there is no reason for them to be particularly weak. It is therefore entirely possible that derivative couplings could be more important than non-derivative ones during reheating. Studies of preheating in models with derivative couplings [51, 52] have been less extensive than those of direct couplings, and therefore our aim here is to carry out one such study: examining preheating in these models and determining whether they lead to a qualitatively different picture of the end of inflation and the onset of reheating. This work appeared in [53], which I will now discuss.

Phenomenologically viable inflationary models require very “flat” potentials. A simple example is provided by our model with quadratic potential $V(\phi) = \frac{1}{2}m^2\phi^2$, in

which sufficient flatness implies that the mass of the field must be $m \approx 10^{-6}M_{\text{Pl}}$. If the inflaton did not couple to matter, this value would not pose any particular problem, as no quantum corrections (other than gravitational) could drive m to higher values. However, the inflaton must couple to matter for reheating to occur, and these couplings will generically be responsible for large quantum corrections.

To be more specific consider an inflationary model with bare Lagrangian given by (2.39). To lowest order in g^2 the effective mass of ϕ receives a correction given by the Feynman diagram in figure 2.5. The loop integral is quadratically divergent, so the corrected mass squared is

$$m^2 \approx m_\phi^2 + \frac{g^2\Lambda^2}{16\pi^2}, \quad (2.52)$$

where Λ is the ultraviolet cut-off of the theory, which is expected to be Planckian. There are hence two different ways to obtain $m \approx 10^{-6}M_{\text{Pl}}$: (i) The coupling of the inflaton to matter is strong, $g \approx 1$, and there has to be a cancellation between the bare mass and the quantum corrections of 1 part in 10^6 , or (ii) the inflaton is very light and it couples very weakly to matter. Case (i) is not technically natural and requires fine tuning. As we shall see, case (ii) is realized in models where the inflaton is a pseudo-Nambu-Goldstone boson. Incidentally, let us point out that if quantum corrections to the mass of the inflaton are to be small, $g^2\Lambda^2/8\pi^2 < m_\phi^2$, the bound in (2.45) has to be violated.

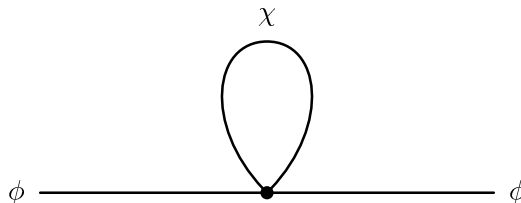


Figure 2.5: One-loop quantum correction to the mass of the inflaton. A quartic coupling between the inflaton ϕ and matter χ leads to a quadratically divergent mass.

Significant efforts have been devoted to develop inflationary models in which the

inflaton is naturally light [47]. Such models require additional symmetries, and perhaps the most promising candidates are those in which the inflaton is a pseudo-Nambu-Goldstone boson, the Goldstone boson of an approximate, spontaneously broken symmetry [49]. In the limit that the symmetry is exact, the Goldstone boson is massless, and the inflaton potential is exactly flat. Small symmetry breaking terms then give a correspondingly small mass to the inflaton, and the remaining approximate symmetry guarantees that quantum corrections remain small.¹

To begin our exploration of reheating in technically natural models of inflation, let us hence consider perhaps the simplest scalar field model with a Goldstone boson: a theory with a single complex field, invariant under a spontaneously broken (approximate) $U(1)$ symmetry $\Phi \rightarrow e^{i\phi}\Phi$,

$$\mathcal{L} = -(\partial_\mu\Phi)\partial^\mu\Phi^* - \lambda(F^2 - \Phi^*\Phi)^2 + \dots \quad (2.53)$$

where the dots denote couplings of Φ to singlets of the $U(1)$ symmetry, which will play no role in our analysis.

The $U(1)$ symmetry is spontaneously broken, because in the vacuum the field Φ has a non-vanishing expectation value, $\langle|\Phi|\rangle = F$. As we shall argue below, in order for the inflaton potential to be sufficiently flat, we need $F \approx M_{\text{Pl}}$. To study the excitations around the vacuum, we define

$$\Phi \rightarrow (F + \chi) \exp\left(i\frac{\phi}{F}\right), \quad (2.54)$$

where the Goldstone boson ϕ will play the role of the inflaton. Substituting this expression into (2.53) we find

$$\mathcal{L} = -(\partial_\mu\chi)\partial^\mu\chi - \left(1 + \frac{\chi}{F}\right)^2 (\partial_\mu\phi)\partial^\mu\phi - 4\lambda F^2\chi^2 \left(1 + \frac{\chi}{2F}\right)^2, \quad (2.55)$$

with the expected derivative couplings between the inflaton ϕ and the field χ . These couplings are model-independent, in the sense that they originate from the kinetic

¹Although, it has been suggested that quantum gravity effects, such as the creation of virtual black holes, explicitly break this symmetry [54].

term of the complex field Φ and the field redefinition (2.54), and are independent of any additional couplings of the field Φ to matter. Since the original $U(1)$ symmetry acts on the field ϕ as a shift by a constant, no term in the Lagrangian can contain an undifferentiated field ϕ . Therefore, ϕ is the Goldstone boson of the spontaneously broken $U(1)$, and is exactly massless so far. On the other hand, the field χ can be quite heavy, with mass $m_\chi^2 = 4\lambda F^2$.

For ϕ to be a viable inflaton, it is necessary to generate a potential for it. To this end, we introduce terms in the Lagrangian that explicitly break the $U(1)$ symmetry. Because the potential has to vanish in the limit of exact symmetry, these terms will generically lead to an inflaton potential of the form

$$V(\phi) \approx \mu^4 \left[1 - \cos\left(\frac{\phi}{F}\right) \right], \quad (2.56)$$

where μ is a parameter with dimensions of mass that characterizes the strength of the symmetry breaking terms. It is easy to verify that the potential (2.56) satisfies the slow-roll conditions only for $F \gtrsim M_{\text{Pl}}$. It is unclear whether we can trust an effective field theory description with $F \gg M_{\text{Pl}}$, so we shall implicitly assume $F \approx M_P$. Note that the potential has to be periodic, since ϕ/F is a phase. However, for $\phi/F < 1$, we can assume that the potential is quadratic, with squared mass $m_\phi^2 = \mu^4/F^2$, which is the form we shall consider in the following. We shall similarly neglect self-interactions of the field χ , because they are also suppressed by the scale $F \approx M_P$.

Taking all this into account, canonically normalizing both scalars, and re-scaling F by $F \rightarrow F/\sqrt{2}$, the Lagrangian (2.55) finally becomes

$$\begin{aligned} \mathcal{L} = & -\frac{1}{2}(\partial_\mu\phi)\partial^\mu\phi - \frac{1}{2}(\partial_\mu\chi)\partial^\mu\chi - \frac{1}{2}m_\phi^2\phi^2 - \frac{1}{2}m_\chi^2\chi^2 - \\ & - \frac{\chi}{F} \left(1 + \frac{\chi}{F} \right) (\partial_\mu\phi)(\partial^\mu\phi). \end{aligned} \quad (2.57)$$

2.7.1 Preheating into Derivatively-Coupled Scalars

We now wish to examine the extent to which parametric resonance may occur in models with derivative couplings, such as (2.57). Varying the action (2.57) with

respect to ϕ and χ respectively, we obtain the equations of motion

$$\begin{aligned} \left[1 - \frac{\chi}{F}\right]^2 \nabla_\mu \nabla^\mu \phi &= \frac{2}{F} \left(1 + \frac{\chi}{F}\right) (\partial_\mu \phi) \partial^\mu \chi + m_\phi^2 \phi, \\ \nabla_\mu \nabla^\mu \chi &= 2 \frac{\chi}{F^2} (\partial_\mu \phi) \partial^\mu \phi + m_\chi^2 \chi + \frac{1}{F} (\partial_\mu \phi) \partial^\mu \phi. \end{aligned} \quad (2.58)$$

Because the inflaton field is homogeneous, the equation of motion for the zero mode of the field χ differs from the equation of motion for the non-zero modes. Expanding equation (2.58) in discrete Fourier modes, we first consider the zero mode χ_0 , obeying

$$\ddot{\chi}_0 + 3H\dot{\chi}_0 + \left[m_\chi^2 - \frac{2}{F^2} \dot{\phi}^2 \right] \chi_0 = \frac{\dot{\phi}^2}{F}, \quad (2.59)$$

which is the equation of motion of a (damped) harmonic oscillator driven by $\dot{\phi}^2/F$. To see how the zero mode responds to the driving term, in the absence of parametric resonance, we need to decouple the two effects. To do this let us first neglect the term $\dot{\phi}^2/F^2$ in the square brackets of (2.59), during the initial stages of reheating, when χ_0 is small. In this case, the solution can be written

$$\chi_0 \approx \frac{\phi_e^2 m_\phi^2}{2F m_\chi^2} [1 - \cos(m_\chi t)] + \frac{\phi_e^2 m_\phi^2}{2F(4m_\phi^2 - m_\chi^2)} [\cos(m_\chi t) - \cos(2m_\phi t)], \quad (2.60)$$

where we have neglected the expansion of the universe and assumed that inflation ends at $t = 0$. It is worth pointing out that the apparent divergence from the denominator of the second term is an artificial consequence of neglecting the expansion of the universe.

Clearly, the inflaton displaces the zero mode of the field from $\chi_0 = 0$ to potentially large amplitudes. In order to estimate how far χ is driven, it suffices to consider the limit $m_\chi \lesssim m_\phi$, which leads to the largest displacement. Evaluating equation (2.60) in this limit at time $t = m_\phi^{-1}$, the characteristic timescale for the evolution of the inflaton, we find $\chi_0 \approx \phi_e^2/2F$. Although this amplitude is sizable, of the order of the Planck mass, we cannot argue that preheating is successful, because excitations of the zero mode cannot be interpreted as radiation. However, if stable, the field χ could play the role of dark matter.

We are mostly interested in the production of actual radiation, so let us now turn our attention to the non-zero modes. Equation (2.58) yields

$$\ddot{\chi}_k + 3H\dot{\chi}_k + \left[\left(\frac{k}{a} \right)^2 + m_\chi^2 - \frac{2}{F^2} \dot{\phi}^2 \right] \chi_k = 0, \quad (2.61)$$

for $k \neq 0$. Note that this would also be the mode equation arising from the Lagrangian (2.57), without the coupling linear in χ . The form of this equation also hints that inflation and preheating in derivatively coupled models may be qualitatively different from the canonical case considered above. This is because the field χ has an effective squared mass given by

$$m_{\text{eff}}^2 = m_\chi^2 - \frac{2}{F^2} \dot{\phi}^2. \quad (2.62)$$

Although $\dot{\phi}^2/F^2$ is small during slow-roll inflation, the correction term becomes large when the inflaton leaves the slow-roll regime. Therefore, for sufficiently small values of m_χ , the effective mass of the field χ may become tachyonic. Obviously, such an instability is absent as long as the effective mass is positive,

$$m_\chi \gtrsim \frac{\sqrt{2}m_\phi M_{\text{Pl}}}{F}. \quad (2.63)$$

Interestingly, this bound is very similar to the requirement that the mass of χ be larger than the Hubble scale during inflation. In fact, since $F \approx M_{\text{Pl}}$, the bound (2.63) simply reads $m_\chi \gtrsim m_\phi$. During slow-roll $H \approx \phi m_\phi / M_{\text{Pl}}$, and because ϕ is of order M_{Pl} during the period of inflation accessible to present observations, (2.63) also follows from requiring $m_\chi > H$. It turns out that the tachyonic instability associated with the violation of the bound (2.63) is harmless, and it is just the production of long-wavelength fluctuations of the field χ that renders light scalar fields undesirable. Tachyonic preheating has been studied in [55].

To further study parametric resonance in this class of models, it is instructive to recast (2.61) into the form of the Mathieu equation. Including the expansion of the universe but neglecting back-reaction from χ , we find that the rescaled variable

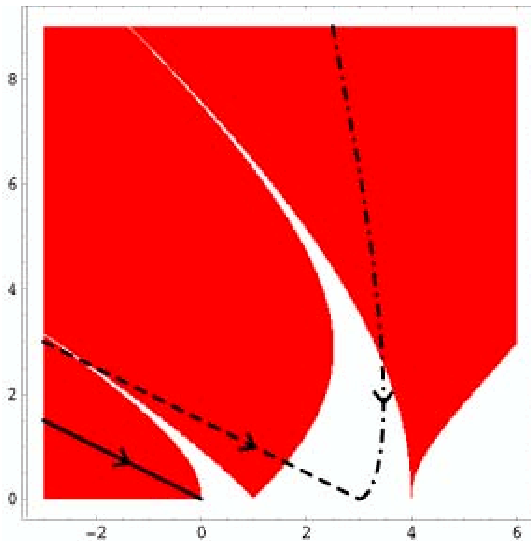


Figure 2.6: Instability diagram for solutions of the Mathieu equation in the δ - ϵ plane. We superimpose the evolution of the parameters in equation (2.64) for different comoving modes and fields: $k = 0, m_\chi = 0$ (continuous), $k = 0, m_\chi \neq 0$ (dashed) and $k \neq 0, m_\chi \neq 0$ (dot-dashed).

$\tilde{\chi}_k \equiv \chi_k a^{3/2}$ satisfies the Mathieu equation (2.47), with

$$\delta = \left(\frac{k}{m_\phi a} \right)^2 + \left(\frac{m_\chi}{m_\phi} \right)^2 - 2\epsilon \quad \text{and} \quad \epsilon = \frac{1}{2} \left(\frac{\phi_e}{Ft} \right)^2. \quad (2.64)$$

The diagram in figure 2.6 shows different trajectories of a mode in the δ - ϵ plane. It is again apparent from the figure that for a given initial value of ϵ preheating is in general more efficient for longer wavelength modes and lighter fields. A crucial property of derivatively coupled models is that ϵ is at most of order one, because $\phi_e \approx M_{\text{Pl}} \approx F$. Hence, any resonance proceeds close to the end of the instability bands, and is clearly ineffective if fields are heavy, $m_\chi \gg m_\phi$ ($\delta \gg 1$). On the other hand, if condition (2.63) is violated, long-wavelength modes will remain inside the instability band as long as the effective mass is negative, which could lead to a significant growth of the homogeneous component of χ .

In order to estimate the efficiency of preheating in the tachyonic regime, let us consider the evolution of a long-wavelength mode $k \approx 0$ mode when the scalar χ is

light, $m_\chi \ll m_\phi$. As we argued above, this is the case where parametric resonance is strongest. After the end of inflation, the mode $k \approx 0$ finds itself in the instability band at $\delta < 0$. To lowest order in ϵ , the characteristic exponent is simply $\mu = \sqrt{-\delta}$. Hence, for adiabatic changes in μ , we expect the solutions to grow as $\exp(\int \mu m_\phi dt)$. However, this is only a good approximation if $\phi_e/F \gg 1$. Indeed the adiabaticity parameter is

$$\frac{\dot{\mu}}{\mu^2} = -\frac{F}{\phi_e}, \quad (2.65)$$

which is of order one instead. Therefore, we shall solve (2.47) directly by approximating

$$\delta = -\left(\frac{\phi_e}{Ft}\right)^2, \quad \epsilon = 0. \quad (2.66)$$

The solution is a linear combination of powers in t . Keeping the growing mode, and returning to the original variable, we find

$$\chi \approx \chi_e \left(\frac{t}{t_e}\right)^p, \quad \text{where } p = -\frac{1}{2} + \sqrt{\frac{1}{4} + \frac{\phi_e^2}{F^2}}, \quad (2.67)$$

and χ_e denotes the value of χ at the end of inflation. Clearly, as seen in figure (2.7), for $\phi_e/F \approx 1$ this amplification is very modest. Hence, parametric resonance is rather ineffective for derivatively coupled scalar fields, no matter whether heavy or light.

2.7.2 Preheating into Gauge Fields

Our analysis so far indicates that in models of inflation in which large quantum corrections are suppressed by a symmetry, the population of the universe with relativistic particles faces several challenges. First, if matter fields are heavier than the inflaton, parametric resonance is absent, and the inflaton cannot decay perturbatively into matter for kinematical reasons. And second, if matter fields are lighter than the inflaton, the perturbative decay is kinematically allowed, even though parametric resonance is inefficient, but then long-wavelength fluctuations of matter are produced during inflation. These conclusions crucially hinge on the assumption that matter

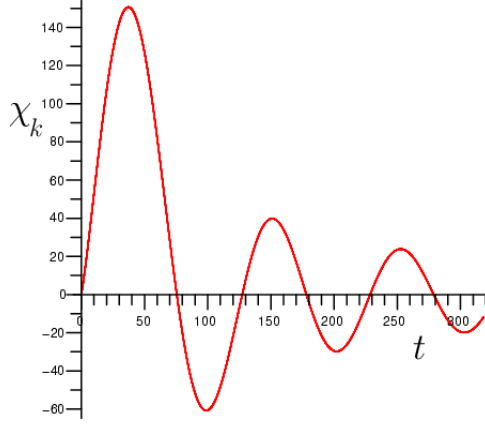


Figure 2.7: The zero mode of χ for $m_\chi = 10^{-2}m_\phi$. During the initial stages, the effective mass is tachyonic, and the mode grows as it remains in the stability band at $\delta < 0$. Once the mode exits the tachyonic regime, the mode function decays. Note that long-wavelength excitations do not admit a particle interpretation.

fields can be represented by minimally coupled scalar fields, which, of course, is not necessarily the case.

There are just two other types of matter fields the inflaton can couple to: fermions (spin 1/2 and 3/2) and vectors (spin 1). Reheating into fermions is not very effective because of the exclusion principle [56], leaving vector fields as the only remaining alternative. These are particularly appealing as decay products of the inflaton for two reasons: their masses are protected by gauge symmetries, so they are naturally light, and the conformal nature of their couplings to gravity prevents the production of long-wavelength fluctuations of these fields during inflation.

Consider therefore an effective theory in which a light pseudo-scalar ϕ (the inflaton) couples derivatively to a $U(1)$ gauge field A_μ (matter),

$$\mathcal{L} = -\frac{1}{2}(\partial_\mu\phi)\partial^\mu\phi - \frac{1}{2}m_\phi^2\phi^2 - \frac{1}{4}A^{\mu\nu}A_{\mu\nu} - \frac{\phi}{4F}\tilde{A}^{\mu\nu}A_{\mu\nu}. \quad (2.68)$$

Here $A_{\mu\nu} = \partial_\mu A_\nu - \partial_\nu A_\mu$ is the field strength of the gauge fields, $\tilde{A}_{\mu\nu} \equiv \varepsilon^{\mu\nu\rho\sigma}A_{\rho\sigma}/2$ is its dual tensor, and F is a symmetry breaking scale, with dimensions of mass. Despite appearances, the field ϕ couples derivatively to the gauge field, because $\tilde{A}_{\mu\nu}A^{\mu\nu}$ is a

total derivative. Effective theories of this type appear in axion-like models [57], in which the coupling of the scalar to the electromagnetic field arises from the triangle anomaly. This sort of coupling between a pseudoscalar and electromagnetism has been suggested as a mechanism to generate primordial magnetic fields in the early universe [58], although a detailed study of coherent magnetic field production during inflation and the subsequent reheating stage has concluded that this generation is not sufficiently strong on the required scales [59].

To analyze the dynamics of reheating in this model, we choose to work in the transverse gauge (where $\partial_i A^i = 0$ and $A^0 = 0$). In this gauge, the equations of motion for the inflaton and the non-vanishing components of A_μ are

$$\nabla_\mu \nabla^\mu \phi = m_\phi^2 \phi + \frac{1}{a^4 F} \epsilon^{ijk} \dot{A}_i \partial_j A_k \quad (2.69)$$

$$\eta^{\mu\nu} \delta^{ij} \partial_\mu A_{\nu j} = \frac{1}{F} \epsilon^{ijk} [\dot{\phi} \partial_j A_k - (\partial_j \phi) \dot{A}_k]. \quad (2.70)$$

We expand A_i in terms of mode functions:

$$\mathbf{A}(\mathbf{x}, t) = \int \frac{d^3 k}{(2\pi)^{3/2}} \sum_{r=\pm} \mathbf{e}_r(\mathbf{k}) A_r(\mathbf{k}, t) e^{i\mathbf{k}\cdot\mathbf{x}}, \quad (2.71)$$

where $\omega_k = |\mathbf{k}| \equiv k$ is the dispersion relation of the photons, and $\mathbf{e}_r(\mathbf{k})$ are circular polarization vectors, obeying $\mathbf{k} \times \mathbf{e}_\pm = \mp i k \mathbf{e}_\pm$. Substituting this expansion into (2.70) yields the decoupled mode equations

$$\ddot{A}_\pm + H \dot{A}_\pm + \left[\left(\frac{k}{a} \right)^2 \mp \frac{k \dot{\phi}}{a F} \right] A_\pm = 0. \quad (2.72)$$

As was the case in the previously considered models, (2.72) exhibits parametric resonance for certain values of k and F^{-1} , which can be interpreted as explosive particle production (e.g., photon production). This can be seen analytically in the regime where back-reaction is neglected by putting (2.72) into the form of the Mathieu equation (2.47). The rescaled field variable,

$$\tilde{A}_\pm \equiv A_\pm a^{1/2} \quad (2.73)$$

satisfies the Mathieu equation (2.47) with parameters

$$\delta = \left(\frac{2k}{m_\phi a} \right)^2 + \frac{2}{9t^2}, \quad \text{and} \quad \epsilon = \pm \frac{k}{m_\phi a} \frac{1}{t} \frac{\phi_e}{F}, \quad (2.74)$$

where we have introduced the dimensionless time variable $t \rightarrow 2m_\phi^{-1}t$.

There is, however, a significant difference that distinguishes couplings to gauge fields from those to scalar fields. Whereas for the latter the value of ϵ is constant in a non-expanding universe, for the former it is proportional to the energy of the photons. Hence, ϵ can become very large. Since the effective theory we are using breaks down at physical momentum $k/a \approx F$, we find that at the end of inflation ϵ can be as large as $\phi_e/m_\phi \approx 10^6$. However, this does not necessarily imply that parametric resonance is very effective. In figure 2.8 we show the trajectories of different modes in the δ - ϵ plane for different values of k and $\phi_e/F = 1$. As seen in the figure, although a mode can cross several instability bands, it does so in the narrow band regime, close to the tips of the instability bands, mainly because ϵ rapidly decays as time evolves.

In order to estimate the efficiency of preheating in this regime, let us estimate how long a mode remains in the first instability band (the one whose tip touches $\epsilon = 0$, $\delta = 1$), and how much its mode function grows during that time. For small ϵ , the characteristic exponent along the first band is

$$\mu = \frac{1}{2} \sqrt{\epsilon^2 - (\delta - 1)^2}. \quad (2.75)$$

Hence, its boundary is $|\delta - 1| = \epsilon$, along which $\mu = 0$. Let us write the time at which a mode enters and leaves the band as $t_1 \mp \Delta t$, where t_1 is the time at which the mode crosses the center of the band, at $\delta = 1$. Using (2.74), and neglecting the factor $2/9t^2$, we find

$$t_1 \approx t_e \left(\frac{2k}{m_\phi a_e} \right)^{3/2}, \quad \Delta t \approx \frac{3}{8} \frac{\phi_e}{F}, \quad (2.76)$$

where $t_e \approx 1$ is the time at the end of inflation, and a_e denotes the value of the scale factor at that time.

We shall now estimate what is the growth of the mode function during that time. Inside the band, we may neglect the term $(\delta - 1)^2$ in (2.75), so that $\mu \approx \epsilon_1/2$, where

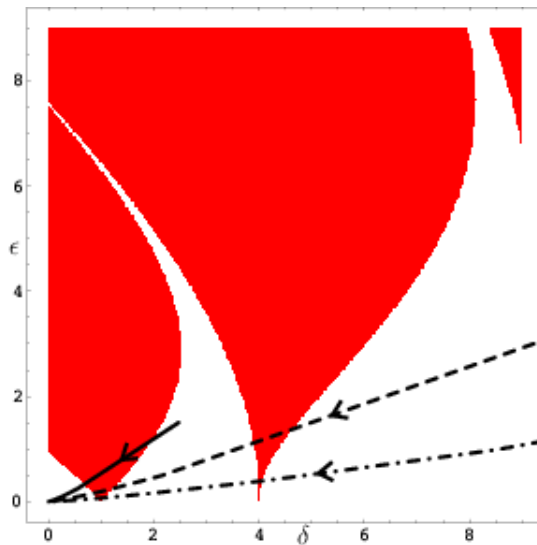


Figure 2.8: Instability diagram for solutions of the Mathieu equation in the δ - ϵ plane. The trajectories follow the evolution of the parameters in (2.74) starting at the end of inflation. The corresponding values of $k_e \equiv k/(m_\phi a_e)$ are $k_e = 3/4$ (continuous), $k_e = 3/2$ (dashed) and $k_e = 3$ (dot-dashed). In all cases $\phi_e/F = 1$.

ϵ_1 is the value of ϵ at time t_1 . Hence, we find that \tilde{A}_+ grows by a factor

$$\exp(\epsilon_1 \cdot \Delta t) \approx \exp \left[\frac{3}{16t_e} \frac{\phi_e^2}{F^2} \left(\frac{m_\phi a_e}{2k} \right)^{3/2} \right], \quad (2.77)$$

while the growth in A_+ is suppressed by an additional factor $(t_e/t)^{1/3}$. Note that the above expression is strictly valid only for $\Delta t \ll t_1$, and provided the change in $\mu = \epsilon/2$ at time t_1 is adiabatic,

$$\left. \frac{\dot{\mu}}{\mu^2} \right|_{t_1} \approx -\frac{20}{3} \frac{F}{\phi_e} \ll 1. \quad (2.78)$$

Hence (2.77) implies that preheating into gauge fields is very effective for $\phi_e/F \gg 1$. However, this is not the regime that applies in technically natural models of inflation, where ϕ_e/F is of order one (a small number for our purposes). In order to estimate the growth in the opposite regime, we shall set $\epsilon \propto \phi_e/F \rightarrow 0$. In that case,

the solution of the Mathieu equation has the growing mode

$$\tilde{A}_+ \propto t^{1/3} \cos\left(\frac{6k t_e^{2/3}}{m_\phi a_e} t^{1/3} + \varphi\right), \quad (2.79)$$

which implies that the original variable A_+ oscillates with constant amplitude. Therefore, there is no parametric resonance in the decay of the inflaton into gauge fields. As before, the lack of parametric resonance is due to the modest value of ϕ_e/F , which is a reflection of the weak couplings between the inflaton and matter. Numerical investigation including the effects of expansion confirms this.

2.8 Conclusions

It is obviously necessary to repopulate the universe with matter after a period of early universe inflation. The detailed process through which this takes place can be of great significance since, although a thermally equilibrated bath ultimately results, non-equilibrium relics from preheating can have important cosmological consequences, even if the ultimate reheat temperature of the universe is below the mass scale of any relics of interest.

The possible implications of preheating include the overclosure of the universe through the production of monopoles, moduli or gravitinos, and new possibilities for the generation of the baryon asymmetry of the universe, either at the Grand Unified (GUT) [60, 61] or electroweak [62–65] scale. It is therefore important to examine the different ways in which parametric resonance may take place in inflationary models.

Because phenomenologically viable inflation requires extremely flat potentials, models in which the couplings of the inflaton to itself and to other fields are naturally suppressed are particularly attractive. One way to achieve this is to construct the inflaton as a pseudo-Nambu-Goldstone boson of a spontaneously broken $U(1)$ symmetry—*natural inflation*. The $U(1)$ symmetry is then realized as a shift symmetry on the inflaton field, and explicit soft breaking terms render this symmetry

approximate, and generate an approximately flat potential for the inflaton. A consequence of the residual approximate symmetry is that direct couplings of the inflaton to matter fields are correspondingly suppressed, leading to the interesting possibility that derivative couplings, unconstrained by a shift symmetry, may be the dominant type of coupling to matter.

In this chapter, we have used analytic and numerical techniques to study reheating in models in which derivative couplings between the inflaton and matter fields are expected to play the dominant role—such as in natural inflation. We have seen that successful reheating places non-trivial constraints on these models and confronts them with several challenges. In particular, for heavy scalar fields ($m_\chi \gg m_\phi$) parametric resonance is ineffective in producing matter particles, and the perturbative decay is forbidden on kinematic grounds. For light scalars ($m_\chi \ll m_\phi$) there are novel long-wavelength instabilities that cause the zero mode of matter to grow, but in this case these excitations do not correspond to relativistic particles, and the production of fluctuations of matter during inflation leads to several cosmological problems. We note that we have not addressed any mechanism to keep matter fields light, which could lead to further constraints.

Some of these problems are avoided when the inflaton couples derivatively to gauge fields, as in axion-like models. Because of the gauge symmetry, these vector fields are automatically light, thus allowing the perturbative decay of the inflaton. At the same time, the conformal nature of their couplings to gravity circumvents all the problems associated with the presence of light scalars during inflation. Nevertheless, we have found that parametric resonance is absent for the values of parameters implied by technically natural inflationary models. As for couplings to scalars, the origin of this absence is the weakness of the coupling of the inflaton to matter, which is characterized by the ratio of the inflaton at the end of inflation to the spontaneous breaking scale, and is hence of order one at most.

Chapter 3

Brief Interlude: Is the Universe Really Accelerating?

In Chapter 2 we saw that a stage of accelerated expansion in the early universe could solve problems with the HBB cosmology. At the turn of the century, evidence emerged that strongly suggested that universe is currently accelerating. Many approaches have emerged in hopes of explaining the cause of this late-time acceleration. One possibility is that a scalar field is driving the accelerated expansion, just as in the case of inflation. Another possibility is that we need to modify our theory of gravity, as given by GR. Still other attempts have been made to explain away the need for acceleration all together. In this chapter I will discuss one such attempt and some possible ways to test such a proposal.

3.1 LTB Cosmology

Homogeneity and isotropy are the cornerstones of the standard cosmological model, providing not only a tremendous simplification of General Relativity, but remarkable agreement with all observations. Homogeneity is supported by the observed galaxy distribution from large-scale structure surveys, while isotropy is supported by,

in particular, the remarkable uniformity of the average temperature of the cosmic microwave background radiation (CMB). Nevertheless, the paradigm-changing observation of cosmic acceleration, now more than a decade old, has forced cosmologists to re-examine even their most cherished assumptions, including the correctness of General Relativity, a vanishing cosmological constant, and, more recently, homogeneity and isotropy.

The primary evidence for the accelerating universe comes from the unexpected dimming of type Ia supernovae [66–73], as measured through their light curves. The connection to cosmic acceleration requires the assumptions of homogeneity and isotropy, and thus this raises the possibility that abandoning one of these principles may allow for the appearance of accelerated expansion without actual acceleration itself.

Of course, the usual cosmological Friedmann-Robertson-Walker (FRW) metric is so simple by virtue of its underlying symmetries. Abandoning these leads to a correspondingly more complicated metric. It is convenient therefore to begin by studying toy models. One class of these that has shown some promise in this direction are the *Lemaitre-Tolman-Bondi* (LTB) metrics, in which we are assumed to live inside a spherically symmetric underdense region of space-time (or “void”) embedded in an otherwise spatially flat and homogeneous Einstein-de Sitter universe [74–80], illustrated in Fig. 3.1. The LTB metric is given by [81–83]

$$ds^2 = -dt^2 + \frac{|R'(t, r)|^2}{1 + \beta(r)} dr^2 + R^2(t, r) d\Omega^2 , \quad (3.1)$$

where $R(t, r)$ is a position-dependent scale factor, $\beta(r)$ is related to the curvature of the spatial slices, and $()' \equiv \partial/\partial r$. The Einstein equations relate $R(t, r)$ to $\beta(r)$ and an additional arbitrary function of integration $\alpha(r)$. Specifying $\alpha(r)$, $\beta(r)$, and an initial condition for $R(t, r)$ completely determines the space-time. In models with an underdense region, or “void”, surrounded by an overdense region, $\alpha(r)$ and $\beta(r)$ roughly correspond to the width of the void and the gradient of the boundary between the inner and outer regions, respectively, and will be specified below. Such a space-

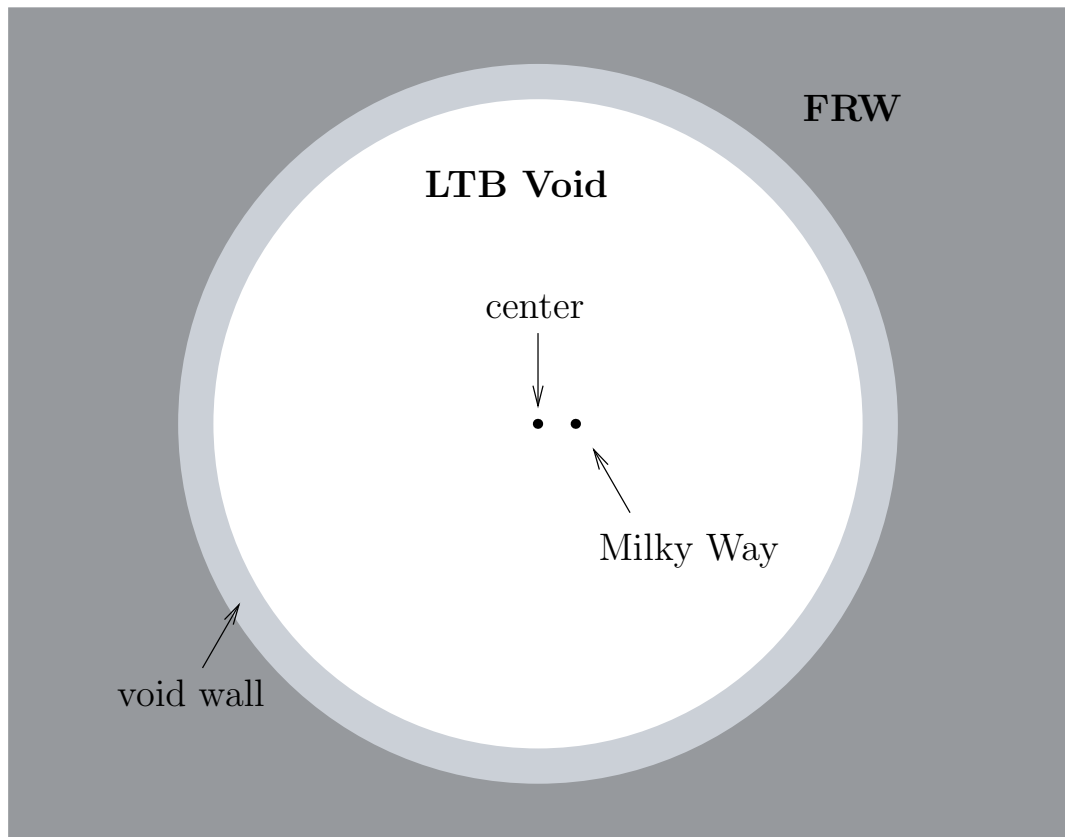


Figure 3.1: In LTB void models our galaxy is located near the center of an underdense region of space-time (void) which is matched to an FRW region outside the void.

time is manifestly inhomogeneous, due to the void, and on its own violates any strong version of the Copernican principle, since we must live inside this void in order to account for the observed supernovae dimming. Nevertheless, it has been shown that these models can provide a satisfactory fit to the luminosity distance-redshift relation of type Ia supernovae and the position of the first peak in the CMB [78, 84]. Thus, LTB models have been suggested as a possible solution to the problem of cosmic acceleration, obviating the need for quintessence fields, modifications of gravity, or a cosmological constant, and considerable effort has been devoted to constraining them [85–89].

3.2 Cosmic Parallax in an LTB Void

The LTB metric describes a region of space-time that is isotropic about the origin but inhomogeneous with respect to the radial direction. Therefore distant galaxies appear to be receding at the same rate in all directions for observers located at the origin. On the other hand, observers located away from the center of the void could in principle observe anisotropic recession. One way to observe this effect [90] is to measure how the angle between the positions of two distant sources evolves over time. This difference is referred to as the cosmic parallax.

The expansion of an FRW universe is isotropic for all observers, and so cosmic parallax would not be observed. Of course although our universe is very close to an FRW universe, it is not exactly so—for example, on large scales bound structures may acquire small peculiar velocities, giving rise to a slight deviation from observed isotropic expansion. However, to any observer living off-center inside the void of an LTB universe, cosmic evolution itself is anisotropic and is an additional source of cosmic parallax. For sufficiently off-center observers the cosmic parallax due to anisotropic expansion would dominate over the contribution from peculiar velocities. Cosmic parallax could therefore provide an interesting test of void models. Upcoming sky surveys such as GAIA [91] may be able to initiate a measurement of this effect, requiring only that a similar survey be completed 10 years later in order to complete the measurement. The absence of cosmic parallax beyond what is expected from peculiar velocities would put an upper bound on how far our galaxy could be from the center of the void in otherwise allowed LTB models. For example, the authors of [90] argue that GAIA may map sufficiently many quasars, with enough accuracy, so that two such surveys spaced 10 years apart could detect the additional LTB contribution to cosmic parallax if the Milky Way is more than 10 megaparsecs from the center of a 1 Gpc void. If after a decade no additional contribution were found, that would constrain the Milky Way to lie unnaturally close to the center of such a void.

To study cosmic parallax, one considers null geodesics in an LTB universe, obeying

$$\frac{d^2 x^\mu}{d\lambda^2} + \Gamma^\mu_{\rho\sigma} \frac{dx^\rho}{d\lambda} \frac{dx^\sigma}{d\lambda} = 0 . \quad (3.2)$$

Here $\Gamma^\mu_{\rho\sigma}$ are the Christoffel symbols, λ is an affine parameter along null geodesics, and the four-velocities $u^\mu \equiv \frac{dx^\mu}{d\lambda}$ satisfy $u^\mu u_\mu = 0$. The goal will be to solve these equations to determine the null geodesics along which light travels from various sources to an observer, and to do this for two different observation times.

Following [90], we work in spherical-polar coordinates (t, r, θ, ϕ) for which the origin coincides with the center of the void (labeled “O” in figure 3.2). Without

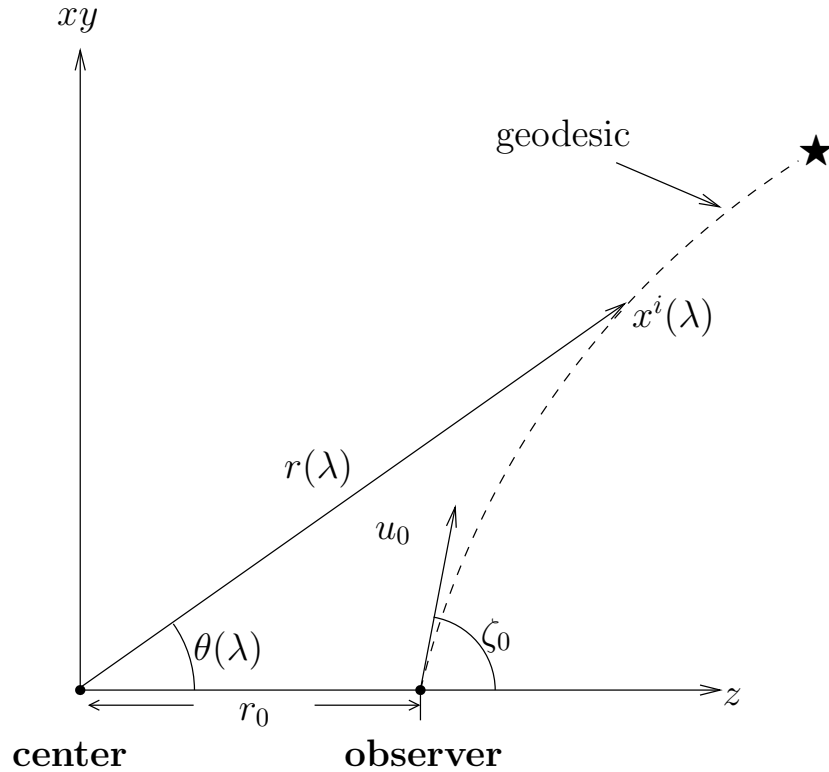


Figure 3.2: In the LTB model the observer is located at a distance r_0 from the center of the void along the axis of symmetry. Each point along the geodesic is described by the spatial coordinates $(\theta(\lambda), r(\lambda))$ or equivalently by $x^i(\lambda)$

loss of generality we choose the observer to lie on the polar axis at a coordinate

distance r_0 along it. Spherical symmetry about the observer is now broken but the remaining cylindrical symmetry applied to (3.2) allows us to neglect the polar angle ϕ dependence. The system then reduces to three second-order geodesic equations, or equivalently six first-order equations. Applying the null geodesic condition further reduces the system to five independent first-order equations for t , r , θ , $p \equiv dr/d\lambda$ and the redshift z as [85, 90]

$$\frac{dt}{d\lambda} = -\sqrt{\frac{(R')^2}{1+\beta}p^2 + \frac{J^2}{R^2}} \quad (3.3)$$

$$\frac{dr}{d\lambda} = p \quad (3.4)$$

$$\frac{d\theta}{d\lambda} = \frac{J}{R^2} \quad (3.5)$$

$$\frac{dz}{d\lambda} = \frac{(1+z)}{\sqrt{\frac{(R')^2}{1+\beta}p^2 + \frac{J^2}{R^2}}} \left[\frac{R'\dot{R}'}{1+\beta}p^2 + \frac{\dot{R}}{R^3}J^2 \right] \quad (3.6)$$

$$\frac{dp}{d\lambda} = 2\dot{R}'p\sqrt{\frac{p^2}{1+\beta} + \left(\frac{J}{RR'}\right)^2} + \frac{1+\beta}{R^3R'}J^2 + \left(\frac{\beta'}{2+2\beta} - \frac{R''}{R'}\right)p^2, \quad (3.7)$$

where $J \equiv R^2 d\theta/d\lambda = J_0$, is constant along the geodesic.

To completely specify the system we require five initial conditions, which we provide for convenience at the initial observation event, and denote with a subscript “0”. Since one would like to specify initial conditions in terms of physically measurable quantities, we consider the angle ξ_0 between the polar axis and the line of sight along an incoming photon trajectory arriving at the observer (see figure 3.2). This angle ξ_0 coincides with the coordinate angle θ when $r_0 = 0$, but in general it is given by [85]

$$\cos \xi_0 = -\frac{R'(t, r)p}{\frac{dt}{d\lambda}\sqrt{1+\beta(r)}}. \quad (3.8)$$

This expression can be used to express J_0 and p_0 in terms of t_0 , r_0 , and ξ_0 , via

$$\begin{aligned} J_0 &= R(t_0, r_0) \sin \xi_0 \\ p_0 &= \frac{\cos \xi_0}{R'(t_0, r_0)} \sqrt{1+\beta(r_0)}. \end{aligned} \quad (3.9)$$

Therefore, the system is completely determined by specifying t_0 , r_0 , θ_0 , z_0 , and ξ_0 .

Clearly, our coordinate choice means that $\theta_0 = 0$, and our conventional definition of redshift yields $z_0 = 0$. Following [90] we choose $r_0 = 15\text{Mpc}$, which is the largest value consistent with the CMB dipole [85]. What remains is to specify a direction on the sky and the time of observation to uniquely determine a geodesic that terminates at the space-time event of observation. This picks out an initial geodesic along which light from a distant source travels to reach the observer.

Given the redshift and line of sight angle of a source at an initial time, we can determine the trajectory of light from that source at a later time in the following way. As just mentioned, the line of sight angle ξ_0 picks out an initial geodesic, terminating at the initial observation event. The observed redshift determines how far backwards in time along this initial geodesic the source lies. We extract the comoving coordinates of the source by numerically integrating backwards along this initial geodesic. Once the comoving coordinates of the observer and source are determined, and the interval of time between observations is specified, we solve a boundary-value problem to determine the final geodesic. We then extract the line of sight angle of this final geodesic ξ_f .

After repeating this procedure for two sources we have four angles: the input angles ξ_{a0} and ξ_{b0} and the output angles ξ_{af} and ξ_{bf} , as shown in Fig. 3.3. We may then compute the difference

$$\Delta\gamma \equiv \gamma_f - \gamma_0 = (\xi_{af} - \xi_{bf}) - (\xi_{a0} - \xi_{b0}) , \quad (3.10)$$

which is the main quantity of interest, hereafter referred to as the cosmic parallax.

In [90] this quantity is calculated for LTB models characterized by the functions

$$\beta(r) = (H_0^{\text{OUT}})^2 r^2 \frac{\Delta\alpha}{2} \left(1 - \tanh \frac{r - r_{\text{vo}}}{2\Delta r} \right) \quad (3.11)$$

$$\alpha(r) = (H_0^{\text{OUT}})^2 r^3 - r\beta(r) , \quad (3.12)$$

which characterize the smooth transition from the inner underdense region to the outer, higher density region. The quantities $\Delta\alpha$, r_{vo} , Δr , and H_0^{OUT} are free parameters of the model that can be tuned to fit CMB and supernovae measurements.

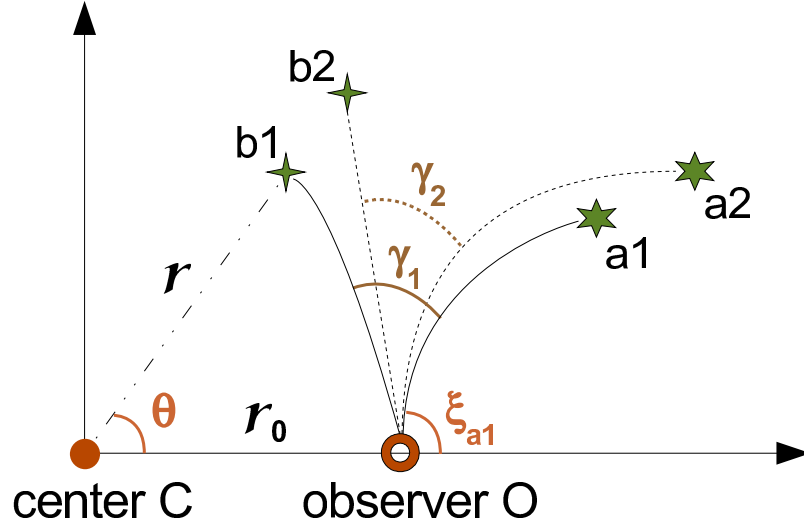


Figure 3.3: Overview of the four geodesics of interest: two geodesics at an earlier time and two geodesics at a later time. Figure appears in [90].

Following [90] and [78], we choose a model which is in good agreement with SNIa observations and the location of the first peak of the CMB, namely $\Delta\alpha = 0.9$, $r_{\text{vo}} = 1.3 \text{ Gpc}$, $\Delta r = 0.4 r_{\text{vo}}$, and $H_0^{\text{OUT}} = 51 \text{ km s}^{-1} \text{ Mpc}^{-1}$. Although this Hubble parameter outside the void seems to be in conflict with the measured Hubble Key project value of $72 \pm 8 \text{ km s}^{-1} \text{ Mpc}^{-1}$ [1], one should keep in mind that the measurements made to determine this value are all made at less than a few hundred megaparsec ($z \approx 0.1$), whereas the size of the void in this model is about 1 Gpc ($z \approx 0.2$). The Hubble parameter inside the void in this model turns out to be $65 \text{ km s}^{-1} \text{ Mpc}^{-1}$, which is consistent with the Hubble Key project value. Recently the SHOES Team [2] was able to reduce the uncertainty on the value of the Hubble parameter to $H_0 = 74.2 \pm 3.6 \text{ km s}^{-1} \text{ Mpc}^{-1}$, raising more doubts about the validity of this model.

The authors of [90] numerically compute the cosmic parallax for two different models. They find an angle-dependent signal with maximal value roughly $0.18 \mu\text{as}$ (micro arcseconds) for sources at redshift of 1, shown in Fig. 3.4. It is claimed that

this signal is within reach of the forthcoming Gaia mission, provided Gaia produces a sky map of the expected number of quasars (roughly 500,000) with final positional error less than $30 \mu\text{as}$, and that such measurements are repeated after 10 years.

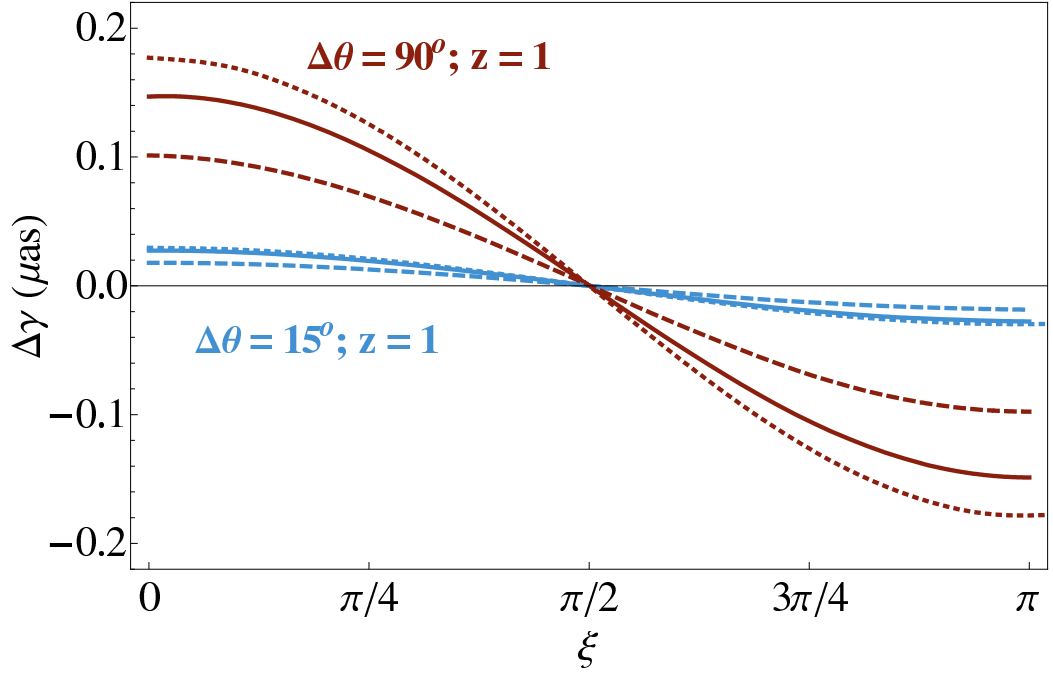


Figure 3.4: Estimate of the cosmic parallax for $\Delta t = 10$ years, $\epsilon = 10^{-6}$, and for sources at $z = 1$ with a separation angle of 90 degrees, plotted as a function of the angle between the trailing source and the symmetry axis (i.e., the angle between the leading source and the symmetry axis is advanced by 90 degrees). The two sets of plotted data correspond to interpolated values found using 100 trials for Δt spread from 5 – 500 years, and interpolated values found using 20 trials in ϵ in the $10^{-6} - 10^{-4}$ range, respectively [90]

3.3 Axisymmetric Bianchi Type I Models

As we have discussed, anisotropic expansion of the universe around a given observer contributes to cosmic parallax. In the case of LTB models, this may allow us to constrain the distance of our galaxy from the center of the void. The further we

are from the center of the void, the more anisotropic the universe would look to us. Of course, LTB space-times are not the only ones that can give rise to anisotropic expansion around a point. This raises the question of how we might interpret any observation of an anomalously large cosmic parallax, since such an observation would not itself be evidence that we live in an LTB universe. To understand this therefore, we study cosmic parallax in alternative anisotropic cosmologies and compare our results with those obtained in [90].

For simplicity we consider anisotropic space-times that are spatially homogeneous [92]. In particular, we focus on a subclass of Bianchi Type I space-times, the metric for which may be written as

$$ds^2 = -dt^2 + a_1^2(t)dx^2 + a_2^2(t)dy^2 + a_3^2(t)dz^2 . \quad (3.13)$$

In general, $a_1(t)$, $a_2(t)$, and $a_3(t)$ are independent scale factors, describing how the three spatial directions scale with time, which reduces to the standard FRW case when $a_1(t) = a_2(t) = a_3(t)$. We specialize to the case when only one of the scale factors differs from the others, say $a_1(t) = a_2(t) \neq a_3(t)$, in which case the expansion is axisymmetric. We do so because we want to compare our results to observations made by an off-center observer in an LTB void. Such an observer will experience axisymmetric cosmic expansion, and so the most direct comparison will be to an axisymmetric Bianchi-I universe. There is, however, an important difference in the symmetries around observers in these two space-times. In the axisymmetric Bianchi-I universe there is an additional plane of symmetry normal to the axis of symmetry. The same is not true for an off-center observer in an LTB universe. To see this, it is sufficient to consider the extremal case of an observer outside the void, who can obviously distinguish the two directions along the polar axis: toward the void and away from it. This suggests that cosmic parallax in these two types of anisotropic models will differ at least qualitatively, if not in magnitude.

Setting $a_1 = a_2 = a(t)$ and $a_3 = b(t)$ in (3.13), the Einstein equations become

$$H_a^2 + 2H_a H_b = 8\pi G\rho \quad (3.14)$$

$$2\dot{H}_a + 3H_a^2 = -8\pi G P_z \quad (3.15)$$

$$\dot{H}_a + H_a^2 + \dot{H}_b + H_b^2 + H_a H_b = -8\pi G P_x, \quad (3.16)$$

where an overdot denotes a derivative with respect to t , $P_x = P_y$ and P_z are anisotropic pressures in the different directions, and we have defined the Hubble parameters $H_a \equiv \dot{a}/a$ and $H_b \equiv \dot{b}/b$. The conservation of energy equation in this case is

$$\dot{\rho} = -2H_a(\rho + P_x) - H_b(\rho + P_z). \quad (3.17)$$

The observational success of FRW cosmology places tight constraints on how anisotropic the universe can be. In order to restrict ourselves to solutions that remain close to an FRW cosmology, we split each of these exact equations into an FRW part which evolves according the FRW equations of motion, and a non-FRW part which we require to remain small, in a sense that we will now make clear. A similar approach was used in [93]. We define

$$H_a(t) = \bar{H}(t) + \epsilon f(t) \quad (3.18)$$

$$H_b(t) = \bar{H}(t) + \epsilon g(t) \quad (3.19)$$

$$\rho(t) = \bar{\rho}(t) + \epsilon r(t) \quad (3.20)$$

$$P_x(t) = P_y(t) = \bar{P}(t) \quad (3.21)$$

$$P_z(t) = \bar{P}(t) + \epsilon s(t) \quad (3.22)$$

where overbars denote the FRW quantities and ϵ is a small perturbative parameter for which we will determine an upper bound later. Substituting these definitions into equations (3.14)-(3.17) and collecting powers of ϵ gives the zeroth-order (or background) equations, which are just the usual ones of the FRW metric, and the

first-order equations

$$2\bar{H}(f + 2g) = 8\pi Gr \quad (3.23)$$

$$6\bar{H}f + 2\dot{f} = -8\pi Gs \quad (3.24)$$

$$3\bar{H}(f + g) + \dot{f} + \dot{g} = 0 \quad (3.25)$$

$$\dot{r} = -3\bar{H}r - \bar{\rho}(2f + g) - \bar{H}s \quad (3.26)$$

These constitute four equations in four variables, but only three of these equations are independent. To close the system we need additional information, which we obtain by assuming an equation of state of the form

$$s(t) = \sigma r(t) \quad (3.27)$$

where the parameter σ is taken to be constant. Note that this is analogous to $\bar{P} = w\bar{\rho}$, except that it relates the anisotropic component of the pressure to the non-FRW correction of the energy density. The value of σ will be important in determining whether the non-FRW parts of equations (3.23)-(3.26) grow or decay in time.

Realistic models will be those for which the amount of anisotropy is sufficiently small in the past and present. Assuming the anisotropy is set (for example by inflation) to be sufficiently small at some early epoch, the question then is whether the anisotropy grows or not. In our set-up this corresponds to asking whether the non-FRW parts of equations (3.23)-(3.26) grow or not, and if so, how quickly. We will see that σ governs the general behavior of the non-FRW quantities, but for a given σ , the details will depend on the background (FRW) solution. Since we are integrating from the present up to redshifts of order 1, our background is well described by the Λ CDM model. Using this background we can analytically find the asymptotic behavior of the non-FRW quantities for different values of the equation state parameter σ .

The background energy density and pressure for Λ CDM are

$$\bar{\rho} = \bar{\rho}_m + \rho_\Lambda$$

$$\bar{P} = -\rho_\Lambda ,$$

where $\bar{\rho}_m$ is the background energy density of matter and ρ_Λ is the effective energy density of the cosmological constant. The background equations become

$$3\bar{H}^2 = 8\pi G(\rho_\Lambda + \bar{\rho}_m) \quad (3.28)$$

$$2\dot{\bar{H}} + 3\bar{H}^2 = 8\pi G\rho_\Lambda \quad (3.29)$$

$$\dot{\bar{\rho}}_m = -3\bar{H}\bar{\rho}_m. \quad (3.30)$$

The solutions can be written simply

$$\bar{H}(t) = A \coth\left(\frac{3}{2}At\right) \quad (3.31)$$

$$\bar{\rho}_m = \rho_\Lambda \left[\sinh\left(\frac{3}{2}At\right) \right]^{-2} \quad (3.32)$$

$$A = \sqrt{\frac{8\pi G\rho_\Lambda}{3}}. \quad (3.33)$$

Using (3.27) and (3.23) in (3.26) then gives

$$\dot{r} = - \left[(3 + \sigma)A \coth\left(\frac{3}{2}At\right) + \frac{12A\pi G}{\sinh\left(\frac{3}{2}At\right)} \right] r(t), \quad (3.34)$$

which can be integrated to find

$$r(t) = c_1 \cosh\left(\frac{3}{2}At\right) \left[\sinh\left(\frac{3}{2}At\right) \right]^{-(3+\frac{2}{3}\sigma)}. \quad (3.35)$$

Using the equation of state (3.27) immediately gives $s(t)$. Equations (3.24) and (3.25) can then be integrated to find the remaining solutions (for $\sigma \neq -9/2$)

$$f(t) = \frac{A}{\left[\sinh\left(\frac{3}{2}At\right) \right]^2} \left(c_2 + \frac{3c_1}{2 \left[\sinh\left(\frac{3}{2}At\right) \right]^{\frac{2}{3}\sigma}} \right) \quad (3.36)$$

$$g(t) = -f(t) - \frac{Ac_2}{\left[\sinh\left(\frac{3}{2}At\right) \right]^2}. \quad (3.37)$$

Now we consider the asymptotic behavior of these solutions for $t \rightarrow \infty$ and $t \rightarrow 0$ in turn.

The behavior as $t \rightarrow \infty$ is

$$r(t) \sim s(t) \sim c_1 \left[\sinh \left(\frac{3}{2} At \right) \right]^{-2(1+\frac{1}{3}\sigma)}. \quad (3.38)$$

$$f(t) \sim -g(t) \sim c_1 \left[\sinh \left(\frac{3}{2} At \right) \right]^{\text{Max}[-2, -2(1+\frac{1}{3}\sigma)]}. \quad (3.39)$$

Here we see that $\sigma = -3$ is the boundary between growing and decaying solutions. If we require all of the non-FRW quantities to decay as $t \rightarrow \infty$, then we must restrict ourselves to $\sigma > -3$.

As $t \rightarrow 0$, the situation is slightly more complicated. The behavior of $f(t)$ and $g(t)$ have a part that depends on the value of σ and a part that does not. The part that does not behaves as

$$c_2 \frac{A}{\left[\sinh \left(\frac{3}{2} At \right) \right]^2} \sim c_2 t^{-2}, \quad t \rightarrow 0,$$

whereas the part that depends on σ behaves as

$$c_1 \frac{3A}{2 \left[\sinh \left(\frac{3}{2} At \right) \right]^{2(1+\frac{1}{3}\sigma)}} \sim c_1 t^{-2(1+\frac{1}{3}\sigma)}, \quad t \rightarrow 0.$$

We require that the expansion history is close to FRW in the far past, which amounts to demanding that $|f/\bar{H}|$, $|g/\bar{H}|$, etc remain $\lesssim \mathcal{O}(1)$ as $t \rightarrow 0$. From the first term, this requires that $c_2 = 0$, while the second term requires that $\sigma < -3/2$. Therefore solutions with decaying anisotropy have an equation of state parameter lying in the range $-3 < \sigma < -3/2$. Turning to $r(t)$ and $s(t)$, as $t \rightarrow 0$ we have

$$r(t) \sim s(t) \sim c_1 \left[\sinh \left(\frac{3}{2} At \right) \right]^{-(3+\frac{2}{3}\sigma)}. \quad (3.40)$$

When $\sigma > -3$ these solutions diverge as $t \rightarrow 0$, but if $\sigma < -3/2$ they diverge slower than $\bar{\rho}$ and \bar{P} , respectively. So the condition

$$-3 < \sigma < -\frac{3}{2} \quad (3.41)$$

will ensure that all non-FRW quantities remain small in the far past, as required. We will restrict ourselves to these models in the rest of this chapter.

What remains is to fix c_1 and the constant A in the solutions (3.35)-(3.37). We do this by imposing observational constraints on the models of interest. First we impose a condition at the surface of last scattering. For an anisotropically expanding universe to be viable it must at the very least predict angular variations in the temperature of the CMB no bigger than 10^{-5} . We can estimate the maximum temperature difference at the time of last scattering by

$$\begin{aligned}\Delta T_0 &= |T_0^{xy} - T_0^z| \\ &= \left| T_{\text{lss}} \left(\frac{a_{\text{lss}}}{a_0} \right) - T_{\text{lss}} \left(\frac{b_{\text{lss}}}{b_0} \right) \right| ,\end{aligned}\quad (3.42)$$

where T^z is the temperature along the axis of symmetry and T^{xy} is the temperature in the transverse plane; subscripts ‘‘0’’ and ‘‘lss’’ refer to quantities today and at the last scattering surface, respectively. Recall that $b(t)$ is the scale factor along the axis of symmetry and $a(t)$ is the scale factor in the transverse plane. From the definitions of H_a and H_b , we have

$$a(t) = a_0 \exp \int_{t_0}^t (\bar{H}(t') + \epsilon f(t')) dt' \quad (3.43)$$

$$b(t) = b_0 \exp \int_{t_0}^t (\bar{H}(t') + \epsilon g(t')) dt' . \quad (3.44)$$

Using these, and choosing $a_0 = b_0 = 1$, we can re-write the expression for ΔT_0 to first order in ϵ as

$$\Delta T_0 = T_{\text{lss}} \left(\frac{b_{\text{lss}}}{b_0} \right) \left| 1 - \left(\frac{a_{\text{lss}} b_0}{b_{\text{lss}} a_0} \right) \right| \simeq 2\epsilon T_0^z \left| \int_{t_0}^{t_{\text{lss}}} f(t) dt \right| , \quad (3.45)$$

where we have used the fact that $g(t) = -f(t)$, which is a consequence of requiring $c_2 = 0$. Inserting the solution for $f(t)$ gives

$$\frac{\Delta T_0}{T_0^z} \simeq 3A\epsilon c_1 \int_{t_0}^{t_{\text{lss}}} \left[\sinh \left(\frac{3}{2} At \right) \right]^{-2(1+\frac{\sigma}{3})} dt . \quad (3.46)$$

Demanding the left-hand side to be at most 1.3×10^{-6} [94] yields one condition on the product ϵc_1 and A for a given equation of state parameter σ .

In order to break the degeneracy between ϵc_1 and A , we need one further condition. Equation (3.46) already requires the difference between H_a and H_b to be small – well within the accepted uncertainty in the measured value of the Hubble parameter [2]. We find it convenient to choose to set the arithmetic average of the Hubble parameters in the three directions equal to the observed value.

$$\begin{aligned} H_{\text{obs}} &= \frac{2H_a + H_b}{3} \\ &= \bar{H} + \frac{\epsilon}{3}f(t) , \end{aligned} \quad (3.47)$$

where again we have used the fact that when $c_2 = 0$, $g(t) = -f(t)$. Alternative choices, such as setting H_a or H_b equal to the measured value of the Hubble parameter, would not change the order of magnitude of ϵc_1 and A and would leave the final result essentially unaltered. Inserting the solution for $f(t)$ into equation (3.47) gives a second condition on ϵc_1 and A

$$\epsilon c_1 = \frac{2}{A}(H_{\text{obs}} - \bar{H}) \left[\sinh \left(\frac{3}{2}At \right) \right]^{2(1+\frac{\sigma}{3})} . \quad (3.48)$$

We can (numerically) solve this equation for A in terms of ϵc_1 and then substitute it back into the first condition (3.46) to obtain an upper bound on ϵc_1 . By taking the maximal allowed value for ϵc_1 , we can then find A using (3.48). For $\sigma = -2$ we find $A \simeq 62(\text{km/s})/\text{Mpc}$ and $\epsilon c_1 \simeq 1.3 \times 10^{-6}$. We always take c_1 to be $\mathcal{O}(1)$, and so in this case we choose $c_1 = 1.3$ and $\epsilon = 10^{-6}$.

In this way we can fully determine solutions to the non-FRW quantities for a given equation of state parameter σ . By restricting ourselves to $-3 < \sigma < -3/2$ we have chosen to focus on models for which these solutions decay in the distant future and which diverge slower than the respective background quantities in the far past as one approaches the initial singularity. These models seem to be the most conservative realizations of a Bianchi-I cosmology, in the sense that they are the easiest to make consistent with observations, or alternatively, the most difficult to rule out. One might try to push the boundaries slightly, for example by considering models with

anisotropies that approach a constant in the distant future rather than vanishing. It may be that such models can be carefully tuned to match observations. We do not consider these more general models here, since our main interest is not model-building, but rather to explore a general effect (cosmic parallax) arising in a Bianchi-I universe.

3.4 Cosmic Parallax in Axisymmetric Bianchi-I Models

As in section 3.2, in order to analyze cosmic parallax we need to find null geodesics in the space-time that connect an observer and various sources at two different times. Letting latin indices run over 1, 2, 3 and $(x^0, x^1, x^2, x^3) = (t, x, y, z)$, the non-zero Christoffel symbol components for the Bianchi-I metric in (3.13) are

$$\Gamma^0_{ij} = a_i^2 H_i \delta_{ij}, \quad \Gamma^i_{0j} = H_i \delta^i_j,$$

where no sum on the index i is implied and H_i is defined as above. The four geodesic equations are then

$$\frac{d^2 t}{d\lambda^2} = - \sum_i H_i \left(a_i \frac{dx^i}{d\lambda} \right)^2 \quad (3.49)$$

$$\frac{d^2 x^i}{d\lambda^2} = -2H_i \frac{dt}{d\lambda} \frac{dx^i}{d\lambda}, \quad (3.50)$$

with the null geodesic condition, $u^\mu u_\mu = 0$, becoming

$$\left(\frac{dt}{d\lambda} \right)^2 = \sum_i \left(a_i \frac{dx^i}{d\lambda} \right)^2. \quad (3.51)$$

As before, $u^\mu \equiv dx^\mu/d\lambda$. We specialize to the axisymmetric case by setting $a_1 = a_2 = a(t)$ and $a_3 = b(t)$, and also $H_1 = H_2 = H_a$ and $H_3 = H_b$. The scale factors, $a(t)$ and $b(t)$, and Hubble parameters, $H_a(t)$ and $H_b(t)$, are fixed after choosing σ and solving the full set of equations as in the previous section.

After fixing the background Bianchi-I space-time, equations (3.49) and (3.50) yield four second-order differential equations and one constraint equation in four dependent variables. To solve this system we must in principle specify initial conditions for the four dependent variables as well as initial velocities (derivatives with respect to λ) giving a total of eight conditions. However, using the constraint equation the system can be reduced to seven independent first-order equations.

Considering the $u^\mu(t) \equiv dx^\mu(t)/d\lambda$ as functions of time along the geodesic, equations (3.50) can be integrated immediately to give

$$\begin{aligned} u^i(t) &= u_0^i e^{-2 \int_{t_0}^t H_i(t') dt'} \\ &= u_0^i a_i^{-2}(t) , \end{aligned} \quad (3.52)$$

which can then be used in equation (3.51) to give

$$\left(\frac{dt}{d\lambda} \right)^2 = \sum_i \left(\frac{u_0^i}{a_i(t(\lambda))} \right)^2 . \quad (3.53)$$

As in the LTB case it is again useful to find an expression for the redshift as it will be one of our observational inputs. To find this expression, as usual, we consider two photons emitted from a source at times t and $t + \tau$, respectively, where τ is taken to be infinitesimally small. The trajectory of the first photon is described by equation (3.53), while to first order in τ , the trajectory of the second photon is described by the geodesic equation

$$\left(\frac{dt}{d\lambda} \right)^2 + 2 \frac{dt}{d\lambda} \frac{d\tau}{d\lambda} = \sum_i (u^i a_i)^2 (1 + 2\tau H_i) . \quad (3.54)$$

Here the variation in time corresponds to a time-delay, and so to a change in geodesic, and not to a change of the time coordinate along a fixed geodesic. Since the $u^i(\lambda)$ are directional derivatives along a given geodesic, they remain unaffected by time variations (derivatives) in obtaining this equation. Using the standard definition of redshift, $1 + z(\lambda_{\text{em}}) \equiv \tau(\lambda_{\text{ob}})/\tau(\lambda_{\text{em}})$, we find the relation

$$\frac{d \log(1 + z(\lambda_{\text{em}}))}{d\lambda_{\text{em}}} = - \frac{1}{\tau(\lambda_{\text{em}})} \frac{d\tau(\lambda_{\text{em}})}{d\lambda_{\text{em}}} , \quad (3.55)$$

where λ_{em} and λ_{ob} are the values of the affine parameter at the emission and observation event, respectively. Using this in (3.54) gives

$$\begin{aligned} \frac{d \log(1+z)}{d\lambda} &= -\frac{\sum_i (u^i a_i)^2 H_i}{\sqrt{\sum_i (u^i a_i)^2}} \\ &= \frac{d \log \sqrt{\sum_i (u^i a_i)^2}}{d\lambda}. \end{aligned} \quad (3.56)$$

In the last step we have also made use of (3.52) and the chain rule

$$\frac{d}{d\lambda}(u^i(\lambda)a_i(\lambda)) = -\frac{dt}{d\lambda}(u^i(t)a_i(t)H_i(t)).$$

With the initial condition $z(\lambda_0) = 0$, integrating (3.56) then gives

$$(1+z) = \frac{\sqrt{\sum_i (u^i a_i)^2}}{\sqrt{\sum_i (u_0^i)^2}}. \quad (3.57)$$

As in section 3.2, we would like to express our results not only in terms of redshift but also in terms of angles, since these are the actual observables. In general there are four pieces of data for each object in the sky, namely the time of observation, two angles with respect to an arbitrary coordinate system, and the observed redshift of the source. In the case of cylindrical symmetry one angle is enough. In contrast with LTB space-times, not much is gained in this case by rewriting the geodesic equations in terms of angles and redshift. Instead, we numerically integrate the equations in the above coordinates and then express the results in terms of angles and redshift.

Our procedure for computing the cosmic parallax for these models is analogous to that in section 3.2. We work in local Cartesian coordinates (t, x_1, x_2, x_3) in which the observer is located at the origin. As seen above, the system of four second-order differential equations plus a constraint reduces to seven independent first-order equations, some of which can be integrated immediately by hand. We are then left

with the problem of fixing initial conditions for our complete set of equations

$$\frac{dt}{d\lambda} = -\sqrt{\sum_i (u^i a^i)^2} \quad (3.58)$$

$$u^i(\lambda) = \frac{u_0^i}{a_i^2} \quad (3.59)$$

$$\frac{dx^i}{d\lambda} = u^i, \quad (3.60)$$

where the subscripts $_0$ refer to quantities at the initial observation event, correspond-

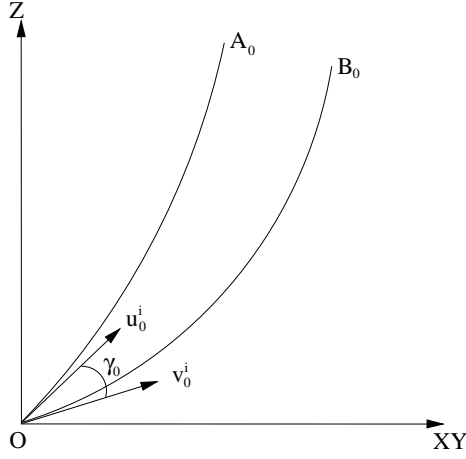


Figure 3.5: Initial angle γ_0 defined by the velocity vectors at observing time for two sources

ing to $\lambda = 0$. To close the system requires seven initial conditions that unfortunately cannot be all specified at the observation event. By construction we have $x^i_0 = 0$, leaving four remaining conditions, three of which are obtained by specifying t_0 and two initial spatial velocities in terms of measurable quantities (angles), while the last one is given by the observed redshift. We integrate backwards along the initial geodesic until reaching the desired redshift and then find the comoving coordinates of the source. To find the final geodesic that connects the same source with the observer at a later time $t_0 + \Delta t$, we solve the corresponding boundary-value problem (namely, to find solutions of the null geodesic equations with two fixed endpoints). We then find the velocities along the final geodesics at the time of observation.

This procedure is repeated for two sources, yielding four sets of velocities: one set for each initial geodesic and one set for each final geodesic. The velocities u^i and v^i along two geodesics at the same observing time (see figure 3.5) are related to the angle γ between them by

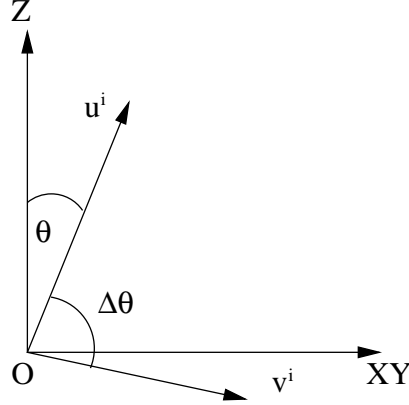


Figure 3.6: Location of sources as seen by an observer at the measuring event. The vertical axis points along the axis of symmetry. We are considering sources at equal redshifts of $z = 1$ and in a plane defined by a fixed value of the polar angle ϕ .

$$\cos(\gamma) = \frac{\sum_i a_i^2 u^i v^i}{\sqrt{\left(\sum_j (a_j u^j)^2\right) \left(\sum_k (a_k v^k)^2\right)}}. \quad (3.61)$$

We then calculate the cosmic parallax $\Delta\gamma$, as defined in (3.10), by taking the difference of the angle between the two sources at the two different times. Finally, we plot the cosmic parallax as a function of the polar coordinate θ for one of the sources. By convention we choose the second, or trailing, source as our reference, as shown in figure 3.6. We find the parallax for two hypothetical sources with the same redshift, initially separated by a given angle on the sky, and for a given Δt and ϵ . In figure 3.7 we plot the parallax for two hypothetical sources at $z = 1$, with an initial separation of 90 degrees on the sky, for $\epsilon = 10^{-6}$ and various values of Δt . For $\Delta t = 500$ years and $\epsilon = 10^{-6}$ we find this maximal value to be of the order of 6×10^{-14} radians. Of course, our true goal is to find the maximal signal for reasonable time scales, say

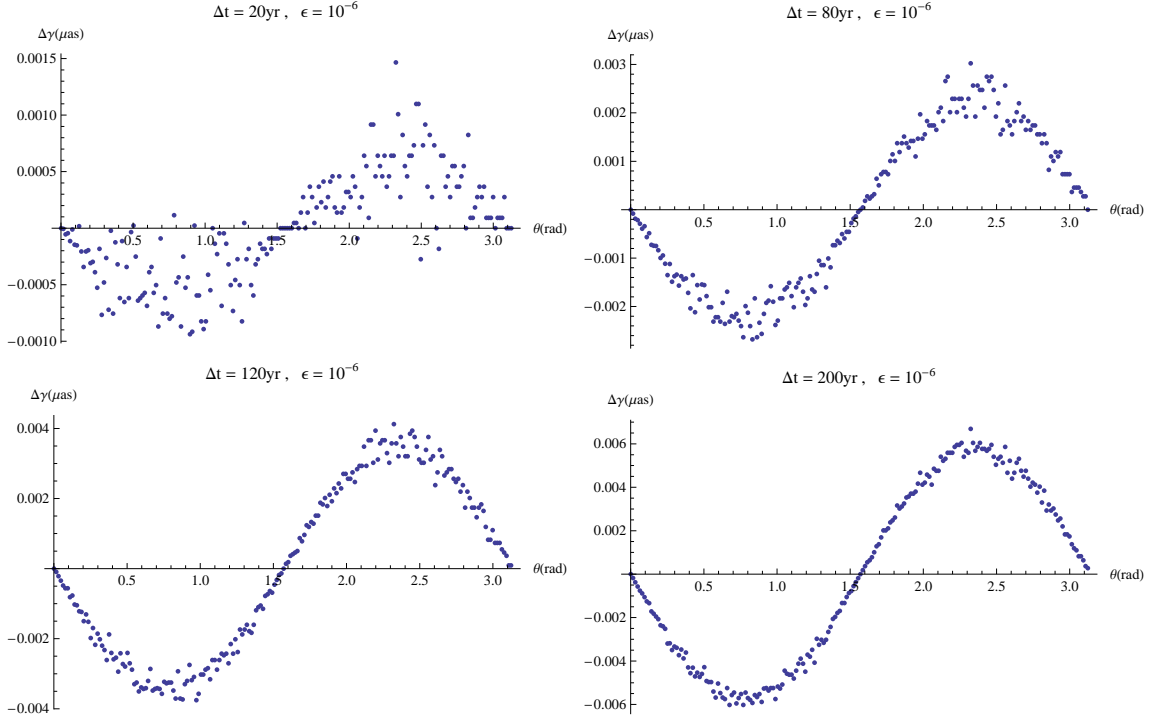


Figure 3.7: A sequence of cosmic parallax signals for different values of Δt and fixed $\epsilon = 10^{-6}$. Top row, left to right: $\Delta t = 20$ yrs, $\Delta t = 80$ yrs. Bottom row, left to right: $\Delta t = 120$ yrs, $\Delta t = 200$ yrs. The signal-to-noise ratio becomes smaller as Δt becomes smaller.

$\Delta t \sim 10$ years, but unfortunately the numerical signal-to-noise ratio approaches 1 for Δt of that magnitude. One can see from the first quadrant of figure 3.7 that by $\Delta t = 20$ years the signal-to-noise ratio starts to diminish. Therefore, although we can directly compute the signal for this model at $\Delta t = 10$ years, as a consistency check we also calculate the cosmic parallax for several values of Δt between 5 and 500 years and interpolate the value at 10 years. Since our primary goal is to find an order of magnitude estimate for the effect, this approach should be acceptable. Figure 3.8 shows the values of the cosmic parallax between two sources for decreasing values of Δt for a specific direction θ in the sky (keeping all other values fixed). For each value of θ , we use a linear fit passing through the origin (because cosmic parallax must vanish for $\Delta t = 0$) to find the interpolated value at 10 years. We could just as well

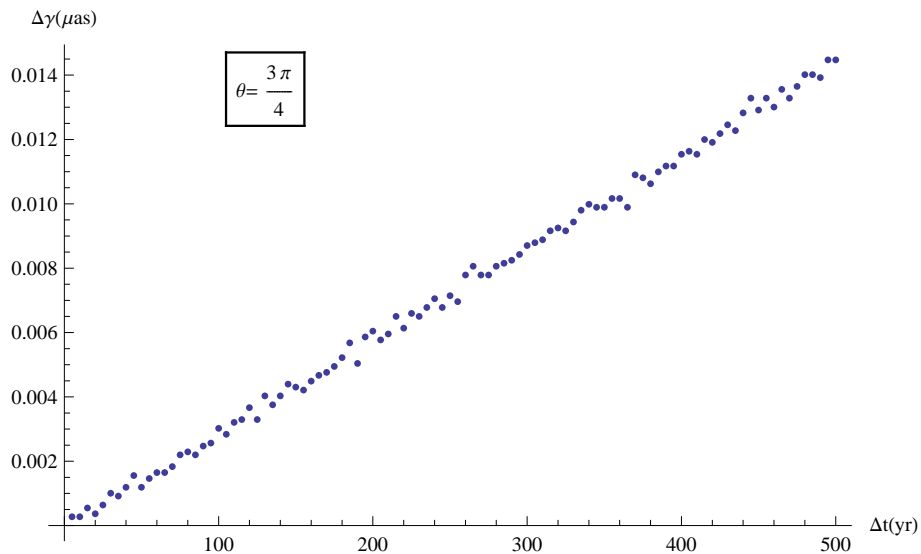


Figure 3.8: Cosmic parallax as a function of Δt . Here $\epsilon = 10^{-6}$ and sources are at $z = 1$, separation angle ($\Delta\theta$) of 90 degrees.

perform an extrapolation by omitting data below some cut-off, say $\Delta t = 50$ years. This does not have any noticeable effects on our results.

As an additional consistency check of this procedure we repeat the same analysis, except now we keep the time interval fixed, namely $\Delta t = 10$ years, and vary the amount of anisotropy by considering values of ϵ between 10^{-6} and 10^{-4} . Also in this case we find a linear dependence of the parallax angle on the varied parameter. In figure 3.9 we plot the angular dependence of the parallax for different values of anisotropy, and in figure 3.10 we plot the parallax as a function of anisotropy for a fixed direction.

After repeating the interpolation for all our data points for both the time and the anisotropy dependence we show our main result in figure 3.11. The two methods give consistent results, strengthening our confidence in the correctness of the linear interpolation procedure.

For the largest allowed values of ϵ consistent with the observed anisotropy of the CMB (i.e., $\epsilon \sim 10^{-6}$) and for time delays on the order of 10 years, we find that

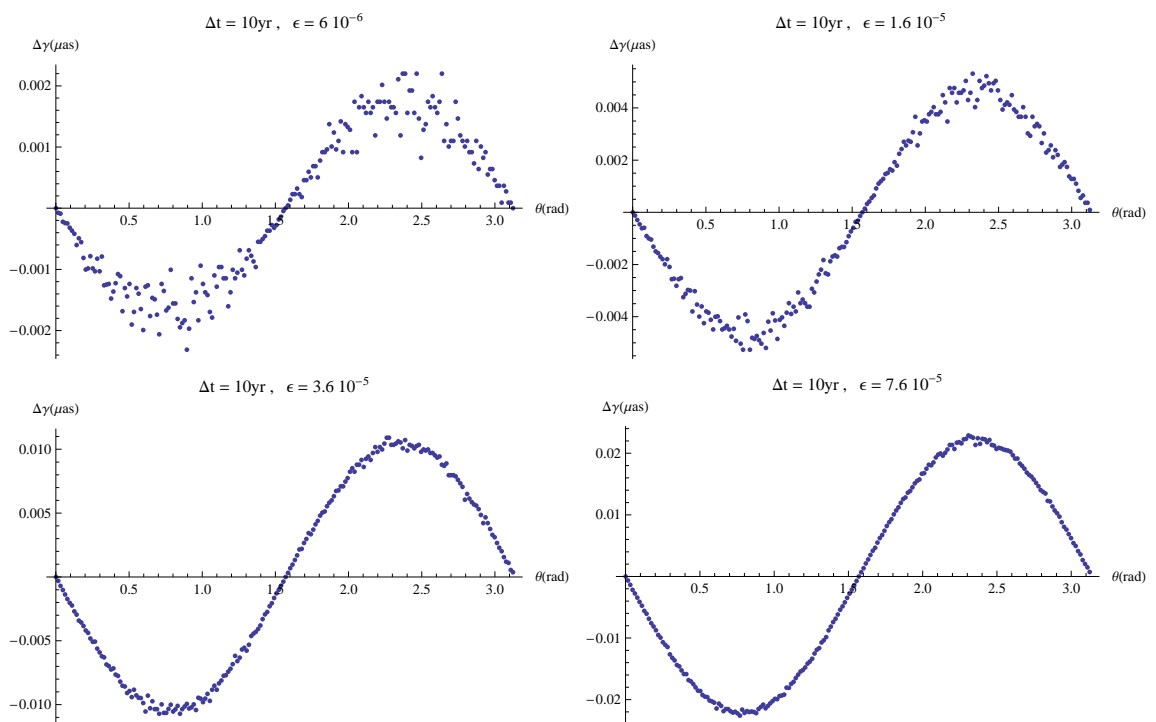


Figure 3.9: A sequence of cosmic parallax signals for different values of ϵ at $\Delta t = 10\text{yrs}$. Top row, left to right: $\epsilon = 6 \cdot 10^{-6}$, $\epsilon = 1.6 \cdot 10^{-5}$. Bottom row, left to right: $\epsilon = 3.6 \cdot 10^{-5}$, $\epsilon = 7.6 \cdot 10^{-5}$.

the maximal cosmic parallax is on the order of 10^{-15} radians, or equivalently 10^{-4} microarcseconds. This is three orders of magnitude smaller than the maximal cosmic parallax seen by [90] for LTB models. It is also three orders of magnitude smaller than the expected level of cosmic parallax from peculiar velocities alone in a Λ CDM universe [95]. In other words, the contribution to cosmic parallax in this model due to anisotropic expansion is sub-dominant to the contribution from peculiar velocities¹.

The qualitative behavior of the cosmic parallax in this model is also quite different from that of LTB models as put forth in [90]. Both LTB and Bianchi models show a sinusoidal (or at least quasi-sinusoidal) cosmic parallax. However, whereas LTB

¹Here we assume that the Bianchi-I models we consider have roughly the same peculiar velocity-redshift relation as an FRW universe.

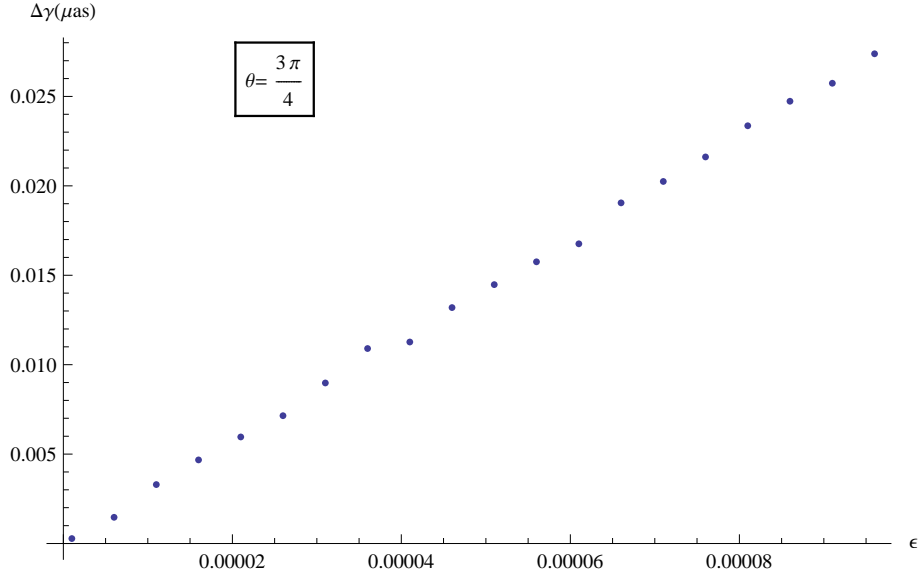


Figure 3.10: Cosmic parallax as a function of ϵ for a fixed value of $\Delta t = 10\text{yrs}$.

models exhibit a 2π -periodic behavior, here we see that Bianchi models exhibit a π -periodic behavior. This is to be expected due to the symmetries of the two types of space-times, as alluded to earlier in the paper. The LTB spacetime is axisymmetric about an off-center observer but is not plane-symmetric about the plane normal to the symmetry axis. If we align the z -axis along the symmetry axis, then in spherical-polar coordinates this amounts to saying that the spacetime is invariant under changes in ϕ (the azimuthal angle) but has no symmetries under (nontrivial) changes in θ (the polar angle). In other words, one would expect cosmic expansion to be 2π -periodic in θ , which is just what was seen for the cosmic parallax in these models in [90]. The Bianchi space-times, on the other hand, are both axisymmetric and plane-symmetric about the plane normal to the axis of symmetry. So one would expect cosmic expansion to be π -periodic in θ , which is what we see for the cosmic parallax in these models.

Although here we have only considered a particular model, preliminary investigations into other models suggest that these results are robust. For example, one might

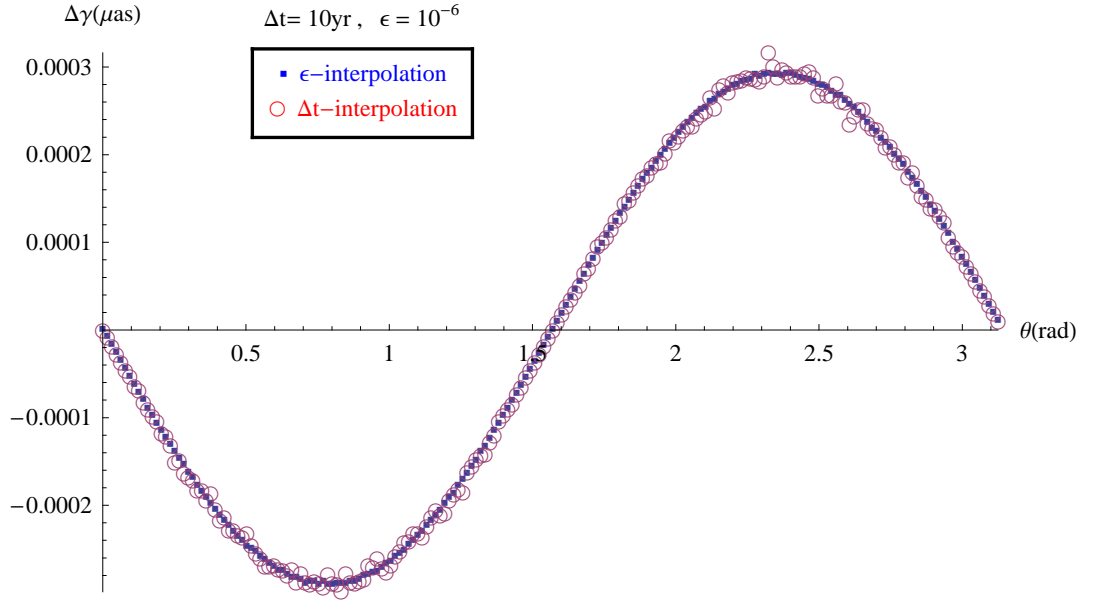


Figure 3.11: Estimate of the cosmic parallax for $\Delta t = 10$ years, $\epsilon = 10^{-6}$, and for sources at $z = 1$ with a separation angle of 90 degrees, plotted as a function of the angle between the trailing source and the symmetry axis (i.e., the angle between the leading source and the symmetry axis is advanced by 90 degrees). The two sets of plotted data correspond to interpolated values found using 100 trials for Δt spread from 5 – 500 years, and interpolated values found using 20 trials in ϵ in the $10^{-6} - 10^{-4}$ range, respectively.

consider models with other constant values for the equation of state parameter σ , a time-varying rather than constant σ , or an equation of state that takes a different form than equation (3.27). None of these modifications seem to affect the order of magnitude of the cosmic parallax (which, due to the symmetry of the metric, is the only free parameter). What this suggests is that the contribution to the cosmic parallax from viable Bianchi-I models is much smaller than the contribution from viable LTB-void models. If the observed cosmic parallax deviates from what is expected in an FRW universe, it is unlikely that this is due to our living in a Bianchi-I spacetime.

Chapter 4

Building Braneworlds

The idea that our universe could be a defect (or “3-brane”) in a higher-dimensional space-time can be used to try to solve many problems in theoretical physics and cosmology. Braneworld models can be used to explain the disparity of scales in the standard model interactions. They can also provide additional fields that can be used to drive inflation or be the missing dark energy. Finally, colliding braneworlds provide one possible explanation for how our universe originated. In this chapter I will introduce some simple braneworld models and discuss their consequences. Then I will discuss recent efforts to construct more realistic braneworld models.

4.1 Why Extra Dimensions?

Extra dimensions have been used in theoretical physics ever since Kaluza [96] and Klein [97] attempted to unify electromagnetism and gravity in a 5-dimensional model. More recently, attempts to unify gravity and quantum mechanics has led to superstring theories, which require a total of 9 spatial dimensions, and supergravity theories, which requires 10 spatial dimensions. Before the 1990’s it was generally thought that the extra spatial dimensions in these theories had to be compactified on microscopic scales and that their effects would therefore be very difficult to detect. With

the discovery of extended objects in extra dimensions, called “branes”, it was realized that standard model fields could be confined to these branes. As a consequence, the size of the extra dimensions could be much larger without conflicting with observations. This led to a wealth of options for particle physics model building [98–112] as well as entirely new approaches for addressing cosmological problems [113–128].

4.2 Factorizable Extra Dimensions

The $(4 + n)$ dimensional Einstein-Hilbert action for gravity (without cosmological constant) can be written as

$$S_{\text{grav}} = -\frac{1}{2} \int d^{(4+n)}x \sqrt{-g^{(4+n)}} M_*^{(2+n)} \mathcal{R}^{(4+n)} \quad (4.1)$$

The simplest models of extra dimensions are ones in which the extra dimensions are flat and compact. For example, if the n extra dimensions are compactified on an n -torus with equal radii r , then the metric can be factorized

$$ds^2 = g_{\mu\nu} dx^\mu dx^\nu + r^2 d\Omega_{(n)}^2 \quad (4.2)$$

where $d\Omega_{(n)}^2$ is the line element for the unit n -torus. Any dependence on the extra dimensions is then factorizable, allowing us to completely integrate over them, leaving us with a 4D effective theory for gravity plus extra fields. In particular the gravitational part of the action becomes

$$S_{\text{grav}} \simeq -\frac{1}{2} \int d^4x d\Omega_{(n)} r^n \sqrt{-g^{(4)}} M_*^{(2+n)} \mathcal{R}^{(4)} \quad (4.3)$$

$$\simeq -\frac{1}{2} \int d^4x \sqrt{-g^{(4)}} (2\pi r)^n M_*^{(2+n)} \mathcal{R}^{(4)} \quad (4.4)$$

where we have neglected the terms containing effective vector and scalar fields. Comparison with the ordinary Einstein-Hilbert action in 4D indicates that the Planck scale must be identified as

$$M_{\text{Pl}} \equiv \sqrt{(2\pi r)^n M_*^{(2+n)}}. \quad (4.5)$$

Here we see that the 4D Planck mass is a derived quantity that depends on the volume of the extra dimensions $V_n = (2\pi r)^n$. Although here we are considering the simple case of compactifying the extra dimensions on an n -torus with equal radii, this dependence on the volume of the extra dimensions hold for general compactification schemes. In this example, we can also invert the above relation in terms of the size of the extra dimensions

$$r = \frac{1}{2\pi} \left(\frac{M_{\text{Pl}}^2}{M_*^{n+2}} \right)^{1/n}. \quad (4.6)$$

The 4D Planck mass is $2.4 \times 10^{15} \text{TeV}$, whereas the hierarchy problem would be solved if $M_* \sim 1 \text{TeV}$. Plugging these in gives

$$\begin{aligned} n = 1 : \quad r &\sim 10^{11} \text{m} \\ n = 2 : \quad r &\sim 10^{-4} \text{m} \\ n = 3 : \quad r &\sim 10^{-9} \text{m} \end{aligned}$$

We obviously would have observed an extra dimension 10^{11}m in radius. But gravity has only been measured precisely to submillimeter distances [129–135]. So in this simplistic model $n \geq 3$ is still viable. The point of this is to show that these models can explain the hierarchy problem with extra dimensions much larger than the Planck length ($\sim 10^{-35} \text{m}$), but still small enough to avoid conflicting with existing probes of gravity.

4.3 The Randall-Sundrum Braneworlds

Next we consider a model with just one extra dimension which is an S^1/Z_2 orbifold. This amounts to considering the extra dimension as an interval $[0, 2\pi]$ where we impose periodic boundary conditions at the end points $y = 0, 2\pi$ as we did when compactifying on the circle, S^1 , but with an additional reflection symmetry around $y = \pi$

We will consider the case where branes are located at the two fixed points of the orbifold. This situation is illustrated in Fig. 4.1. The gravitational action in five

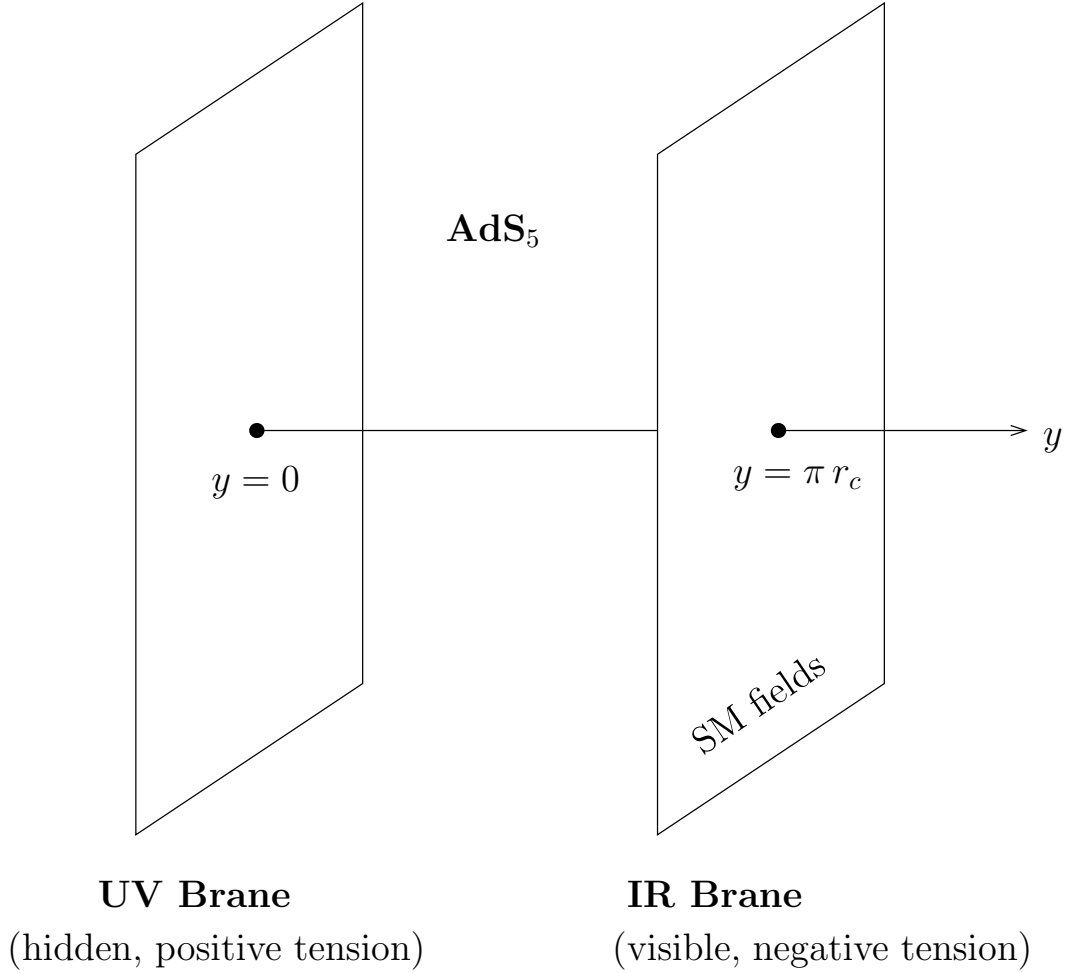


Figure 4.1: Illustration of the RS1 model. Two branes are located at the fixed points of an S^1/Z_2 orbifold. The bulk between the branes is AdS_5 and the brane tensions are tuned to be equal and opposite. In order for this model to solve the hierarchy problem, standard model fields are localized on the IR brane.

dimensions is

$$S_{\text{grav}} = -\frac{1}{2} \int d^5x \sqrt{-g^{(5)}} (M_*^3 \mathcal{R}^{(5)} + \Lambda_5) \quad (4.7)$$

where we have included a cosmological constant in the bulk Λ_5 . The action for the two branes, located at $y = y_1, y_2$, is

$$S_{\text{brane}} = \int d^5x \sqrt{-g^{(5)}} \sum_{i=1,2} \delta(y - y_i) \lambda_i \quad (4.8)$$

where $\lambda_{1,2}$ are the tensions of each brane (we have not yet included matter on the branes). Randall and Sundrum [103] showed that this setup admits the following static solution

$$ds^2 = e^{-2\sigma(y)} \eta_{\mu\nu} dx^\mu dx^\nu + r_c^2 dy^2 \quad (4.9)$$

where σ is called the warp-factor and r_c is the compactification radius of the extra dimension. Plugging this ansatz into the 5D Einstein equations gives

$$\sigma'^2 = - \left(\frac{\Lambda_5}{24M_*^3} \right) r_c^2 \quad (4.10)$$

$$\sigma'' = \frac{1}{2} \sigma'^2 + \frac{\Lambda_5}{12M_*^3} r_c^2. \quad (4.11)$$

Integrating (4.10) shows that $\sigma(y) = k|y|$, where $k = \sqrt{\frac{-\Lambda_5}{24M_*^3}}$. Requiring that the metric is real, we have $\Lambda_5 < 0$. In other words the 5D space-time is found to be a slice of Anti de Sitter (AdS) space-time.

As in the case with flat extra dimensions, the 4D Planck mass M_{Pl} is a derived quantity that depends on the fundamental scale of gravity and the volume of the extra dimensions

$$M_{\text{Pl}}^2 = \frac{M_*^3}{k} (1 - e^{-2kr_c\pi}) \quad (4.12)$$

By tuning $kr_c \approx 50$, a fundamental mass of $\sim 1\text{TeV}$ will generate the Planck mass $\sim 10^{19}\text{GeV}$ on our visible brane, thereby solving the hierarchy problem (see Fig. 4.2). Because the fundamental scale of gravity is so low, this model has distinct phenomenological signatures that could be detected in colliders such as the LHC [103].

4.4 Inclusion of Bulk Fields

We now turn to the task of constructing more realistic braneworld setups. In the above implementations, Standard Model (SM) fields were assumed to be confined to the brane, while in other scenarios not discussed here they populate the entire extra-dimensional space. Common to both approaches, however, is the inclusion of bulk

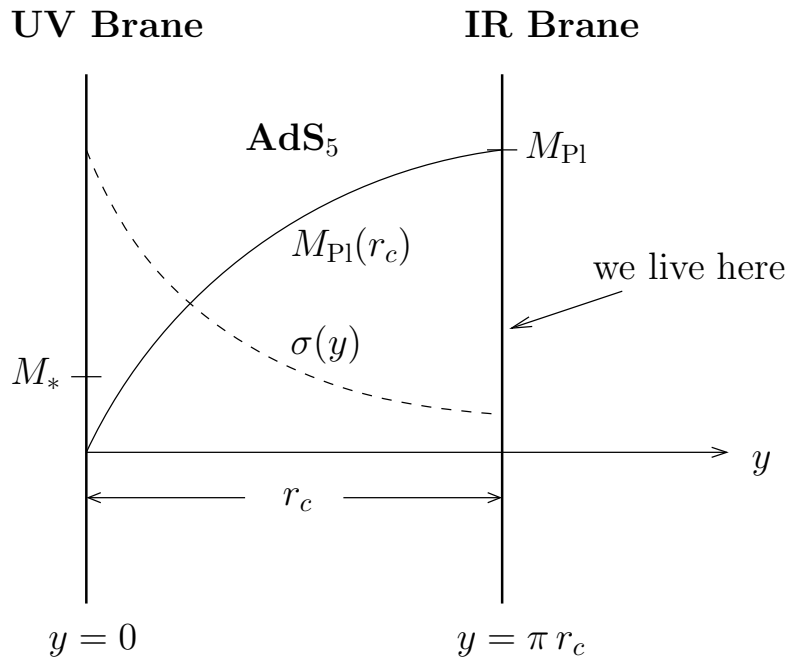


Figure 4.2: Illustration of the RS1 solution to the hierarchy problem. The warp-factor σ drops off exponentially from the (hidden) UV brane, while the Planck mass M_{Pl} on the (visible) IR brane is lifted relative to the fundamental scale M_* on the UV brane. The amount by which M_{Pl} is lifted depends on the size of the extra dimension, given by the compactification radius r_c .

fields beyond pure gravity, either because they are demanded by a more complete theory, such as string theory, or because they are necessary to stabilize the extra-dimensional manifold. So a complete understanding of the predictions and allowed phenomenology of extra dimension models necessarily includes a comprehensive consideration of the configurations of these bulk fields, the simplest of which are real scalars. Indeed, 4D Poincare invariance allows for these new bulk fields to acquire nontrivial static configurations along the extra dimensions.

Bulk scalar fields may also prove useful for model building. Static one-dimensional scalar configurations with a node (where the field vanishes) are known to localize wave functions of other fields near that node. In the context of extra dimensions, these kink-like scalar backgrounds can be used for example to localize bulk fermions near

either boundary [136–139], allowing for interesting constructions of flavor models. They can also affect the localization of other scalar or vector fields leading to a field theoretic description of fat branes (see for example the constructions in [140–143]). More recently, multiple bulk scalar fields have been used to construct so-called soft wall models, in which the profiles of the scalar fields, coupled to the gravitational background, play the role of a dynamical IR boundary (as opposed to a hard-wall IR boundary or brane, located at a specific location in the IR). Phenomenological model building in these scenarios [144, 145] has drawn attention to this possibility, specially because it may alleviate some of the problems of the hard-wall approach, such as the generic tension with precision electroweak measurements [146].

The above examples all make use of static solutions of bulk scalar fields, assuming that such configurations can be dynamically realized. This latter aspect, however, has received little attention, in part because of the difficulty of analyzing a coupled multi-field system in the presence of gravity. Kink-like scalar configurations are a particularly interesting case to consider because the boundary conditions make it possible to obtain non-trivial general results regarding both the existence and the stability of such configurations, at least in the case of one flat extra dimension without gravity [147, 148].

4.5 Kinked Scalar in a Flat Extra Dimension

In [147, 148] a 5D flat scenario including one real scalar field with an arbitrary scalar potential was studied and the general conditions for the existence and perturbative stability of static, nontrivial, background scalar field configurations were presented. In this section we briefly review the main results of [147, 148] and extend the discussion of the energy densities of different kink configurations [149].

Consider a real scalar field in 5 dimensions (labeled by indices $M, N, \dots = 0, 1, 2, 3, 5$)

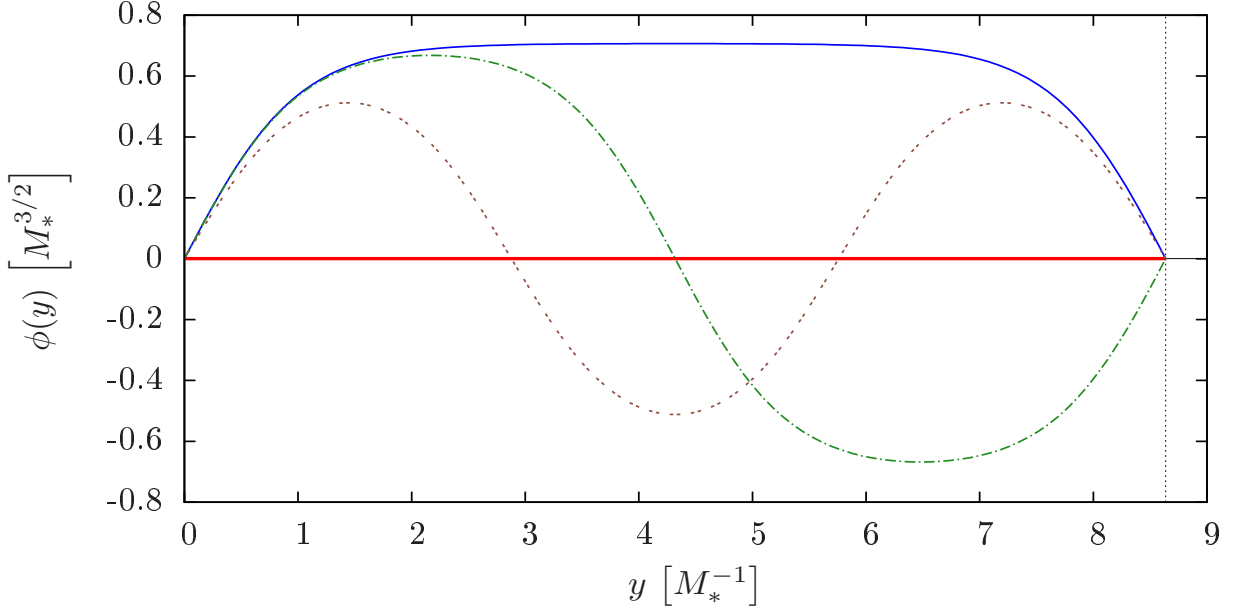


Figure 4.3: Profiles in the extra dimension interval $[0, \pi R]$ of different static configurations of the Dirichlet scalar field ϕ , defined by the scalar potential $V(\phi) = -\frac{1}{2}|\mu^2|\phi^2 + |\lambda|\phi^4$ ($\mu^2 = 2M_*^2$, $\lambda = 1M_*^{-1}$, $\pi R = 8.6375M_*^{-1}$). The solutions with nodes in the interval (dashed curves) are unstable, while the stability of the nodeless and trivial solutions (solid curves) depend on the parameters of the model. The vertical dashed line indicates the location of the second brane.

with a flat background metric, and defined by the action

$$S = \int d^5x \left[\frac{1}{2}\eta^{MN}(\partial_M\phi) \partial_N\phi - V(\phi) \right]. \quad (4.13)$$

The extra dimension is compactified on an S^1/Z_2 orbifold with the scalar field $\phi(x, y)$ being odd under Z_2 reflections along the extra coordinate $x^5 \equiv y$ (i.e. $\phi(x, y) = -\phi(x, -y)$). Here the orbifold interval is defined as $[0, \pi R]$, with its size πR assumed to be fixed. The potential $V(\phi)$ must then be invariant under the discrete symmetry $\phi \rightarrow -\phi$, and is chosen to have at least two degenerate global minima at $\phi = \pm v$, with $v \neq 0$. To simplify notation, we will also choose the potential to vanish at $\phi = 0$.

Under these conditions, it was shown in [147] that there will always be static

solutions, nontrivial along the extra coordinate y , satisfying the (static) field equation

$$\phi'' - \frac{\partial V}{\partial \phi} = 0 , \quad (4.14)$$

where a prime denotes a derivative with respect to y . The profiles of these solutions, satisfying Dirichlet boundary conditions, resemble that of a kink solution patched to an anti-kink in the middle of the interval. The possible solutions were classified in two groups, namely those with nodes in the interval (multiple kink-antikink solutions patched together) and those with no nodes, vanishing only at the end-points of the orbifold (see Fig. 4.3). It was shown that all static kink solutions with nodes are perturbatively unstable, whereas the stability of nodeless solutions depends on the parameters of the model in a particularly simple way.

The Dirichlet solutions of Eq. (4.14) with no nodes in the interval form a continuous one-parameter family of functions. A simple choice for the parameter is the amplitude A of the solution, i.e., the maximum value of the nontrivial solution $\phi_A(y)$. Solutions with different amplitudes A generally vanish at different points along the extra dimension, which correspond to different possible orbifold radii R (see Fig. 4.4). However, in order to obtain the stability condition for these solutions it is extremely useful to consider the full family of solutions.

The value of the 4D effective energy density of a given static solution $\phi_A(y)$ is

$$E(A) = \int_0^{T(A)} \left(\frac{1}{2} \phi_A'^2 + V(\phi_A) \right) dy , \quad (4.15)$$

where $T(A)$ is the length of the solution in the extra dimension. This can be conveniently rewritten as an integral over ϕ using properties of Eq. (4.14) and its solutions $\phi_A(y)$

$$E(A) = 2\sqrt{2} \int_0^A \frac{V(A) - 2V(\phi)}{\sqrt{V(\phi) - V(A)}} d\phi . \quad (4.16)$$

We are now equipped to state the general results of [147, 148] in a slightly modified, although more revealing, version:

Proposition 1 *A static solution to equation (4.14), with $\delta > 0$ nodes inside the orbifold interval is always unstable.*

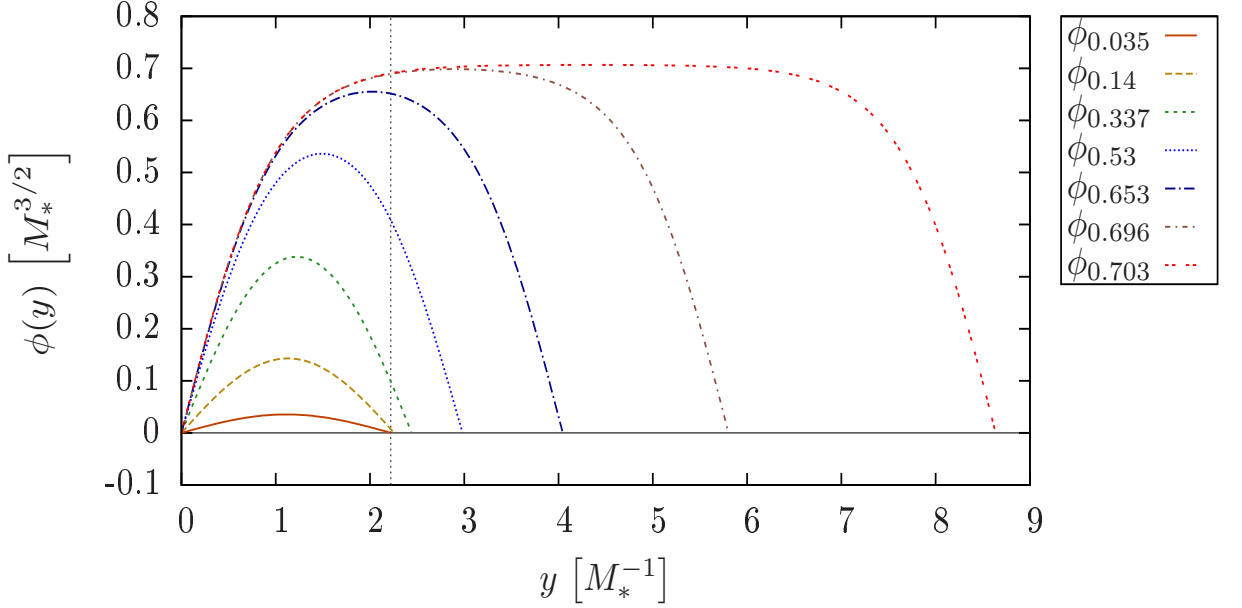


Figure 4.4: Nodeless static configurations of the kink scalar field ϕ , defined by the scalar potential $V(\phi) = -\frac{1}{2}|\mu^2|\phi^2 + |\lambda|\phi^4$ ($\mu^2 = 2M_*^2$, $\lambda = 1M_*^{-1}$). Configurations with different amplitudes are solutions to different physical problems, corresponding to different stabilization radii of the extra dimension. The vertical dashed line indicates the minimal radius R_c , below which nodeless solutions do not exist with this potential.

Proposition 2 *A static, nodeless solution $\phi_{A_*}(y)$ to equation (4.14), with amplitude A_* , and associated energy density $E(A_*)$ is stable if*

$$\left. \frac{dE}{dA} \right|_{A=A_*} < 0 . \quad (4.17)$$

This is a powerful result since it means that given any scalar potential $V(\phi)$ we immediately know which of the nontrivial nodeless solutions ϕ_A will be stable or unstable, without the need to actually know explicitly their analytic form.

With this result it is possible to understand the vacuum structure of any single scalar field theory with Dirichlet boundary conditions in 5D when the metric along the extra dimension is flat. Possible static solutions consist of the trivial solution $\langle \phi \rangle = 0$ (which may or may not be stable), kink-like solutions with nodes in the interval

(which are always unstable), and kink-like solutions without nodes in the interval (some stable and some unstable, depending on condition (4.17)). As remarked in [147, 148], the trivial solution may be the true vacuum solution even in the case of a negative mass term $-\mu^2|\phi^2$ in the 5D potential, as long as the inequality $|\mu^2| < |1/R^2|$ is preserved. Therefore, for a given orbifold radius R , many different perturbatively stable vacuum solutions are possible, and it is necessary to identify which one is the true vacuum of the theory.

The true vacuum of the theory will depend on the size of the radius R . This can be seen as follows: Without loss of generality, one may define the energy density of the trivial solution to be zero by choosing the 5D potential $V(\phi)$ to vanish at $\phi = 0$. It was shown in [147, 148] that there is a critical radius R_c below which nontrivial nodeless solutions do not exist (see Fig. 4.4). The energy density associated with the critical nontrivial nodeless solution will be either positive or exactly zero, so that the transition from one vacuum to another can be either second order or first order, as one varies the radius R .

In Fig. 4.5 we show an example of a simple setup defined by the scalar field potential $V(\phi) = -\frac{1}{2}|\mu^2|\phi^2 - \frac{1}{4}|\lambda|\phi^4 + \frac{1}{6}|\xi|\phi^6$, with $\mu^2 = 4M_*^2$, $\lambda = 4M_*^{-1}$ and $\xi = 0.6M_*^{-4}$. In the right panel, the energy density of two static solutions is plotted as a function of R , showing clearly that below a critical radius R_1 only the trivial solution is possible and above a critical radius R_2 only the kink solution is possible. For $R_1 < R < R_2$, both solutions are perturbatively stable. At the radius R_* the two solutions are degenerate, marking the transition from one true vacuum to another (ϕ_{triv} for $R < R_*$ and ϕ_{kink} for $R > R_*$). From this we see that the inverse length scale $1/R$ plays the role of an order parameter of a phase transition, much like temperature T in finite temperature field theory. For a very small radius R (analogous to high T) the system is stable only around its trivial solution, with all symmetries restored. As the radius increases (analogous to T decreasing) the system can undergo a phase transition, which could be of either first or second order. The analogy with temperature, however,

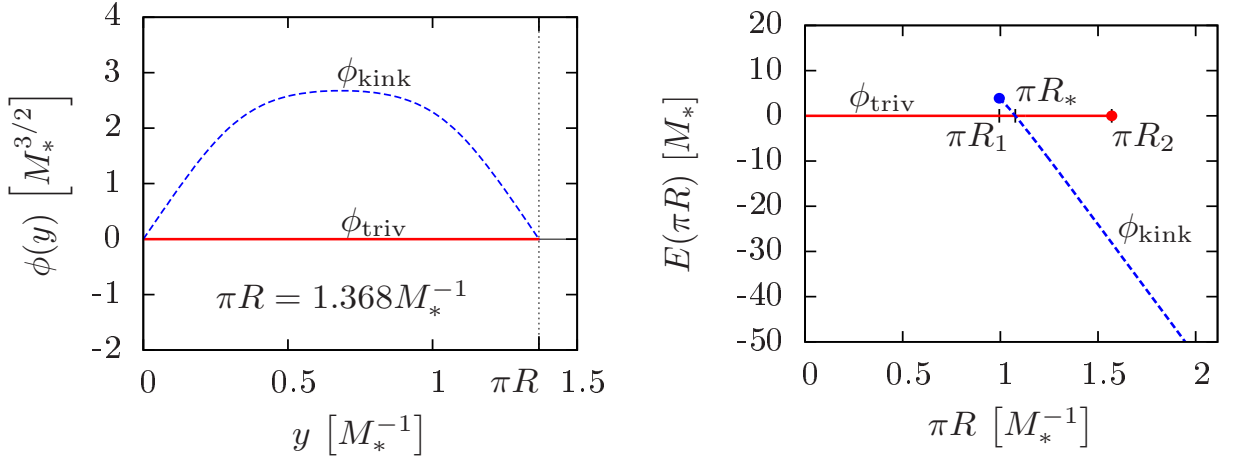


Figure 4.5: Profiles (left panel) in the extra dimension interval $[0, \pi R]$ of the two possible stable static configurations of the Dirichlet scalar field ϕ , defined by the scalar potential $V(\phi) = -\frac{1}{2}|\mu^2|\phi^2 - \frac{1}{4}|\lambda|\phi^4 + \frac{1}{6}|\xi|\phi^6$ (with $\mu^2 = 4M_*^2$, $\lambda = 4M_*^{-1}$, $\xi = 0.6M_*^{-4}$, and $\pi R = 1.368M_*^{-1}$). In the right panel, we show the energy of the two stable solutions as a function of πR , and it is seen how the absolute stability of coexisting static configurations is determined by the size of the radius R . The dots show critical points where the scalar perturbations contain a massless mode.

is not meant to be taken literally. For whereas the temperature in any 4D effective cosmology must be monotonically decreasing for most of its history, the orbifold radius R could in principle increase, decrease or oscillate on very long time scales, depending on the dynamics of the stabilization mechanism (which we have so far ignored).

4.6 Kinked Scalar in a Warped Background

In this section we begin considering bulk fields in a warped background. This original work appeared in [149].

Case 1: *AdS* Background

We can extend the previous investigations to the case of a scalar field in a warped extra dimension, while neglecting any backreaction on the warping from the scalar field itself. In this case one includes the effects of the curved metric along the extra dimension on the scalar field solutions while still ignoring the dynamics of the gravitational sector. We therefore consider the action

$$S = \int d^5x \sqrt{-g} \left[\frac{1}{2} g^{MN} (\partial_M \phi) \partial_N \phi - V(\phi) \right], \quad (4.18)$$

where the form of the metric is now taken to be

$$ds^2 = e^{-2\sigma(y)} \gamma_{\mu\nu}(x) dx^\mu dx^\nu - dy^2, \quad (4.19)$$

and where $\sigma(y)$ is the warp-factor and $\gamma_{\mu\nu}$ the 4D metric on slices of constant y . The purpose of considering scalar field configurations on a fixed background is to explore whether our previous results continue to hold in the presence of a warped background in a regime where we still have semi-analytical control over the solutions. We postpone a discussion of the full dynamical problem, including the backreaction on the metric due to the presence of the scalar field, until the next section.

In the original Randall-Sundrum (RS) model [103], the metric takes the form (4.19) with $\sigma(y) = k|y|$ and $\gamma_{\mu\nu} = \eta_{\mu\nu}$, where k has dimensions of mass and is related to the 5D cosmological constant of *AdS*₅. In this background any static nontrivial field configurations $\bar{\phi}(y)$ are solutions of

$$\bar{\phi}'' - 4k\bar{\phi}' - \left. \frac{\partial V}{\partial \phi} \right|_{\bar{\phi}} = 0. \quad (4.20)$$

Scalar perturbations around this kink background, $\varphi(x, y) = \phi(x, y) - \bar{\phi}(y)$, can be decomposed as

$$\varphi(x, y) = \sum_n \varphi_x^{(n)}(x) \varphi_y^{(n)}(y) \quad (4.21)$$

such that the normal modes $\varphi_x^{(n)}(x)$ and $\varphi_y^{(n)}(y)$ are solutions of

$${}^{(4)}\square \varphi_x + m_n^2 \varphi_x = 0 \quad (4.22)$$

$$\varphi_y'' - 4k\varphi_y' - (\mu^2(y) - m_n^2 e^{2ky}) \varphi_y = 0, \quad (4.23)$$

where $\mu^2 \equiv \left. \frac{\partial^2 V}{\partial \phi^2} \right|_{\bar{\phi}}$ and $(4)\square \equiv \eta^{\mu\nu} \partial_\mu \partial_\nu$. Taking the derivative of the kink equation (4.20) gives

$$\varphi_M'' - 4k\varphi_M' - \mu^2(y)\varphi_M = 0, \quad (4.24)$$

where we have defined $\varphi_M \equiv \bar{\phi}'$. Thus φ_M is a massless solution ($m_n^2 = 0$) of the perturbation equation (4.23), although it satisfies mixed boundary conditions rather than the Dirichlet boundary conditions imposed on φ_y .

At this point we are already able to state a new result of this work, which is an extension of the previous result related to the impossibility of having stable kink solutions with nodes inside the interval. Suppose that $\bar{\phi}(y)$ happens to have δ nodes inside the interval. We have just shown that $\bar{\phi}' \equiv \varphi_M$ will solve the equation for a massless excitation, but with mixed boundary conditions. Since $\bar{\phi}$ has δ nodes, $\bar{\phi}' = \varphi_M$ must have $\delta + 1$ nodes inside the interval. The following inequalities relating the eigenvalues λ_n^D for the Dirichlet case and the eigenvalues λ_n^M for a general mixed boundary condition case hold from Sturm-Liouville theory

$$\lambda_n^D \leq \lambda_{n+2}^M \leq \lambda_{n+2}^D. \quad (4.25)$$

Since we have $\lambda_{\delta+1}^M = 0$ (i.e. the eigenvalue of the solution with $\delta + 1$ nodes), we can immediately deduce that the mass-squared of the lowest excitation of the Dirichlet problem must be negative since $\lambda_{\delta-1}^D \leq \lambda_{\delta+1}^M = 0$ with $\delta \geq 1$.

Proposition 3 *In a warped background on a slice of AdS_5 , any static solution to equation (4.20), with $\delta > 0$ nodes inside the interval is always unstable.*

However, for nodeless static solutions (when $\delta = 0$) the results for the flat case obtained in [147, 148] cannot be extended here. Lacking a general stability condition, we will instead propose a weaker sufficient stability condition for these and other more generic solutions in the next subsection.

Case 2: General Background

In a general warped background with metric ansatz (4.19) the equation for a static scalar background configuration is

$$\bar{\phi}'' - 4\sigma'\bar{\phi}' - \left. \frac{\partial V}{\partial \phi} \right|_{\bar{\phi}} = 0 . \quad (4.26)$$

In this situation, although we have been unable to extend the stability theorems found earlier, we are still able to find a general *sufficient* condition for perturbative stability of the background configurations.

Small perturbations around the background $\bar{\phi}(y)$ may be defined as in (4.21). The spectrum of these perturbations consists of solutions to the eigenvalue problem

$$\varphi_y(y_1) = \varphi_y(y_2) = 0 \quad (4.27)$$

$$\varphi_y'' - 4\sigma'\varphi_y' - [\mu^2(y) - m_n^2 e^{2\sigma(y)}] \varphi_y = 0 . \quad (4.28)$$

A useful form of this equation is obtained by performing a change of variables $e^{\sigma(y)} dy = dz$ and defining $\sigma(z) = -\frac{2}{3} \ln(J(z))$ and $W(z) = \mu^2(z) e^{-2\sigma(y(z))}$ to yield

$$\frac{(J\varphi)''}{J\varphi} - \frac{J''}{J} - (W(z) - m_n^2) = 0 . \quad (4.29)$$

To proceed, we make use of the following integral inequality. For any function $f(z)$, such that $f(a) = f(b) = 0$, and with n nodes within the interval $[a, b]$, there exists $\rho \in \mathcal{R}$ such that

$$\int_a^b e^{-\rho f''(z)/f(z)} dz \geq (n+1)e\sqrt{\rho\pi} . \quad (4.30)$$

Applied to (4.29), this implies

$$e^{\rho m_n^2} \int_a^b e^{-\rho[\frac{J''}{J} + W(z)]} dz \geq (n+1)e\sqrt{\rho\pi} , \quad (4.31)$$

the logarithm of which yields

$$m_n^2 \geq \frac{1}{\rho} \ln[(n+1)e\sqrt{\rho\pi}] - \frac{1}{\rho} \ln \left(\int_a^b e^{-\rho[\frac{J''}{J} + W(z)]} dz \right) \quad (4.32)$$

which is a lower bound for the eigenvalues in terms of the background quantities $\sigma(z)$ and $\mu(z)$ (which are contained in J and W). In the case of the lowest eigenvalue we have

$$m_0^2 \geq \frac{1}{\rho} \ln(e\sqrt{\rho\pi}) - \frac{1}{\rho} \ln \left(\int_a^b e^{-\rho[\frac{J''}{J} + W(z)]} dz \right) \quad (4.33)$$

and so a sufficient condition for perturbative stability ($m_0^2 \geq 0$) is

$$\int_a^b e^{-\rho[\frac{J''}{J} + W(z)]} dz \leq e\sqrt{\rho\pi} . \quad (4.34)$$

We may formulate this explicitly in terms of the warp factor $\sigma(z)$ so that finally, a static solution $\bar{\phi}(z)$ of (4.26), obeying Dirichlet boundary conditions, is stable if

$$\int_a^b e^{-\rho[-\frac{3}{2}\sigma'' + \frac{9}{4}\sigma'^2 + \mu^2(z)e^{-2\sigma}]} dz \leq e\sqrt{\rho\pi} , \quad (4.35)$$

where $\mu^2(z) \equiv \frac{\partial^2 V}{\partial \phi^2} \Big|_{\bar{\phi}(z)}$ and where the actual value of ρ is that which extremizes the right hand side. This is a sufficient condition, but not a necessary one. In order to demonstrate how effective this *weaker* stability condition can be, we now turn to a simple example in which the condition can actually be evaluated.

Consider a flat metric, where $\sigma(y) \equiv 0$, and a trivial background scalar configuration, i.e., $\bar{\phi}(y) \equiv 0$, but where the 5D scalar potential is allowed to have a tachyonic mass. In this case equation (4.28) becomes

$$\varphi_y'' - (\mu^2 - m_n^2) \varphi_y = 0 . \quad (4.36)$$

If φ_y has Dirichlet boundary conditions, the solutions to this problem are

$$\varphi_y = \sin(\sqrt{m_n^2 - \mu^2} y) \quad (4.37)$$

where $m_n^2 - \mu^2 = n^2\pi^2/L^2$ and $L = b - a$ is the size of the extra dimension. The mass of the lightest mode is $m_0^2 = \mu^2 + \pi^2/L^2$ and so the condition for stability is $m_0 \leq 0$, which means that the bulk scalar mass μ^2 can be negative, but not arbitrarily so:

$$\mu^2 \geq -\pi^2/L^2 . \quad (4.38)$$

Therefore in this case (where $\sigma' = \sigma'' = 0$), our *sufficient* condition (4.35) becomes

$$e^{-\rho\mu^2} \int_a^b dz \leq e\sqrt{\rho\pi}, \quad (4.39)$$

which leads to

$$\mu^2 \geq \frac{1}{\rho} \ln\left(\frac{L}{e\sqrt{\rho\pi}}\right). \quad (4.40)$$

The value of ρ that extremizes this bound is $\rho = \pi L^2/e$, and so our weaker bound is

$$\mu^2 \geq -\frac{e\pi}{2} \frac{1}{L^2}. \quad (4.41)$$

This result is a factor of $2\pi/e$ weaker than the exact bound (4.38). Nevertheless this result is nontrivial as it clearly demonstrates that it is possible to have negative bulk masses and retain a stable system.¹

4.7 Bulk Scalars in Gravitating Warped Extra Dimensions

So far we have examined static scalar field configurations in a fixed background. We have found that some of the results that were shown to hold in a flat extra-dimensional background continue to hold in a fixed warped background, and we have found useful generalizations of other results. We now want to include the dynamics of the gravitational sector and explore how these results can be extended when the gravitational backreaction is included. Therefore we now seek nontrivial static field configurations in which the warp factor has its own dynamics determined by the 5D Einstein equations.

As soon as we include a dynamical gravitational sector, we are required to worry about stabilization of the extra dimension. In the above discussion we assumed that

¹The stability conditions of the trivial vacuum in the presence of negative bulk mass terms in an extra-dimensional scalar field theory have been analyzed and generalized to general warped backgrounds in [150].

the extra dimension was stabilized and that the dynamics of the stabilization mechanism were frozen out. Here we want to include the backreaction of any matter fields on the 5D metric, and so we must include the dynamics of stabilization. A natural question to ask is whether the kink fields of interest could provide a stabilization mechanism. Unfortunately, in [151] it was shown that when one considers static solutions for both the warp factor and a single scalar field, the lightest scalar perturbative mode (the radion) will be tachyonic whenever the derivative of the scalar profile vanishes inside the interval. In other words, the system is unstable whenever the scalar field profile passes through an extremum in the bulk. This means that if we insist on obtaining a nontrivial configuration for a single scalar field with Dirichlet boundary conditions, we are guaranteed to obtain a tachyonic radion and the extra dimension will be unstable. To address this issue we will add extra scalar fields whose purpose will be to stabilize the radion as in [152].

The resulting system becomes considerably more difficult to analyze than the case with only one bulk scalar field, particularly with regard to questions about stability. On the other hand, the case with three or more scalar fields is formally no more difficult to analyze than the case with only two scalar fields. Hence we will keep our treatment general to include an arbitrary number of scalar fields χ_a ($a, b = 1, \dots, \mathcal{N}$), although when we consider particular examples below, we will specialize to the case with only two scalar fields (a kink field and a non-kink field). For simplicity we will assume that the scalar fields are only coupled gravitationally. The following results in this and the next section appear in [149].

We therefore consider the 5D action for gravity and \mathcal{N} free scalar fields

$$\begin{aligned}
S &= -\frac{M_*^3}{2} \int d^5x \sqrt{-g} [\mathcal{R} - 2\Lambda] \\
&+ \int d^5x \sqrt{-g} \left[\sum_{a=1}^{\mathcal{N}} \frac{1}{2} g^{MN} (\partial_M \chi_a) (\partial_N \chi_a) - W(\chi_a) - \sum_{i=1,2} \lambda_i(\chi_a) \delta(y - y_i) \right] \quad (4.42)
\end{aligned}$$

where $M_* \equiv (8\pi G)^{-1/3}$, G is the 5D Newton's constant, \mathcal{R} is the 5D Ricci scalar, and Λ is the 5D cosmological constant. The full scalar potential in the bulk is $W(\chi_a)$,

and the brane potentials are $\lambda_i(\chi_a)$. As before, we take the 5D line element of the form

$$ds^2 = e^{-2\sigma(y)} \gamma_{\mu\nu}(x) dx^\mu dx^\nu - dy^2, \quad (4.43)$$

where $\gamma_{\mu\nu}$ is the induced metric on the 4D hypersurfaces of constant y , which foliate the extra dimension. The 5D Einstein and field equations are

$$\sigma'' - \sigma'^2 + \frac{\Lambda}{6} = \frac{1}{2M_*^3} \left(\sum_a^{\mathcal{N}} \frac{1}{2} \chi_a'^2 + \frac{1}{3} W(\chi_a) + \frac{2}{3} \sum_{i=1,2} \lambda_i(\chi_a) \delta(y - y_i) \right) \quad (4.44)$$

$$\sigma'^2 - \frac{\Lambda}{6} + \frac{{}^{(4)}\mathcal{R}}{12} e^{2\sigma} = \frac{1}{6M_*^3} \left(\sum_a^{\mathcal{N}} \frac{1}{2} \chi_a'^2 - W(\chi_a) \right) \quad (4.45)$$

$$\chi_a'' - 4\sigma' \chi_a' - \frac{\partial W}{\partial \chi_a} - \sum_{i=1,2} \frac{\partial \lambda_i}{\partial \chi_a} \delta(y - y_i) = 0, \quad (4.46)$$

where ${}^{(4)}\mathcal{R}$ is the 4D Ricci scalar associated with the induced 4D metric $\gamma_{\mu\nu}$, which we have left arbitrary. The boundary conditions for the system are determined by Israel junction conditions at each brane. These are obtained by integrating the equations of motion over an infinitesimally small interval across each brane, giving

$$[\sigma']_{y_i} \equiv \lim_{\epsilon \rightarrow 0} [\sigma'(y_i + \epsilon) - \sigma'(y_i - \epsilon)] = \frac{1}{3M_*^3} \lambda_i(\chi_a)|_{y_i} \quad (4.47)$$

$$[\chi_a']_{y_i} \equiv \lim_{\epsilon \rightarrow 0} [\chi_a'(y_i + \epsilon) - \chi_a'(y_i - \epsilon)] = \frac{\partial \lambda_i}{\partial \chi_a} \Big|_{y_i}. \quad (4.48)$$

These yield \mathcal{N} conditions on each brane, which is exactly the number of data that need to be specified in order for equations (4.44) and (4.46) to form a well-posed problem.

Note that the above boundary value problem consists of a system of coupled nonlinear differential equations. Finding solutions analytically for such a setup is highly unlikely, although it is still possible to proceed in the opposite direction, i.e. given a particular analytical solution one can obtain the setup from which it originates. To do so, one relies on the powerful method of the superpotential [153–155], which can be useful even for two or more scalar fields (see, for example, [144] in the context of soft-wall models). However, even if one solution is constructed in this way, there

is no guarantee that this is the only solution with the same action. We will now describe how to look for all possible solutions of a given action using a combination of numerical and graphical techniques.

Whenever there is more than one static solution to the above boundary value problem *with the same action*, we say that multiple solutions exist. In general, the bulk scalar fields can have Dirichlet boundary conditions, Neumann boundary conditions or more general mixed boundary conditions. Here we focus on the case where we have one kink field ϕ (obeying Dirichlet boundary conditions), with the remaining $\mathcal{N} - 1$ fields χ_a having Neumann or mixed boundary conditions. When the profiles of these extra fields are monotonic, they will tend to stabilize the extra dimension, whereas if their profiles have vanishing derivatives inside the interval, they will tend to destabilize the extra dimension [151]. Despite this subtlety, we will generically refer to the non-kink fields as “stabilization” fields.

To find solutions we proceed as follows: we specify the Lagrangian in the bulk and on one of the branes, and we numerically solve an initial value problem to determine the profiles of the fields along the extra dimension. Dirichlet boundary conditions are imposed on the kink field ϕ at the initial brane by demanding that it vanish there. For this to hold, we assume the kink field has a sufficiently heavy brane mass so that it decouples from the stabilization fields on the branes. As a result, the kink field disappears from the junction conditions (4.47)-(4.48), which then yield only \mathcal{N} conditions on the initial brane. This leaves $\mathcal{N} + 1$ initial conditions that need to be specified, which we take to be the boundary values for the derivatives ϕ' , $\chi'_1 \dots \chi'_{\mathcal{N}-1}$, and σ' . After solving the initial value problem for a given choice of initial conditions, we impose Dirichlet boundary conditions on ϕ at the final boundary by locating the second brane at a point where the profile of ϕ vanishes. In general, the profile will vanish at several points along the extra dimension, and one may study kinks with the desired number of nodes by choosing the location of the second brane accordingly. Here, as in the flat case, we are primarily interested in nodeless kink solutions, and

we therefore place the second brane at the first zero of the profile function.

We now have a solution to a *boundary* value problem whose boundary conditions on the second brane are not yet known. We parameterize the brane potential on the second brane $\lambda_2(\chi_a)$ in terms of P parameters α_b (for example, the brane tension Σ_2 , the brane mass term m_a^2 of each scalar, the quartic coupling of each scalar, etc.)

$$\lambda_2(\chi_a) = f(\Sigma_2, m_1^2, m_2^2, \dots, m_{\mathcal{N}}^2, \dots) . \quad (4.49)$$

Then the junction conditions (4.47)-(4.48) at the second brane ($i = 2$) give \mathcal{N} linear equations for the P unknowns α_b . By evaluating the fields on the second brane, and using the parameterization in (4.49), we then invert the \mathcal{N} junction conditions to determine the α_b . If this is possible, then the solution to our initial value problem is also a solution to a corresponding boundary value problem. From this we see that we must have $P \geq \mathcal{N}$ in order to guarantee that the field configuration we obtained is the solution to a corresponding boundary value problem. If $P = \mathcal{N}$, the α_b are uniquely determined, and there is a unique Lagrangian for which the above field configuration is a solution. On the other hand if $P > \mathcal{N}$, some of the α_b are arbitrary and so there is a family of solutions for these final-boundary conditions. In that case there is a family of Lagrangians which yield the obtained field configuration, and one can proceed by focusing on one member of this family. If $P < \mathcal{N}$, the linear system of parameters α_b may be overdetermined, in which case the obtained field configuration is not a solution to any corresponding boundary value problem.

We can find additional solutions by changing the initial-boundary conditions and repeating the above process. Note that by freely varying the field derivatives (ϕ' , $\chi'_1 \dots \chi'_{\mathcal{N}-1}$) at the initial brane and determining the remaining quantities from the junction conditions, it is possible to leave the initial-brane potential unchanged. This is necessary in order that the action remains unchanged (it is not sufficient because part of the action is determined by the final-brane potential). A solution and the resulting final-boundary conditions (the α_b) are then found as before. Since each set of initial shooting values yields a set of α_b , each α_b is a function of the \mathcal{N} initial-

boundary derivatives. Each α_b therefore defines an \mathcal{N} -dimensional surface whose level-surfaces can be projected onto the $\phi'(y_1)$ - $\chi'_a(y_1)$ parameter space (which is an \mathcal{N} -dimensional space). In the above construction there are P such quantities, and so P level-surfaces intersect at every point in this parameter space, representing one solution for this action. The question of whether multiple solutions exist for the same action is equivalent to the question of whether the same P surfaces simultaneously intersect at more than one point in the parameter space.

We will now show how this works in two simple examples. In both cases, we will consider a kink field ϕ in addition to just one stabilization field χ , with no interaction terms among them in the scalar potential. In both examples there will be regions of parameter space in which two distinct static configurations are possible for the same action.

Example 1: Quartic Potential

In both of the following examples we consider a Lagrangian for two scalar fields

$$\begin{aligned} \mathcal{L}_{matter} = & \frac{1}{2} g^{MN} (\partial_M \phi) \partial_N \phi - V(\phi) - \sum_{i=1,2} \beta_i(\phi) \delta(y - y_i) \\ & + \frac{1}{2} g^{MN} (\partial_M \chi) \partial_N \chi - U(\chi) - \sum_{i=1,2} \lambda_i(\chi) \delta(y - y_i) , \end{aligned} \quad (4.50)$$

where ϕ is the kink field and χ is the stabilization field with potentials

$$U(\chi) = \frac{1}{2} m_\chi^2 \chi^2 \quad (4.51)$$

$$\lambda_i(\chi) = M_*^{-1} \left(\frac{1}{2} \mu_i^2 \chi^2 + \Sigma_i \right) . \quad (4.52)$$

The fact that the second brane potential for χ is parameterized in terms of two parameters, μ_2^2 and Σ_2 , will allow us to find unique solutions to the boundary conditions on the second brane. The junction conditions (4.47)-(4.48) become

$$\sigma'(y_i) = (-1)^{i-1} \frac{1}{6M_*^4} \left(\frac{1}{2} \mu_i^2 \chi^2(y_i) + \Sigma_i \right) \quad (4.53)$$

$$\chi'(y_i) = (-1)^{i-1} \frac{1}{2} \mu_i^2 \chi(y_i) . \quad (4.54)$$

On the second brane ($i = 2$) these can be inverted to give

$$\mu_2^2 = -2 \frac{\chi'(y_2)}{\chi(y_2)} \quad (4.55)$$

$$\Sigma_2 = -6M_*^4 \sigma(y_2) + \chi'(y_2)\chi(y_2) \quad (4.56)$$

so that once we determine the fields on the second brane, we can extract the boundary conditions (and therefore Lagrangian) to which those fields are a solution.

The only things left to specify are the bulk potential for the kink field and the initial-boundary conditions. In this first example, we take the kink potential to be

$$V(\phi) = -\frac{1}{2} m_\phi^2 \phi^2 + \frac{1}{4} \lambda \phi^4. \quad (4.57)$$

Taking the initial brane to be located at $y = 0$, we find solutions to the initial-boundary value problem at this brane with Dirichlet boundary conditions imposed on the field ϕ . Examples of nodeless solutions to the initial value problem are shown in Fig. 4.6. To ensure that ϕ obeys Dirichlet boundary conditions on the second brane, we locate the second brane at the first point (other than $y = 0$) where the profile of ϕ vanishes (the vertical dashed lines in Fig. 4.6).² Once the position of the second brane is identified, the final-boundary conditions are determined from (4.55) and (4.56). By varying the initial shooting conditions, $\phi'_1 \equiv \phi'(y_1)$ and $\chi'_1 \equiv \chi'(y_1)$, and repeating this process of finding solutions, identifying the location of the second brane, and determining the final-boundary conditions, we generate level-curves of μ_2^2 and Σ_2 . These are plotted in Fig. 4.7. Notice that most μ_2^2 contours cross each Σ_2 just once, signifying that there is a single solution for the corresponding action with the kink potential of Eq. (4.57). However, some contours cross each other more than once (see, for example, the circles in Fig. 4.7.) Furthermore there is only a finite region in the ϕ'_1 - χ'_1 parameter space where solutions exist. If either $|\phi'_1|$ or $|\chi'_1|$ are increased sufficiently, the solution to the initial value problem blows up. In that case

²For certain initial conditions, the profile of ϕ will blow up before it vanishes for a second time. When this happens the initial conditions used do not lead to a solution of our boundary value problem.

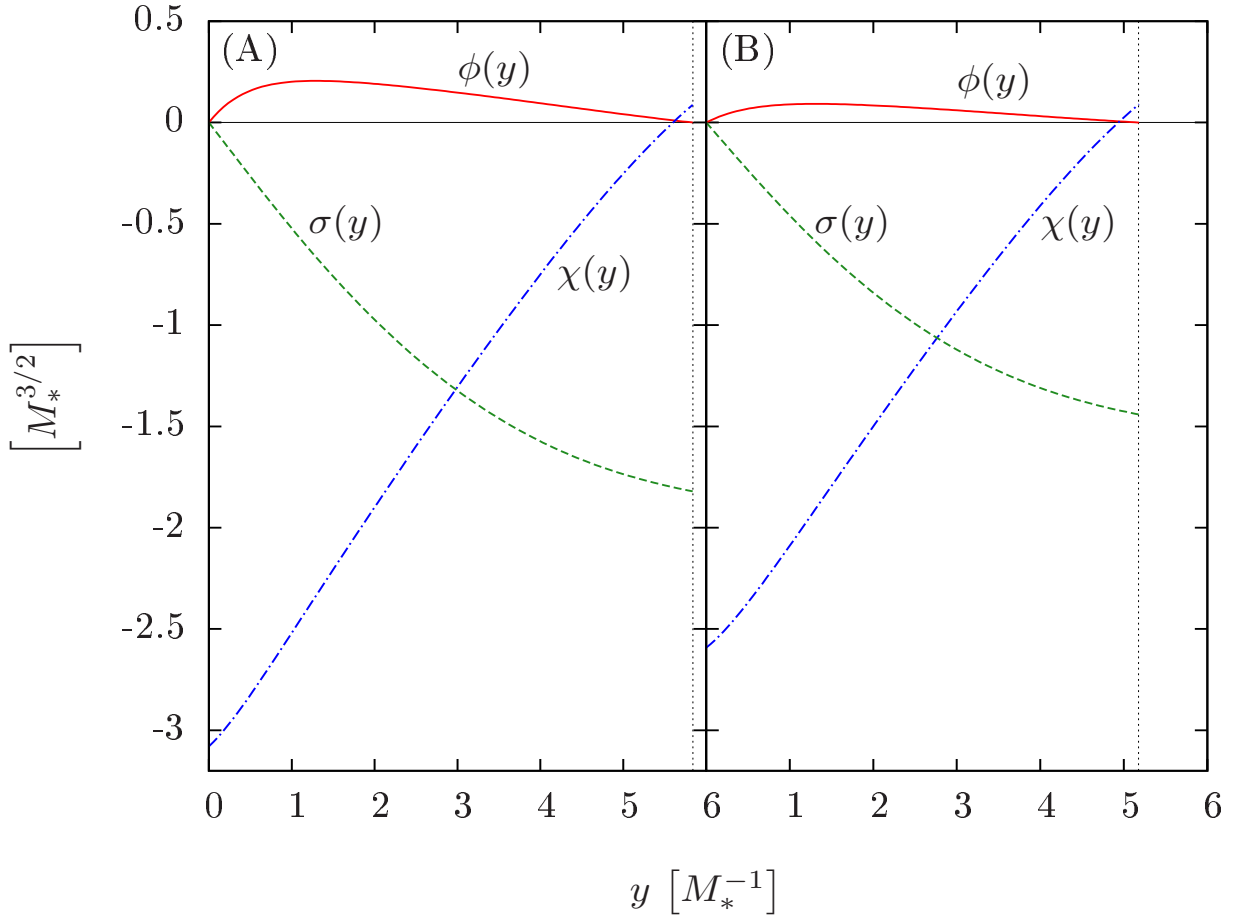


Figure 4.6: Profiles of the scalar backgrounds $\phi(y)$ and $\chi(y)$ as well as the warp factor $\sigma(y)$, showing the two possible solutions (panels A and B) to the same boundary value problem defined by the physical parameters $m_\chi^2 = -0.5M_*^2$, $\mu_1^2 = -0.25M_*^2$, $\mu_2^2 = -8M_*^2$, $\Sigma_1 = -2M_*^4$, $\Sigma_2 = 0.52M_*^4$, $m_\phi^2 = 0.5M_*^2$, $\lambda = 2M_*^{-1}$, and $\Lambda = 0$.

the *boundary* value problem has no solution, since a second boundary where $\phi = 0$ does not exist. It is therefore possible to scan the entire allowed ϕ'_1 - χ'_1 space and examine whether multiple solutions with the same action exist.

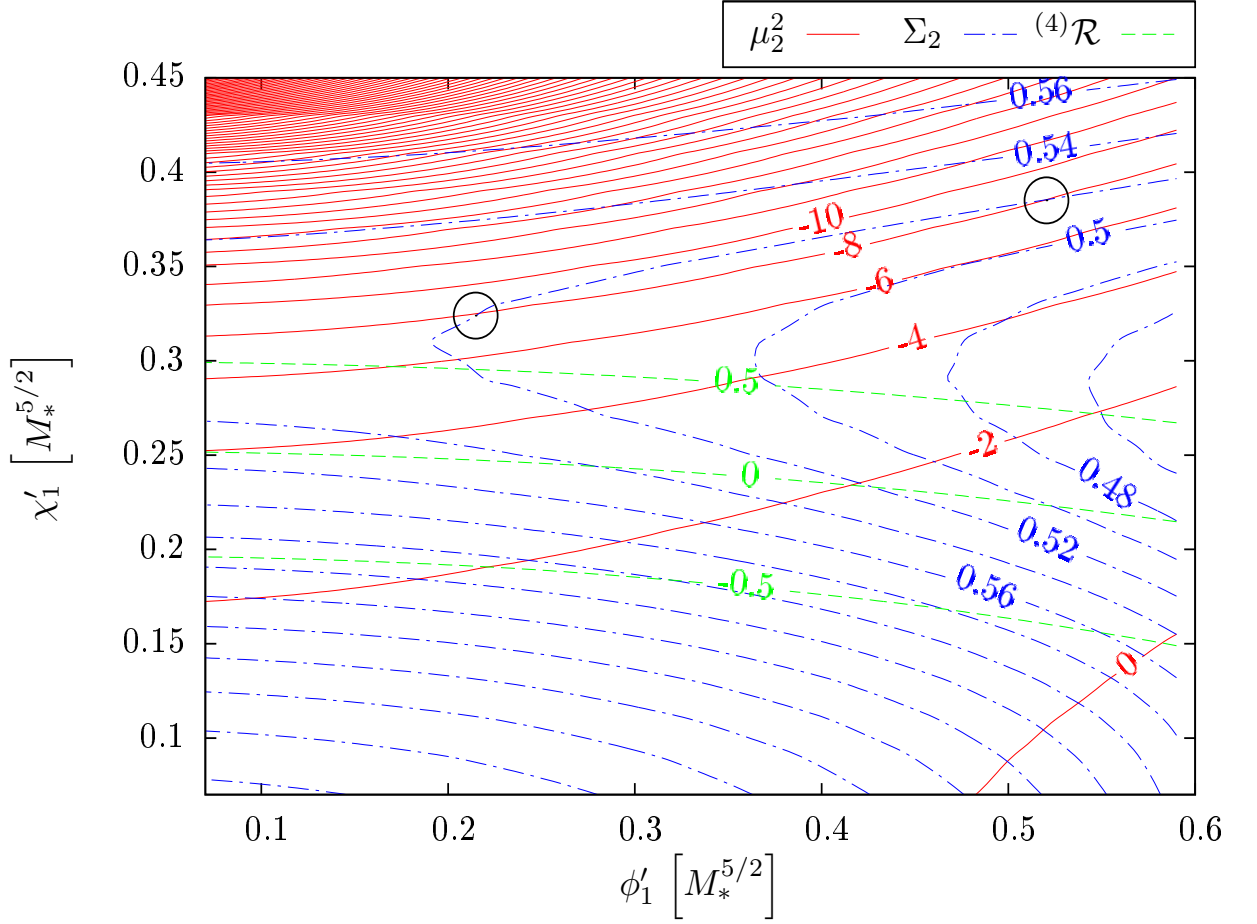


Figure 4.7: Level-curves of μ_2^2 and Σ_2 in the ϕ'_1 - χ'_1 parameter space for example 1 with $m_\chi^2 = -0.5M_*^2$, $\mu_1^2 = -0.25M_*^2$, $\Sigma_1 = -2M_*^4$, $m_\phi^2 = 0.5M_*^2$, $\lambda = 2M_*^{-1}$, and $\Lambda = 0$. Circled are two points in the ϕ'_1 - χ'_1 parameter space with the same values of μ_2^2 and Σ_2 , corresponding to two solutions with the same Lagrangian (plotted in Fig. 4.6).

Example 2: Higher-Order Potential

In this second example we take a slightly more complicated kink potential

$$V(\phi) = -\frac{1}{2}m_\phi^2\phi^2 - \frac{1}{4}\lambda\phi^4 + \frac{1}{6}\xi\phi^6. \quad (4.58)$$

The other potentials and boundary conditions are the same as in the previous example, the only difference being the dynamical evolution of the system due to the

new potential $V(\phi)$. We choose this potential because, contrary to the potential in our first example, in the limit of weak gravity and flat spacetime, it leads to multiple solutions to the same boundary value problem [147, 148] due to the nonlinear nature of the equations.

In our more general setting, including gravity and a stabilization field, we find numerically that there exists more than one solution for the same Lagrangian in a large portion of the parameters space. In Fig. 4.8 we show two such solutions. Note that these solutions would be extremely difficult to discover by randomly guessing initial-boundary conditions. To be more methodical we follow the same procedure as before to find level-curves of the final-boundary conditions, shown in Fig. 4.9. Again, solutions to a particular action will be given by the intersection of the appropriate contours for the brane mass squared μ_2^2 and brane tension Σ_2 . As can be seen, there are regions in which some contours intersect at more than one point, showing that multiple solutions for the same action are possible as expected. In particular, we again circle two such points, corresponding to the solutions plotted in Figs. 4.8. As an interesting remark, note that both of these particular solutions happen to lie near the region of parameter space where the 4D cosmological constant vanishes.

4.8 Stability of Kink Solutions

Having shown how different nontrivial static field configurations exist in warped extra dimensions, the next question to ask is whether these solutions are stable. As we reviewed above, in the case of flat extra dimensions there exist [148] techniques for determining the stability of such solutions. Indeed, for certain potentials, in that case perturbative stability can be determined analytically. Unfortunately, in the case of warped extra dimensions, the question of stability is complicated by the presence of multiple scalar fields and their coupled dynamics. Here we begin to study the perturbative stability of these kinked configurations. We derive the linearized equations

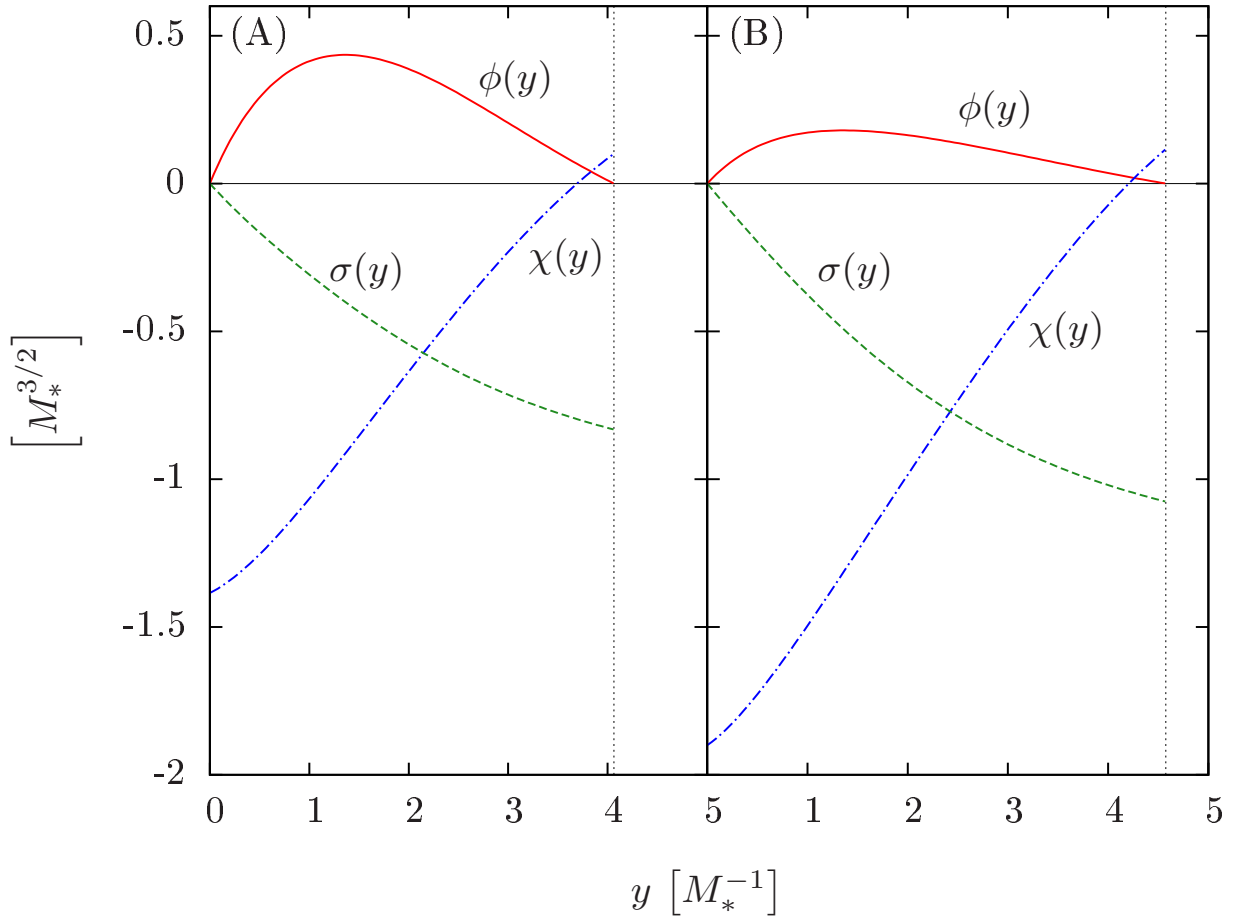


Figure 4.8: Profiles of the scalar backgrounds $\phi(y)$ and $\chi(y)$ as well as the warp factor $\sigma(y)$, showing the two possible solutions (panels A and B) to the same boundary value problem defined by the physical parameters $m_\chi^2 = -0.5M_*^2$, $\mu_1^2 = -0.25M_*^2$, $\mu_2^2 = -5M_*^2$, $\Sigma_1 = -2M_*^4$, $\Sigma_2 = 0.56M_*^4$, $m_\phi^2 = 0.5M_*^2$, $\lambda = 2M_*^{-1}$, $\xi = 6M_*^{-4}$, and $\Lambda = 0$.

and reformulate the problem in terms of a matrix Sturm-Liouville problem. However, the full analysis requires matrix Sturm-Liouville methods which we omit and leave for future work. Although incomplete, our approach here will be completely general for the stability of any coupled, multi scalar field system, in the presence of a warped extra dimension. In particular, although we have been interested in kink-like field configurations with Dirichlet boundary conditions, in this section we leave the

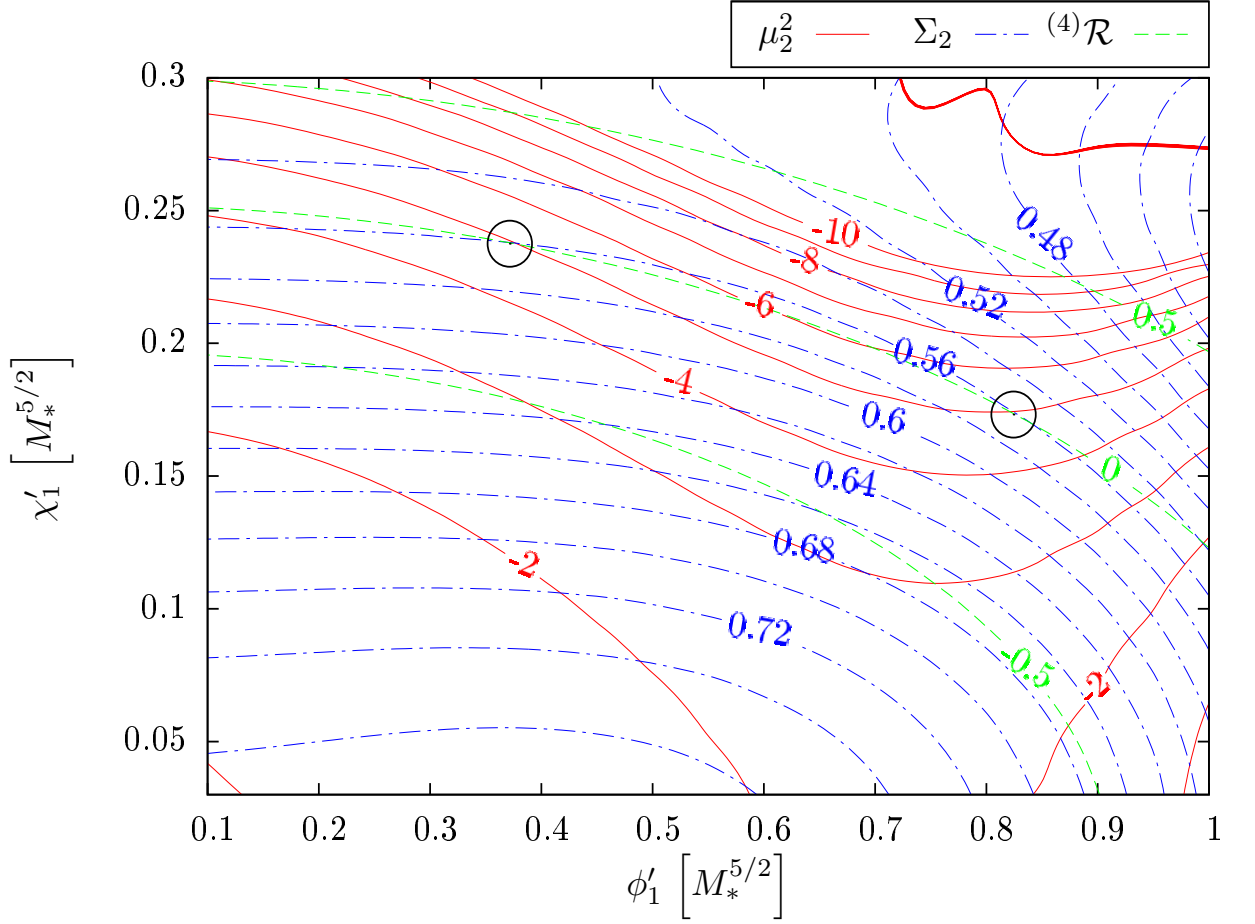


Figure 4.9: Level-curves of μ_2^2 and Σ_2 in the ϕ'_1 - χ'_1 parameter space for example 2 with $m_\chi^2 = -0.5M_*^2$, $\mu_1^2 = -0.25M_*^2$, $\Sigma_1 = -2M_*^4$, $m_\phi^2 = 0.5M_*^2$, $\lambda = 2M_*^{-1}$, $\xi = 6M_*^{-4}$ and $\Lambda = 0$. Circled are two points in the ϕ'_1 - χ'_1 parameter space with the same values of μ_2^2 and Σ_2 , corresponding to two solutions with the same Lagrangian. These solutions are plotted in Fig. 4.8.

boundary conditions in a general form.

We begin by expanding the metric to first-order. Instead of the coordinates in (4.19), in this section it will be more convenient to choose coordinates so that the metric takes the form

$$ds^2 = a^2(y) (\gamma_{\mu\nu}(x) dx^\mu dx^\nu - dy^2) . \quad (4.59)$$

The background Einstein and field equations in these coordinates are

$$\mathcal{H}' - \frac{\Lambda}{6}a^2 = -\frac{\kappa^3}{2} \left(\sum_a \frac{1}{2}\chi_a'^2 + \frac{1}{3}a^2 W(\chi_a) + \frac{2}{3}a^2 \sum_i \lambda_i(\chi_a)\delta(y - y_i) \right) \quad (4.60)$$

$$\mathcal{H}^2 - \frac{\Lambda}{6}a^2 + \frac{{}^{(4)}\mathcal{R}}{12} = \frac{\kappa^3}{6} \left(\sum_a \frac{1}{2}\chi_a'^2 - a^2 W(\chi_a) \right) \quad (4.61)$$

$$\chi_a'' + 3\mathcal{H}\chi_a' - a^2 \frac{\partial W}{\partial \chi_a} - a^2 \sum_i \frac{\partial \lambda_i}{\partial \chi_a} \delta(y - y_i) = 0, \quad (4.62)$$

where $\mathcal{H} \equiv \frac{a'}{a}$, ${}^{(4)}\mathcal{R}$ is the 4D Ricci scalar with respect to the background 4D metric $\gamma_{\mu\nu}$. To first-order in scalar perturbations, the 5D metric can be written

$$ds^2 = a^2(y) \left[\{ (1 + 2\Phi(x, y))\gamma_{\mu\nu}(x) + 2E(x, y)|_{\mu\nu} \} dx^\mu dx^\nu + 2B(x, y)|_\mu dx^\mu dy - (1 + 2\Psi(x, y))dy^2 \right] \quad (4.63)$$

where $|$ indicates a covariant derivative with respect to the 4D slices of the bulk. Choosing to work in the generalized longitudinal gauge, we set $B = E = 0$, and the linearized metric simplifies to

$$ds^2 = a^2(y) \left[(1 + 2\Phi(x, y))\gamma_{\mu\nu}(x) dx^\mu dx^\nu - (1 + 2\Psi(x, y))dy^2 \right]. \quad (4.64)$$

We also expand the scalar fields to first-order

$$\chi_a(x, y) = \bar{\chi}_a(y) + \xi_a(x, y), \quad (4.65)$$

where the fields $\bar{\chi}_a$ obey the background equations of motion (4.60)-(4.62) above and $\xi_a(x, y)$ are small perturbations. The linearized Einstein and field equations are

$$2\Phi + \Psi = 0 \quad (4.66)$$

$$\Phi' - \mathcal{H}\Psi = -\frac{1}{3M_*^3} \sum_a \bar{\chi}_a' \xi_a \quad (4.67)$$

$$\begin{aligned} {}^{(4)}\square(2\Phi + \Psi) - 4\Phi'' + 8\mathcal{H}'\Psi &+ 8\mathcal{H}^2\Psi + 4\mathcal{H}(\Psi' - 3\Phi') + \frac{2}{3}{}^{(4)}\mathcal{R}\Phi \\ &= \frac{4}{3M_*^3} \sum_a \left(\bar{\chi}_a' \xi_a' - \bar{\chi}_a'^2 \Psi + a^2 \frac{\partial W}{\partial \chi_a} \Big|_{\bar{\chi}} \xi_a \right) \end{aligned} \quad (4.68)$$

$$\begin{aligned}
{}^{(4)}\square\Phi - 4\mathcal{H}\Phi' + 4\mathcal{H}^2\Psi + \frac{1}{3}{}^{(4)}\mathcal{R}\Psi \\
= -\frac{1}{3M_*^3} \sum_a \left(\bar{\chi}'_a \xi'_a - \bar{\chi}_a'^2 \Psi - a^2 \frac{\partial W}{\partial \chi_a} \Big|_{\bar{\chi}} \xi_a \right) \quad (4.69)
\end{aligned}$$

$${}^{(4)}\square\xi_a - \xi_a'' - 3\mathcal{H}\xi'_a + a^2 \sum_b \frac{\partial^2 W}{\partial \chi_a \partial \chi_b} \Big|_{\bar{\chi}} \xi_b = -2\bar{\chi}_a'' \Psi - \bar{\chi}_a' (\Psi' - 4\Phi' + 6\mathcal{H}\Psi), \quad (4.70)$$

where ${}^{(4)}\square \equiv \gamma^{\mu\nu} \partial_\mu \partial_\nu$ is the 4D wave operator. Applying the constraint equation (4.66) to equations (4.67)-(4.70), and making use of the background equations (4.60)-(4.62), yields

$$\Psi' + 2\mathcal{H}\Psi = \frac{2}{3M_*^3} \sum_a \bar{\chi}'_a \xi_a \quad (4.71)$$

$$\Psi'' + 5\mathcal{H}\Psi' + \left(4\mathcal{H}' + 4\mathcal{H}^2 - \frac{1}{6}{}^{(4)}\mathcal{R} + \frac{2}{3M_*^3} \sum_a \bar{\phi}_a'^2 \right) \Psi = \frac{2}{3M_*^3} \sum_a \left(\bar{\chi}'_a \xi'_a + a^2 \frac{\partial W}{\partial \chi_a} \Big|_{\bar{\chi}} \xi_a \right) \quad (4.72)$$

$${}^{(4)}\square\Psi - 4\mathcal{H}\Psi' - \left(8\mathcal{H}^2 - \frac{1}{3}{}^{(4)}\mathcal{R} - \frac{2}{3M_*^3} \sum_a \bar{\chi}_a'^2 \right) \Psi = \frac{2}{3M_*^3} \sum_a \left(\bar{\chi}'_a \xi'_a - a^2 \frac{\partial W}{\partial \chi_a} \Big|_{\bar{\chi}} \xi_a \right) \quad (4.73)$$

$${}^{(4)}\square\xi_a - \xi_a'' - 3\mathcal{H}\xi'_a + \sum_b \left(a^2 \frac{\partial^2 W}{\partial \chi_a \partial \chi_b} \Big|_{\bar{\chi}} - \frac{2}{M_*^3} \bar{\chi}'_a \bar{\chi}'_b \right) \xi_b = -2 \left(3\mathcal{H}\bar{\chi}'_a - a^2 \frac{\partial W}{\partial \chi_a} \Big|_{\bar{\chi}} \right) \Psi. \quad (4.74)$$

We obtain a 5D wave-like equation for Ψ by subtracting (4.72) from (4.73) to give

$${}^{(4)}\square\Psi - \Psi'' - 9\mathcal{H}\Psi' - \left(4\mathcal{H}' + 12\mathcal{H}^2 - \frac{1}{2}{}^{(4)}\mathcal{R} \right) \Psi = -\frac{4a^2}{3M_*^3} \sum_a \frac{\partial W}{\partial \chi_a} \Big|_{\bar{\chi}} \xi_a. \quad (4.75)$$

Equations (4.75) and (4.74) comprise $\mathcal{N} + 1$ dynamical equations for the $\mathcal{N} + 1$ perturbation variables Ψ and ξ_a . However, since these variables are connected through the constraint (4.71), only \mathcal{N} of them are independent. Therefore we may use (4.71) to eliminate one of the variables in terms of the others. Choosing to eliminate the \mathcal{N} th scalar field, $\xi_{\mathcal{N}}$, in terms of $\xi_{a < \mathcal{N}}$ and Ψ , equation (4.71) gives

$$\xi_{\mathcal{N}} = -\frac{1}{\bar{\chi}'_{\mathcal{N}}} \left(\sum_{b=1}^{\mathcal{N}-1} \bar{\chi}'_b \xi_b - \frac{3M_*^3}{2} (\Psi' + 2\mathcal{H}\Psi) \right). \quad (4.76)$$

Note that we cannot eliminate Ψ in terms of the scalar fields ξ_a , since this requires an integration over unknown functions. This is understandable since doing so would

amount to reducing the problem to one in flat spacetime, which ought to be impossible. Substituting this into (4.75) and (4.74) and rearranging gives

$$\begin{aligned} {}^{(4)}\square\Psi - \Psi'' - \left(9\mathcal{H} - 2a^2\frac{1}{\bar{\chi}'_{\mathcal{N}}}\frac{\partial W}{\partial\chi_{\mathcal{N}}}\Big|_{\bar{\chi}}\right)\Psi' &= \left(12\mathcal{H}^2 + 4\mathcal{H}' - \frac{1}{2}{}^{(4)}\mathcal{R} - 4a^2\mathcal{H}\frac{1}{\bar{\chi}'_{\mathcal{N}}}\frac{\partial W}{\partial\chi_{\mathcal{N}}}\Big|_{\bar{\chi}}\right)\Psi \\ &= -\frac{4a^2}{3M_*^3}\sum_{a=1}^{\mathcal{N}-1}\left(\frac{\partial W}{\partial\chi_a}\Big|_{\bar{\chi}} - \frac{\bar{\chi}'_a}{\bar{\chi}'_{\mathcal{N}}}\frac{\partial W}{\partial\chi_{\mathcal{N}}}\Big|_{\bar{\chi}}\right)\xi_a \end{aligned} \quad (4.77)$$

$$\begin{aligned} {}^{(4)}\square\xi_a - \xi_a'' - 3\mathcal{H}\xi_a' + a^2\sum_{b=1}^{\mathcal{N}-1}\left(\frac{\partial^2 W}{\partial\chi_b\partial\chi_a}\Big|_{\bar{\chi}} - \frac{\bar{\chi}'_b}{\bar{\chi}'_{\mathcal{N}}}\frac{\partial^2 W}{\partial\chi_{\mathcal{N}}\partial\chi_a}\Big|_{\bar{\chi}}\right)\xi_b \\ = 3\left(\bar{\chi}'_a - \frac{M_*^3 a^2}{2}\frac{1}{\bar{\chi}'_{\mathcal{N}}}\frac{\partial^2 W}{\partial\chi_{\mathcal{N}}\partial\chi_a}\Big|_{\bar{\chi}}\right)\Psi' + 2a^2\left(\frac{\partial W}{\partial\chi_a}\Big|_{\bar{\chi}} - \frac{3M_*^3\mathcal{H}}{2}\frac{1}{\bar{\chi}'_{\mathcal{N}}}\frac{\partial^2 W}{\partial\chi_{\mathcal{N}}\partial\chi_a}\Big|_{\bar{\chi}}\right)\Psi. \end{aligned} \quad (4.78)$$

We may write these more compactly as

$${}^{(4)}\square\Psi + \mathcal{D}_1^y\Psi = \sum_{a=1}^{\mathcal{N}-1}(\mathcal{D}_2^y)_a\xi_a \quad (4.79)$$

$${}^{(4)}\square\xi_a + \sum_{b=1}^{\mathcal{N}-1}(\mathcal{D}_3^y)_{ab}\xi_b = (\mathcal{D}_4^y)_a\Psi, \quad (4.80)$$

where

$$\begin{aligned} \mathcal{D}_1^y &\equiv -\partial_y^2 - \left(9\mathcal{H} - 2a^2\frac{1}{\bar{\chi}'_{\mathcal{N}}}\frac{\partial W}{\partial\chi_{\mathcal{N}}}\Big|_{\bar{\chi}}\right)\partial_y - \left(12\mathcal{H}^2 + 4\mathcal{H}' - \frac{1}{2}{}^{(4)}\mathcal{R} - 4a^2\mathcal{H}\frac{1}{\bar{\chi}'_{\mathcal{N}}}\frac{\partial W}{\partial\chi_{\mathcal{N}}}\Big|_{\bar{\chi}}\right) \\ (\mathcal{D}_2^y)_a &\equiv -\frac{4a^2}{3M_*^3}\left(\frac{\partial W}{\partial\chi_a}\Big|_{\bar{\chi}} - \frac{\bar{\chi}'_a}{\bar{\chi}'_{\mathcal{N}}}\frac{\partial W}{\partial\chi_{\mathcal{N}}}\Big|_{\bar{\chi}}\right) \\ (\mathcal{D}_3^y)_{ab} &\equiv -\delta_{ab}(\partial_y^2 + 3\mathcal{H}\partial_y) + \mathcal{M}_{ab} \\ \mathcal{M}_{ab} &\equiv a^2\left(\frac{\partial^2 W}{\partial\chi_b\partial\chi_a}\Big|_{\bar{\chi}} - \frac{\bar{\chi}'_b}{\bar{\chi}'_{\mathcal{N}}}\frac{\partial^2 W}{\partial\chi_{\mathcal{N}}\partial\chi_a}\Big|_{\bar{\chi}}\right) \\ (\mathcal{D}_4^y)_a &\equiv 3\left(\bar{\chi}'_a - \frac{M_*^3 a^2}{2}\frac{1}{\bar{\chi}'_{\mathcal{N}}}\frac{\partial^2 W}{\partial\chi_{\mathcal{N}}\partial\chi_a}\Big|_{\bar{\chi}}\right)\partial_y + 2a^2\left(\frac{\partial W}{\partial\chi_a}\Big|_{\bar{\chi}} - \frac{3M_*^3\mathcal{H}}{2}\frac{1}{\bar{\chi}'_{\mathcal{N}}}\frac{\partial^2 W}{\partial\chi_{\mathcal{N}}\partial\chi_a}\Big|_{\bar{\chi}}\right). \end{aligned} \quad (4.81)$$

If we suppress the discrete indices in equations (4.79) and (4.80) they take an even

simpler form

$${}^{(4)}\square\Psi + \mathcal{D}_1^y\Psi = \mathcal{D}_2^y\xi \quad (4.82)$$

$${}^{(4)}\square\xi + \mathcal{D}_3^y\xi = \mathcal{D}_4^y\Psi . \quad (4.83)$$

This is the generic form that the scalar perturbation equations of motion take for $\mathcal{N} - 1$ coupled scalar fields and a graviscalar. Note that these equations include any direct couplings between the 5D scalar fields in the scalar potential.

We now specialize to the case in which the bulk scalar fields are only coupled through gravity. In this case the above equations simplify, but can still be written in the compact form (4.82) and (4.83). The boundary conditions are determined by integrating the equations of motion across each brane. Integrating equations (4.77) and (4.78), these are found to be

$$\begin{aligned} [\Psi']_{y_i} - 2a^2 \frac{1}{\bar{\chi}_{\mathcal{N}}} \frac{\partial W}{\partial \chi_{\mathcal{N}}} \Big|_{\bar{\chi}} \Psi' \Big|_{y_i} - 4 a^2 \mathcal{H} \frac{1}{\bar{\chi}'_{\mathcal{N}}} \frac{\partial W}{\partial \chi_{\mathcal{N}}} \Big|_{\bar{\chi}} \Psi \Big|_{y_i} \\ = \frac{4a^2}{3M_*^3} \sum_{a=1}^{\mathcal{N}-1} \left(\frac{\partial W}{\partial \chi_a} \Big|_{\bar{\chi}} - \frac{\bar{\chi}'_a}{\bar{\chi}'_{\mathcal{N}}} \frac{\partial W}{\partial \chi_{\mathcal{N}}} \Big|_{\bar{\chi}} \right) \xi_a \Big|_{y_i} \end{aligned} \quad (4.84)$$

$$[\xi'_a]_{y_i} + a^2 \frac{\partial^2 W}{\partial \chi_a^2} \Big|_{\bar{\chi}} \xi_a \Big|_{y_i} = 2 a^2 \frac{\partial W}{\partial \chi_a} \Big|_{\bar{\chi}} \Psi \Big|_{y_i} . \quad (4.85)$$

These boundary conditions can be put in the form

$$\Psi'(x, y_i) = A_1(y_i)\Psi(x, y_i) + A_2(y_i)\xi(x, y_i) \quad (4.86)$$

$$\xi'(x, y_i) = B_1(y_i)\Psi(x, y_i) + B_2(y_i)\xi(x, y_i) , \quad (4.87)$$

where $A_{1,2}$ and $B_{1,2}$ are functions of y_i , defined via (4.85), and we have used (4.86) in (4.84) to obtain (4.87).

The plan now is to perform a separation of variables in order to obtain a Sturm-Liouville eigenvalue problem, and then to analyze this eigenvalue problem to determine stability of the system. Because the 5D equations of motion of the scalar

perturbations are coupled, the correct separation of variables ansatz is a coupled one

$$\Psi^{(n)}(x, y) = \Psi_y^{(n)}(y) u^{(n)}(x) \quad (4.88)$$

$$\xi^{(n)}(x, y) = \xi_y^{(n)}(y) u^{(n)}(x) , \quad (4.89)$$

where $u^{(n)}(x)$ is the n^{th} 4D Kaluza-Klein physical mode and $\Psi_y^{(n)}(y)$ and $\xi_y^{(n)}(y)$ are the wave functions. Plugging this ansatz into equations (4.82) and (4.83) leads to the following coupled equations

$$\Psi_y(y) \square u(x) + u(x) \mathcal{D}_1^y \Psi_y(y) = u(x) \mathcal{D}_2^y \xi_y(y) \quad (4.90)$$

$$\xi_y(y) \square u(x) + u(x) \mathcal{D}_3^y \xi_y(y) = u(x) \mathcal{D}_4^y \Psi_y(y) . \quad (4.91)$$

The separation of variables thus yields a 4D wave equation for $u(x)$

$$\square u(x) + m_u^2 u(x) = 0 \quad (4.92)$$

and a system of two coupled differential equations

$$\mathcal{D}_1^y \Psi_y(y) - m_u^2 \Psi_y(y) = \mathcal{D}_2^y \xi_y(y) \quad (4.93)$$

$$\mathcal{D}_3^y \xi_y(y) - m_u^2 \xi_y(y) = \mathcal{D}_4^y \Psi_y(y) \quad (4.94)$$

with boundary conditions for the profiles

$$\Psi_y'(y_i) = A_1(y_i) \Psi_y(y_i) + A_2(y_i) \xi_y(y_i) \quad (4.95)$$

$$\xi_y'(y_i) = B_1(y_i) \Psi_y(y_i) + B_2(y_i) \xi_y(y_i) . \quad (4.96)$$

The system of equations (4.93) and (4.94) constitute an eigenvalue problem. The stability of the static background around which we have added scalar perturbations therefore depends on the existence, or absence, of a negative eigenvalue m_u^2 associated with a solution to eqs. (4.93) and (4.94).

This situation is somewhat unusual, since generally the Kaluza-Klein eigenvalue problem arising from dimensional reduction consists of a single second order differential equation, which can be put in standard Sturm-Liouville form. Analyzing that

Sturm-Liouville eigenvalue problem is straightforward, since in particular it is known that the eigenvalues are bounded from below, and that the eigenfunction corresponding to the smallest eigenvalue has no zeros within the interval. Therefore, the question of stability in practical terms becomes the search for a solution to the Kaluza-Klein equation such that it contains no nodes. Its associated eigenvalue will be the lightest possible eigenvalue and, if positive, the system will have no classical instabilities.

In the present case, however, the Kaluza-Klein problem is a system of coupled differential equations. Consequently, matrix Sturm-Liouville techniques are required. In order to analyze stability further, one must extend the theory of oscillations and the concept of nodes of solutions to a higher dimensional problem. Such an analysis is currently under way.

4.9 Discussion and Outlook

Braneworld theories generally lead to scalar degrees of freedom that propagate in the extra-dimensional bulk. Understanding the vacuum structure of these models in the presence of bulk scalar fields is therefore a prerequisite to fully appreciating their phenomenological possibilities. Furthermore, bulk scalars may provide a useful way to localize fermions and build braneworld models purely with field theory (e.g., fat branes and soft walls).

In this chapter I have examined the vacuum structure of braneworld models with one warped extra dimension and multiple bulk scalar fields. In particular I have focused on static configurations along the extra space coordinate where one of the fields—with Dirichlet boundary conditions—acquires a nontrivial kink-like profile. To find these solutions one needs to solve both the Einstein and the scalar field equations. In the limit of a flat 5D metric and weak gravity such solutions are known to exist, and the problem of finding all possible static configurations as well as determining their perturbative stability has been addressed and solved [147, 148]. Here I have

built upon this previous work to determine how warping along the extra dimension effects the existence and stability of these kink-like solutions.

When considering a fixed warped background, it was sufficient to look for nontrivial solutions for a single scalar field. In this case, neglecting any backreaction of the scalar field on the gravitational dynamics, we found that such kink-like solutions do indeed exist. As in the case of a flat extra dimension, we were able to prove that any kink-like solution with nodes in the bulk is unstable. Thus we have focused on nodeless kink solutions and the trivial solution. However, in contrast to the flat case, in the presence of warping we were only able to find a sufficient condition for determining the stability of these solutions. We were therefore unable to analytically determine stability for nontrivial solutions in a warped background, even when that background is fixed (e.g., in the Randall-Sundrum model with no backreaction). Instead we were forced to determine stability numerically.

Including the dynamics of the gravitational sector forces the inclusion of additional scalar fields whose purpose is to stabilize the size of the extra dimension. In that case we were again able to find nontrivial kink-like configurations, except now for a coupled multiple-field system. We have described a general graphical technique to find all possible static configurations of the background equations with one kink scalar field and an arbitrary number of additional “stabilization” fields. The technique amounts to generating solution surfaces by varying the shooting parameters needed to solve the coupled system of equations. This technique also allows us to look for multiple solutions with the same action. We have demonstrated how to implement this technique in two simple examples, where we considered one kink field and one stabilization field in the presence of gravity. As in the flat case, when the potential for the kink field is a higher-order polynomial (leading to higher-order nonlinearity in the field equations), we found that multiple solutions may exist for the same action. Interestingly, however, we also found multiple solutions for the same action when the kink potential was a fourth-order polynomial, which differs from the result obtained

in a flat background.

I have addressed the issue of stability only partially, deriving the full 5D perturbative equations, including gravitational perturbations, for multiple scalar fields in the presence of a warped extra dimension, and with general boundary conditions. The system of equations constitute a matrix eigenvalue problem, which must be analyzed using an extension of the usual theorems coming from oscillation theory or Sturm-Liouville eigenvalue problems. Such a project is currently underway.

Conclusions

Cosmic acceleration is a common ingredient in many of our current ideas about the universe. In the early universe, cosmic acceleration is often evoked in order to solve many of the outstanding problems with the Hot Big Bang cosmology. Adding this element, called inflation, to our picture of the early universe not only solves some of these problems, but it also makes predictions that are in remarkable agreement with observations. However the inflationary paradigm, as it is sometimes called, has its own shortcomings. One of these is that we do not fully understand the details of how the universe transitions from a cold and empty place at the end of inflation, to a hot and radiation-filled place which is required by the very successful Hot Big Bang cosmology. This transitional period, called reheating, has also proven to contain some surprises. In chapter 2 I discussed a resonance that may occur during this stage of the early universe, called preheating. I discussed some possible models of preheating that involved fields that are derivatively-coupled to the inflaton field.

Whereas cosmic acceleration in the early universe was originally motivated by theoretical arguments, cosmic acceleration in the late universe was seemingly forced upon us by observations. With the unexpected discovery that an accelerating universe seems to best explain several orthogonal observations, the search has been on for what could possibly be causing such behavior. However, there have been attempts to explain away the data in a way that would not require cosmic acceleration. One such approach is to call for a re-examination of how we interpret our observables. We know that we live in a universe which is inhomogeneous, or clumpy, on small scales. Yes our

cosmological observables are based on a model of space-time which is perfectly smooth and homogeneous. At some level the predictions we make with such a model cannot be trusted, since we know that the model is not exact. By using an alternative model of the universe, namely the LTB void model, some authors have recently argued that the observations which seem to lead to the conclusion that the universe is accelerating can be explained in these models without requiring acceleration.

One consequence, or prediction, of these LTB void models is that they would give rise to cosmic parallax. By looking for a cosmic parallax signal, we might hope to test or constrain such models. But LTB void models are not the only possible models of the universe that would give rise to a cosmic parallax signal. In chapter 3 I showed that anisotropic models of the universe would also give rise to cosmic parallax. There I focussed on Bianchi type-I models, for the sake of simplicity. I showed that for realistic Bianchi-I models, the expected cosmic parallax would be several orders of magnitude smaller than the expected signal from the most optimistic LTB void models. If future surveys detect a statistically significant cosmic parallax signal, that would therefore be strong evidence for the LTB void scenario. If, on the other hand, no such signal is observed, that could place significant constraints on LTB void models.

Finally, we do not have a firm understanding of what causes, or drives, cosmic acceleration in the early or late universe. One possibility is that cosmic acceleration could be a physical manifestation of our universe having extra spatial dimensions that have thus far gone undetected. Recent ideas in string theory and high energy particle physics have re-opened this possibility, and efforts are currently underway to test whether extra spatial dimensions really do exist. In chapter 4 I discussed the complications that arise when trying to build realistic braneworld models. In a space-time with extra spatial dimensions, one expects scalar fields (related to the higher-dimensional space-time geometry) to exist in the low-energy description of the theory. Furthermore, one expects that these scalar fields have profiles that extend into the bulk of the extra dimensions. In chapter 4 I searched for scalar field configurations

in such an extra-dimensional setup with non-trivial profiles in the bulk. This required adding an additional scalar field to the setup with the function of stabilizing the extra dimension, which in turn complicated the search for such solutions. I discussed a method that I helped develop to search for these non-trivial solutions in this multi-field situation. I also showed that interesting non-linear effects are possible when one includes gravity into the setup. The stability of the non-trivial configurations in the multi-field case was left for future work, as was showing how such models could give rise to cosmic acceleration.

Bibliography

- [1] W. L. Freedman et al. (HST), *Astrophys. J.* **553**, 47 (2001), [astro-ph/0012376](#).
- [2] A. G. Riess et al., *Astrophys. J.* **699**, 539 (2009), [0905.0695](#).
- [3] D. Tytler, J. M. O’Meara, N. Suzuki, and D. Lubin, *Phys. Scripta* **T85**, 12 (2000), [astro-ph/0001318](#).
- [4] E. Komatsu et al. (2010), [1001.4538](#).
- [5] M. Kowalski et al. (Supernova Cosmology Project), *Astrophys. J.* **686**, 749 (2008), [0804.4142](#).
- [6] E. R. Harrison, *Phys. Rev.* **D1**, 2726 (1970).
- [7] T. W. B. Kibble, *J. Phys.* **A9**, 1387 (1976).
- [8] Y. B. Zeldovich and M. Y. Khlopov, *Phys. Lett.* **B79**, 239 (1978).
- [9] J. Preskill, *Phys. Rev. Lett.* **43**, 1365 (1979).
- [10] A. H. Guth and S. H. H. Tye, *Phys. Rev. Lett.* **44**, 631 (1980).
- [11] E. W. Kolb and M. S. Turner, *Front. Phys.* **69**, 1 (1990).
- [12] A. A. Starobinsky, *Phys. Lett.* **B91**, 99 (1980).
- [13] A. H. Guth, *Phys. Rev.* **D23**, 347 (1981).

- [14] A. Albrecht, P. J. Steinhardt, M. S. Turner, and F. Wilczek, *Phys. Rev. Lett.* **48**, 1437 (1982).
- [15] A. D. Linde, *Phys. Lett.* **B108**, 389 (1982).
- [16] A. D. Linde, *Phys. Lett.* **B129**, 177 (1983).
- [17] S. W. Hawking and I. G. Moss, *Phys. Lett.* **B110**, 35 (1982).
- [18] K. Sato, *Mon. Not. Roy. Astron. Soc.* **195**, 467 (1981).
- [19] D. H. Lyth and A. Riotto, *Phys. Rept.* **314**, 1 (1999), [hep-ph/9807278](#).
- [20] W. H. Press and E. T. Vishniac, *Astrophys. J.* **239**, 1 (1980).
- [21] V. N. Lukash, *Sov. Phys. JETP* **52**, 807 (1980).
- [22] V. F. Mukhanov and G. V. Chibisov, *JETP Lett.* **33**, 532 (1981).
- [23] A. H. Guth and S. Y. Pi, *Phys. Rev. Lett.* **49**, 1110 (1982).
- [24] S. W. Hawking, *Phys. Lett.* **B115**, 295 (1982).
- [25] A. A. Starobinsky, *Phys. Lett.* **B117**, 175 (1982).
- [26] J. M. Bardeen, P. J. Steinhardt, and M. S. Turner, *Phys. Rev.* **D28**, 679 (1983).
- [27] A. D. Linde, *Phys. Lett.* **B116**, 335 (1982).
- [28] Y. B. Zeldovich, *Mon. Not. Roy. Astron. Soc.* **160**, 1P (1972).
- [29] L. F. Abbott, E. Farhi, and M. B. Wise, *Phys. Lett.* **B117**, 29 (1982).
- [30] A. D. Dolgov and A. D. Linde, *Phys. Lett.* **B116**, 329 (1982).
- [31] A. D. Dolgov and D. P. Kirilova, *Sov. J. Nucl. Phys.* **51**, 172 (1990).
- [32] J. H. Traschen and R. H. Brandenberger, *Phys. Rev.* **D42**, 2491 (1990).

- [33] L. Kofman, A. D. Linde, and A. A. Starobinsky, Phys. Rev. Lett. **73**, 3195 (1994), [hep-th/9405187](#).
- [34] Y. Shtanov, J. H. Traschen, and R. H. Brandenberger, Phys. Rev. **D51**, 5438 (1995), [hep-ph/9407247](#).
- [35] L. Kofman, A. D. Linde, and A. A. Starobinsky, Phys. Rev. Lett. **76**, 1011 (1996), [hep-th/9510119](#).
- [36] D. Boyanovsky, H. J. de Vega, R. Holman, D. S. Lee, and A. Singh, Phys. Rev. **D51**, 4419 (1995), [hep-ph/9408214](#).
- [37] D. Boyanovsky, H. J. de Vega, R. Holman, and J. F. J. Salgado, Phys. Rev. **D54**, 7570 (1996), [hep-ph/9608205](#).
- [38] P. B. Greene, L. Kofman, A. D. Linde, and A. A. Starobinsky, Phys. Rev. **D56**, 6175 (1997), [hep-ph/9705347](#).
- [39] D. I. Kaiser, Phys. Rev. **D56**, 706 (1997), [hep-ph/9702244](#).
- [40] S. Y. Khlebnikov and I. I. Tkachev, Phys. Rev. Lett. **77**, 219 (1996), [hep-ph/9603378](#).
- [41] S. Y. Khlebnikov and I. I. Tkachev, Phys. Lett. **B390**, 80 (1997), [hep-ph/9608458](#).
- [42] L. Kofman, A. D. Linde, and A. A. Starobinsky, Phys. Rev. **D56**, 3258 (1997), [hep-ph/9704452](#).
- [43] D. Boyanovsky (1995), prepared for 4th Workshop on Thermal Field Theories and Their Applications, Dalian, China, 7-12 Aug 1995.
- [44] B. A. Bassett, S. Tsujikawa, and D. Wands, Rev. Mod. Phys. **78**, 537 (2006), [astro-ph/0507632](#).

- [45] G. N. Felder, L. Kofman, and A. D. Linde, Phys. Rev. **D60**, 103505 (1999), [hep-ph/9903350](#).
- [46] I. Zlatev, G. Huey, and P. J. Steinhardt, Phys. Rev. **D57**, 2152 (1998), [astro-ph/9709006](#).
- [47] N. Arkani-Hamed, H.-C. Cheng, P. Creminelli, and L. Randall, JCAP **0307**, 003 (2003), [hep-th/0302034](#).
- [48] A. D. Linde, Phys. Rev. **D49**, 748 (1994), [astro-ph/9307002](#).
- [49] K. Freese, J. A. Frieman, and A. V. Olinto, Phys. Rev. Lett. **65**, 3233 (1990).
- [50] P. B. Greene, L. Kofman, and A. A. Starobinsky, Nucl. Phys. **B543**, 423 (1999), [hep-ph/9808477](#).
- [51] A. Dolgov and K. Freese, Phys. Rev. **D51**, 2693 (1995), [hep-ph/9410346](#).
- [52] A. Dolgov, K. Freese, R. Rangarajan, and M. Srednicki, Phys. Rev. **D56**, 6155 (1997), [hep-ph/9610405](#).
- [53] C. Armendariz-Picon, M. Trodden, and E. J. West, JCAP **0804**, 036 (2008), [0707.2177](#).
- [54] R. Kallosh, A. D. Linde, D. A. Linde, and L. Susskind, Phys. Rev. **D52**, 912 (1995), [hep-th/9502069](#).
- [55] G. N. Felder et al., Phys. Rev. Lett. **87**, 011601 (2001), [hep-ph/0012142](#).
- [56] P. B. Greene and L. Kofman, Phys. Rev. **D62**, 123516 (2000), [hep-ph/0003018](#).
- [57] J. E. Kim, Phys. Rept. **150**, 1 (1987).
- [58] M. S. Turner and L. M. Widrow, Phys. Rev. **D37**, 2743 (1988).
- [59] W. D. Garretson, G. B. Field, and S. M. Carroll, Phys. Rev. **D46**, 5346 (1992), [hep-ph/9209238](#).

- [60] E. W. Kolb, A. D. Linde, and A. Riotto, Phys. Rev. Lett. **77**, 4290 (1996), hep-ph/9606260.
- [61] E. W. Kolb, A. Riotto, and I. I. Tkachev, Phys. Lett. **B423**, 348 (1998), hep-ph/9801306.
- [62] L. M. Krauss and M. Trodden, Phys. Rev. Lett. **83**, 1502 (1999), hep-ph/9902420.
- [63] E. J. Copeland, D. Lyth, A. Rajantie, and M. Trodden, Phys. Rev. **D64**, 043506 (2001), hep-ph/0103231.
- [64] J. Smit and A. Tranberg, JHEP **12**, 020 (2002), hep-ph/0211243.
- [65] J. Garcia-Bellido, D. Y. Grigoriev, A. Kusenko, and M. E. Shaposhnikov, Phys. Rev. **D60**, 123504 (1999), hep-ph/9902449.
- [66] A. G. Riess et al. (Supernova Search Team), Astron. J. **116**, 1009 (1998), astro-ph/9805201.
- [67] S. Perlmutter et al. (Supernova Cosmology Project), Astrophys. J. **517**, 565 (1999), astro-ph/9812133.
- [68] N. A. Bahcall, J. P. Ostriker, S. Perlmutter, and P. J. Steinhardt, Science **284**, 1481 (1999), astro-ph/9906463.
- [69] P. J. E. Peebles and B. Ratra, Rev. Mod. Phys. **75**, 559 (2003), astro-ph/0207347.
- [70] E. J. Copeland, M. Sami, and S. Tsujikawa, Int. J. Mod. Phys. **D15**, 1753 (2006), hep-th/0603057.
- [71] J. Frieman, M. Turner, and D. Huterer, Ann. Rev. Astron. Astrophys. **46**, 385 (2008), 0803.0982.

- [72] R. R. Caldwell and M. Kamionkowski, *Ann. Rev. Nucl. Part. Sci.* **59**, 397 (2009), 0903.0866.
- [73] A. Silvestri and M. Trodden, *Rept. Prog. Phys.* **72**, 096901 (2009), 0904.0024.
- [74] K. Tomita, *Mon. Not. Roy. Astron. Soc.* **326**, 287 (2001), [astro-ph/0011484](#).
- [75] K. Tomita, *Prog. Theor. Phys.* **106**, 929 (2001), [astro-ph/0104141](#).
- [76] K. Tomita, *Prog. Theor. Phys.* **108**, 103 (2002), [astro-ph/0203125](#).
- [77] J. W. Moffat, *JCAP* **0510**, 012 (2005), [astro-ph/0502110](#).
- [78] H. Alnes, M. Amarzguioui, and O. Gron, *Phys. Rev.* **D73**, 083519 (2006), [astro-ph/0512006](#).
- [79] K. T. Inoue and J. Silk, *Astrophys. J.* **648**, 23 (2006), [astro-ph/0602478](#).
- [80] K. T. Inoue and J. Silk, *Astrophys. J.* **664**, 650 (2007), [astro-ph/0612347](#).
- [81] G. Lemaitre, *Gen. Rel. Grav.* **29**, 641 (1997).
- [82] R. C. Tolman, *Proc. Nat. Acad. Sci.* **20**, 169 (1934).
- [83] H. Bondi, *Mon. Not. Roy. Astron. Soc.* **107**, 410 (1947).
- [84] D. J. H. Chung and A. E. Romano, *Phys. Rev.* **D74**, 103507 (2006), [astro-ph/0608403](#).
- [85] H. Alnes and M. Amarzguioui, *Phys. Rev.* **D74**, 103520 (2006), [astro-ph/0607334](#).
- [86] J. Garcia-Bellido and T. Haugboelle, *JCAP* **0804**, 003 (2008), 0802.1523.
- [87] J. Garcia-Bellido and T. Haugboelle, *JCAP* **0809**, 016 (2008), 0807.1326.
- [88] J. Garcia-Bellido and T. Haugboelle, *JCAP* **0909**, 028 (2009), 0810.4939.

- [89] J. P. Zibin, A. Moss, and D. Scott, Phys. Rev. Lett. **101**, 251303 (2008), 0809.3761.
- [90] C. Quercellini, M. Quartin, and L. Amendola, Phys. Rev. Lett. **102**, 151302 (2009), 0809.3675.
- [91] M. A. C. Perryman et al., Astron. Astrophys. **369**, 339 (2001), astro-ph/0101235.
- [92] G. F. R. Ellis and M. A. H. MacCallum, Commun. Math. Phys. **12**, 108 (1969).
- [93] J. D. Barrow, Phys. Rev. **D55**, 7451 (1997), gr-qc/9701038.
- [94] G. Hinshaw et al. (WMAP), Astrophys. J. Suppl. **180**, 225 (2009), 0803.0732.
- [95] F. Ding and R. A. C. Croft (2009), 0903.3402.
- [96] T. Kaluza, Sitzungsber. Preuss. Akad. Wiss. Berlin (Math. Phys.) **1921**, 966 (1921).
- [97] O. Klein, Z. Phys. **37**, 895 (1926).
- [98] V. A. Rubakov and M. E. Shaposhnikov, Phys. Lett. **B125**, 136 (1983).
- [99] K. Akama, Lect. Notes Phys. **176**, 267 (1982), hep-th/0001113.
- [100] I. Antoniadis, Phys. Lett. **B246**, 377 (1990).
- [101] J. D. Lykken, Phys. Rev. **D54**, 3693 (1996), hep-th/9603133.
- [102] I. Antoniadis, N. Arkani-Hamed, S. Dimopoulos, and G. R. Dvali, Phys. Lett. **B436**, 257 (1998), hep-ph/9804398.
- [103] L. Randall and R. Sundrum, Phys. Rev. Lett. **83**, 3370 (1999), hep-ph/9905221.

- [104] L. Randall and R. Sundrum, Phys. Rev. Lett. **83**, 4690 (1999), [hep-th/9906064](#).
- [105] J. D. Lykken and L. Randall, JHEP **06**, 014 (2000), [hep-th/9908076](#).
- [106] I. Antoniadis and K. Benakli, Phys. Lett. **B326**, 69 (1994), [hep-th/9310151](#).
- [107] K. R. Dienes, E. Dudas, and T. Gherghetta, Nucl. Phys. **B537**, 47 (1999), [hep-ph/9806292](#).
- [108] N. Kaloper, J. March-Russell, G. D. Starkman, and M. Trodden, Phys. Rev. Lett. **85**, 928 (2000), [hep-ph/0002001](#).
- [109] D. Cremades, L. E. Ibanez, and F. Marchesano, Nucl. Phys. **B643**, 93 (2002), [hep-th/0205074](#).
- [110] C. Kokorelis, Nucl. Phys. **B677**, 115 (2004), [hep-th/0207234](#).
- [111] N. Arkani-Hamed, S. Dimopoulos, and G. R. Dvali, Phys. Lett. **B429**, 263 (1998), [hep-ph/9803315](#).
- [112] N. Arkani-Hamed, S. Dimopoulos, G. R. Dvali, and N. Kaloper, Phys. Rev. Lett. **84**, 586 (2000), [hep-th/9907209](#).
- [113] C. Macesanu and M. Trodden, Phys. Rev. **D71**, 024008 (2005), [hep-ph/0407231](#).
- [114] G. D. Starkman, D. Stojkovic, and M. Trodden, Phys. Rev. Lett. **87**, 231303 (2001), [hep-th/0106143](#).
- [115] G. D. Starkman, D. Stojkovic, and M. Trodden, Phys. Rev. **D63**, 103511 (2001), [hep-th/0012226](#).
- [116] C. Deffayet, G. R. Dvali, and G. Gabadadze (2001), [astro-ph/0106449](#).

- [117] C. Deffayet, G. R. Dvali, and G. Gabadadze, Phys. Rev. **D65**, 044023 (2002), [astro-ph/0105068](#).
- [118] G. R. Dvali, G. Gabadadze, and M. Porrati, Phys. Lett. **B485**, 208 (2000), [hep-th/0005016](#).
- [119] C. Deffayet, S. J. Landau, J. Raux, M. Zaldarriaga, and P. Astier, Phys. Rev. **D66**, 024019 (2002), [astro-ph/0201164](#).
- [120] C. Deffayet, Phys. Lett. **B502**, 199 (2001), [hep-th/0010186](#).
- [121] P. Binetruy, C. Deffayet, U. Ellwanger, and D. Langlois, Phys. Lett. **B477**, 285 (2000), [hep-th/9910219](#).
- [122] P. Binetruy, C. Deffayet, and D. Langlois, Nucl. Phys. **B615**, 219 (2001), [hep-th/0101234](#).
- [123] P. Binetruy, C. Deffayet, and D. Langlois, Nucl. Phys. **B565**, 269 (2000), [hep-th/9905012](#).
- [124] D. J. H. Chung and K. Freese, Phys. Rev. **D61**, 023511 (2000), [hep-ph/9906542](#).
- [125] C. Csaki, M. Graesser, L. Randall, and J. Terning, Phys. Rev. **D62**, 045015 (2000), [hep-ph/9911406](#).
- [126] J. M. Cline and J. Vinet, JHEP **02**, 042 (2002), [hep-th/0201041](#).
- [127] S. Nasri, P. J. Silva, G. D. Starkman, and M. Trodden, Phys. Rev. **D66**, 045029 (2002), [hep-th/0201063](#).
- [128] N. Arkani-Hamed, S. Dimopoulos, and G. R. Dvali, Phys. Rev. **D59**, 086004 (1999), [hep-ph/9807344](#).
- [129] C. D. Hoyle et al., Phys. Rev. Lett. **86**, 1418 (2001), [hep-ph/0011014](#).

- [130] J. Chiaverini, S. J. Smullin, A. A. Geraci, D. M. Weld, and A. Kapitulnik, Phys. Rev. Lett. **90**, 151101 (2003), [hep-ph/0209325](#).
- [131] J. C. Long et al. (2002), [hep-ph/0210004](#).
- [132] J. C. Long et al., Nature **421**, 922 (2003).
- [133] E. G. Adelberger, B. R. Heckel, and A. E. Nelson, Ann. Rev. Nucl. Part. Sci. **53**, 77 (2003), [hep-ph/0307284](#).
- [134] C. D. Hoyle et al., Phys. Rev. **D70**, 042004 (2004), [hep-ph/0405262](#).
- [135] D. J. Kapner et al., Phys. Rev. Lett. **98**, 021101 (2007), [hep-ph/0611184](#).
- [136] H. Georgi, A. K. Grant, and G. Hailu, Phys. Rev. **D63**, 064027 (2001), [hep-ph/0007350](#).
- [137] D. E. Kaplan and T. M. P. Tait, JHEP **11**, 051 (2001), [hep-ph/0110126](#).
- [138] B. Grzadkowski and M. Toharia, Nucl. Phys. **B686**, 165 (2004), [hep-ph/0401108](#).
- [139] N. Arkani-Hamed and M. Schmaltz, Phys. Rev. **D61**, 033005 (2000), [hep-ph/9903417](#).
- [140] P. Q. Hung and N.-K. Tran, Phys. Rev. **D69**, 064003 (2004), [hep-ph/0309115](#).
- [141] Z. Surujon, Phys. Rev. **D73**, 016008 (2006), [hep-ph/0507036](#).
- [142] R. Davies, D. P. George, and R. R. Volkas, Phys. Rev. **D77**, 124038 (2008), 0705.1584.
- [143] Y.-X. Liu, L.-D. Zhang, L.-J. Zhang, and Y.-S. Duan, Phys. Rev. **D78**, 065025 (2008), 0804.4553.
- [144] B. Batell and T. Gherghetta, Phys. Rev. **D78**, 026002 (2008), 0801.4383.

- [145] B. Batell, T. Gherghetta, and D. Sword, Phys. Rev. **D78**, 116011 (2008), 0808.3977.
- [146] A. Falkowski and M. Perez-Victoria, JHEP **12**, 107 (2008), 0806.1737.
- [147] M. Toharia and M. Trodden, Phys. Rev. Lett. **100**, 041602 (2008), 0708.4005.
- [148] M. Toharia and M. Trodden, Phys. Rev. **D77**, 025029 (2008), 0708.4008.
- [149] M. Toharia, M. Trodden, and E. J. West, Phys. Rev. **D82**, 025009 (2010), 1002.0011.
- [150] M. Toharia (2008), 0803.2503.
- [151] J. Lesgourgues and L. Sorbo, Phys. Rev. **D69**, 084010 (2004), hep-th/0310007.
- [152] W. D. Goldberger and M. B. Wise, Phys. Rev. Lett. **83**, 4922 (1999), hep-ph/9907447.
- [153] K. Skenderis and P. K. Townsend, Phys. Lett. **B468**, 46 (1999), hep-th/9909070.
- [154] O. DeWolfe, D. Z. Freedman, S. S. Gubser, and A. Karch, Phys. Rev. **D62**, 046008 (2000), hep-th/9909134.
- [155] C. Csaki, M. L. Graesser, and G. D. Kribs, Phys. Rev. **D63**, 065002 (2001), hep-th/0008151.

Biographical Information

NAME OF AUTHOR: Eric J. West

PLACE OF BIRTH: St. Cloud, Minnesota

DATE OF BIRTH: May 23, 1977

GRADUATE AND UNDERGRADUATE SCHOOLS ATTENDED:

University of Minnesota Duluth, Duluth, Minnesota

Syracuse University, Syracuse, New York

DEGREES AWARDED:

Bachelor of Arts in Philosophy, 1999, University of Minnesota Duluth

Bachelor of Science in Biochemistry, 1999, University of Minnesota Duluth

Masters of Science in Physics, 2006, Syracuse University

AWARDS AND HONORS:

Outstanding Teaching Assistant Award, 2005

PROFESSIONAL EXPERIENCE:

Teaching Assistant, Department of Philosophy, Syracuse University, 2000-2002

Instructor, Department of Philosophy, Syracuse University, Fall 2002

Teaching Assistant, Department of Physics, Syracuse University, 2003-2007

Instructor, Department of Physics, Syracuse University, Summer 2004